MODELING TURBULENT GAS-LIQUID BUBBLY FLOW IN A VERTICAL PIPE

A Thesis

Submitted to the College of Graduate and Postdoctoral Studies

in Partial Fulfillment of the Requirements for the Degree of

Doctor of Philosophy

in the Department of Mechanical Engineering at the

University of Saskatchewan

Saskatoon, Canada

By

A S M Atiqul Islam

Permission to Use

In presenting this thesis in partial fulfillment of the requirements for a Doctor of Philosophy (PhD) degree from the University of Saskatchewan, I agree that the libraries of this University may make it freely available for inspection. I further agree that permission for copying this thesis in any manner, in whole or in part, for scholarly purposes may be granted by the professor or professors who supervised my thesis work or, in their absence, by the Head of the Department or the Dean of the College in which my thesis work was done. It is understood that any copying, publication, or use of this thesis or parts thereof for financial gain shall not be allowed without my written permission. It is also understood that due recognition shall be given to me and to the University of Saskatchewan in any scholarly use which may be made of any material in my thesis.

Requests for permission to copy or to make other use of material in this thesis in whole or part should be addressed to:

Head
Department of Mechanical Engineering
University of Saskatchewan
Engineering Building, 57 Campus Drive
Saskatoon, SK S7N 5A9
Canada

OR

Dean
College of Graduate and Postdoctoral Studies
University of Saskatchewan
116 Thorvaldson Building, 110 Science Place
Saskatoon, SK S7N 5C9
Canada

Abstract

Bubbly gas-liquid turbulent flow occurs in various industrial applications, for example oil and gas production, petrochemical plants, nuclear reactors, etc. The analysis of bubbly gas-liquid turbulent flow remains a challenging task due to complexities such as the dispersed gas phase effects on the continuous liquid phase turbulence, interphase momentum exchange, and redistribution of the gas volume fraction due to bubble coalescence and breakup. The focus of this thesis is to develop a computational model to address these challenges. The model developed in this thesis uses a state-of-the-art two-fluid method, which minimizes computational resources and is based on the Reynolds-Averaged Navier-Stokes (RANS) equations. The predictions obtained for bubbly upward flow in a vertical pipe were validated against the available experimental data.

The first part of this thesis, chapter 2, documents a one-dimensional Eulerian-Eulerian two-fluid model for mono-disperse bubbly gas-liquid flow. The main challenge is the prediction of the gas volume fraction profile, based on the radial force balance of the non-drag forces for the gas phase. The shape of the volume fraction profile across the pipe changes depending on the bubble size. The volume fraction profile exhibits a peak value near the wall and at the centre line of the pipe for smaller and larger bubbles, respectively, which is consistent with experimental measurements. For the model tested, the turbulence kinetic energy was observed to increase for larger size bubbles compared to the smaller size bubbles.

The second part of the thesis, chapter 3, reports a thorough investigation of the effect of bubbles on the liquid phase turbulence, referred to as turbulence modulation. The presence of bubbles in the flow can either enhance or attenuate the liquid phase turbulence. For the same flow conditions, the effect of the turbulence modulation shows both enhancement and suppression for the turbulence kinetic energy in different locations in the pipe. A budget analysis of the turbulence transport equations was used to provide insight on the relative importance of the turbulence modulation and to identify the region where it plays a significant role. The turbulence modulation was often found to have an insignificant effect on the prediction for the mean flow variables.

The third part of the thesis, chapter 4, describes a numerical study of poly-disperse gas-liquid flow, which contains bubbles of different diameter. For a poly-disperse distribution of gas bubbles, the model must account for the consequences of bubbles either breaking up or coalescing with each

other. To explore their effect, an inhomogeneous multiple size group (iMUSIG) approach with a bubble coalescence and breakup model was implemented. The developed model was shown to correctly redistribute the gas volume fraction among the bubble groups based on the coalescence and breakup processes. The turbulence modulation for the poly-disperse flow was found to be larger than for the mono-disperse case, which indicates one additional effect of a poly-disperse distribution of gas bubbles.

Overall, this thesis research implemented a two-fluid model that is able to capture important features of bubbly gas-liquid flow for both mono-disperse and poly-disperse cases. Some significant features of the model are: the use of a radial force balance for the gas volume fraction evaluation; a turbulence modulation contribution based on source terms in the turbulence transport equations; and incorporating the effect of coalescence and breakup processes and the resultant exchange of gas volume fraction among different bubble groups. As such, the thesis documents an improved predictive model for RANS simulations of bubbly gas-liquid flow in industrial applications.

Acknowledgements

I would like to express my sincere gratitude and appreciation to my esteemed supervisor, Prof. D J Bergstrom, for his proper guidance, continuous support and encouragement throughout my research work during this graduate program. His critical assessment and suggestions have been invaluable at every stage of this research work.

I would like to extend my acknowledgement to the advisory committee members Prof. Jerzy A Szpunar, Prof. Carey J Simonson, Prof. James D Bugg and Prof. Richard W Evitts for their valuable suggestions and feedback.

I would also take this opportunity to thank my research colleagues of the CFD lab, friends and Shawn Reinink of the Mechanical Engineering Department for their assistance and making my stay at the University of Saskatchewan a memorable one.

Furthermore, I would like to thank Prof. D J Bergstrom, Canadian Nuclear Laboratories (CNL) formerly known as Atomic Energy of Canada Limited (AECL), and the Natural Sciences and Engineering Research Council of Canada (NSERC) for providing the financial support for this research work.

Dedication

I dedicate this thesis to my parents, sister, brother, and wife for their generous support and continuous motivation throughout the PhD program.

Table of Contents

List of Tables

List of Figures

List of Symbols

A	Effective cross-sectional area for collision (m^2)
B_{eddy}	Constant in breakup model
B_{fric}	Constant in breakup model
B_{turb}	Constant in breakup model
$B_{\mathrm{B,k}}$	The birth rates of bubbles in size group k due to breakup of bubbles of larger size ($kg/s{\cdot}m^3$)
$B_{\mathrm{C,k}}$	The birth rates of bubbles in size group k due to coalescence of bubbles of smaller size ($kg/s{\cdot}m^3$)
C_{buoy}	Constant in coalescence model
C_{eff}	Constant in coalescence efficiency
C_{shear}	Constant in coalescence model
C_{turb}	Constant in coalescence model
C_{D}	Drag force coefficient
$C_{\mathrm{D,Eo}}$	Turbulent dispersion force coefficient based on modified Eötvös number (m^2/s^2)
C_{L}	Lift force coefficient
C_{TD}	Turbulent dispersion force coefficient
C_{W}	Wall (lubrication) force coefficient
d_{b}	Gas bubble diameter (m)
d_{i}	Gas bubble diameter of a velocity group over its size group i (m)
d_{j}	Gas bubble diameter of a velocity group over its size group j (m)
d_{k}	Gas bubble diameter of a velocity group over its size group k (m)
d_{l}	Gas bubble diameter of a velocity group over its size group l (m)
d_{H}	Long axis bubble diameter (m)

D Pipe diameter (m)

$D_{B,k}$ Death rates of bubbles in size group k due to breakup into smaller bubbles (kg/s·m^3)

$D_{C,k}$ Death rates of bubbles in size group k due to coalescence with other bubbles to form a larger one (kg/s·m^3)

E Energy (J)

Eo Eötvös number

$E_{\sigma,i}$ Surface energy during the breakage of bubble i (J)

$E_{\sigma,j}$ Surface energy during the breakage of bubble j (J)

$E_{\sigma,k}$ Surface energy during the breakage of bubble k (J)

f Size fraction of a velocity group

F^{D} Drag force (N/m^3)

F^{L} Lift force (N/m^3)

F^{TD} Turbulent dispersion force (N/m^3)

$F^{TD,Eo}$ Turbulent dispersion force based on modified Eötvös number (N/m^3)

F^{W} Wall (lubrication) force (N/m^3)

g Gravitational acceleration (m/s^2)

h Collision frequency (m^3/s)

k Turbulence kinetic energy (m^2/s^2)

m Mass (kg)

P Pressure (N/m^2)

r Radial variable (m)

R Pipe radius (m)

Re Reynolds number (flow)

Re_b Bubble Reynolds number

S_I Mass transfer between velocity groups due to CAB for bubble group I ($kg/s \cdot m^3$)

S_{II} Mass transfer between velocity groups due to CAB for bubble group II ($kg/s \cdot m^3$)

$S_{M,I}$ Momentum transfer between velocity groups due to CAB for bubble group I (N/m^3)

$S_{M,II}$ Momentum transfer between velocity groups due to CAB for bubble group II (N/m^3)

u_{rel} Approach velocity between bubbles (m/s)

u_τ Friction velocity (m/s)

u_z Liquid phase mean velocity (m/s)

u_T The terminal velocity (m/s)

v_z Gas phase mean velocity (m/s)

$v_{z,I}$ Gas phase mean velocity (m/s) for bubble group I

$v_{z,II}$ Gas phase mean velocity (m/s) for bubble group II

We Weber number

X_{ilk} Fraction of mass for size group k due to coalescence between group i and l

y Distance from the wall (m)

z Longitudinal variable (m)

Greek Symbols

α_g Gas volume fraction

$\alpha_{g,I}$ Gas volume fraction for bubble group I

$\alpha_{g,II}$ Gas volume fraction for bubble group II

$\alpha_{g,III}$ Gas volume fraction for bubble group III

$\alpha_{g,IV}$ Gas volume fraction for bubble group IV

α_l Liquid volume fraction

γ Shear strain rate (1/s)

Γ Coalescence frequency (m^3/s)

ε Dissipation rate of turbulence kinetic energy (m^2/s^3)

η Kolmogorov length scale (m)

λ Coalescence efficiency

λ_{eff} Effective coalescence efficiency

μ_{eff} Effective viscosity of liquid phase ($N{\cdot}s/m^2$)

μ_{g} Dynamic viscosity of gas phase ($N{\cdot}s/m^2$)

μ_{l} Dynamic viscosity of liquid phase ($N{\cdot}s/m^2$)

μ_{t} Turbulent viscosity of liquid phase ($N{\cdot}s/m^2$)

ν Kinematic viscosity (m^2/s)

ρ_{g} Density of gas phase (kg/m^3)

ρ_{l} Density of liquid phase (kg/m^3)

σ Surface tension of liquid phase (N/m)

τ Characteristic time scale (s)

τ_{w} Wall shear stress (N/m^2)

Ω Bubble breakup rate (1/s)

Subscripts

b Bubble

g Gas phase

i Size group index

j Size (bubble or velocity) group index

k Size group index

l Liquid phase

List of Abbreviations

1D	One-Dimensional
2D	Two-Dimensional
3D	Three-Dimensional
ABND	Average Bubble Number Density
BIT	Bubble Induced Turbulence
BSL	Baseline
CAB	Coalescence And Breakup
CFD	Computational Fluid Dynamics
DNS	Direct Numerical Simulation
FVM	Finite Volume Method
iMUSIG	Inhomogeneous Multiple Size Group
IATE	Interfacial Area Transport Equation
LS	Level-Set
MTLoop	Measurement Test Loop
MUSIG	Multiple Size Group
RANS	Reynolds-Averaged Navier-Stokes
SST	Shear Stress Transport
TDMA	Tri-Diagonal Matrix Algorithm
TFM	Two-Fluid Model
TKE	Turbulence Kinetic Energy
TM	Turbulence Modulation
TOPFLOW	Transient TwO-Phase FLOW
URANS	Unsteady Reynolds-Averaged Navier-Stokes
VOF	Volume Of Fluid

Chapter 1

Introduction

In fluid mechanics, the presence of more than one phase in a flow is referred to as multiphase flow, such as gas-solid, gas-liquid, liquid-liquid or liquid-solid flow. Typically, one of the phases, known as the dispersed phase is distributed throughout the corresponding continuous phase in the form of droplets, bubbles or particles. Each phase has a distinct velocity and occupies a fraction of the total flow volume, which is termed the volume fraction.

Gas-liquid flow is considered in this thesis since this flow occurs in many industrial and engineering applications, e.g. the oil and gas, chemical, and nuclear industries. More specifically, oil-gas flow occurs during the process of extraction and pipeline transmission in the oil and gas industry; bubble columns where gas bubbles move through a stationary liquid phase occur in the chemical industry; and gas bubbles form due to boiling heat transfer within reactor systems in the nuclear industry.

Arguably, the most common geometry for fluid flow in industry is a circular pipe because of its ease of installation and maintenance. Depending on the distribution and size of bubbles, different flow regimes, e.g. bubbly, slug, churn, and annular, are identified for gas-liquid flow in a pipe. A general knowledge of these flow regimes is necessary to understand the associated flow phenomena. Bubbly flow occurs when the dispersed bubbles are smaller than the pipe diameter and occupy a relatively small volume of the flow. In contrast, slug and churn flow prevail at larger bubble sizes that are comparable to the pipe diameter in flows with a large gas fraction. For annular flow, the core region of the pipe is occupied by bubbles that are surrounded by a relatively thin liquid film travelling on the pipe walls.

This thesis considers gas-liquid bubbly flow because it is so prevalent in engineering applications. For upward flow in a vertical pipe, the gas bubbles flow co-currently within the liquid phase which is driven by a specified pressure gradient. The pressure forces acting on the interface between the gas and liquid phase is balanced by the surface tension of the water-air interface. The size of a bubble depends mainly on the nature of the gas distribution and the physical properties of the water-air interface, e.g. surface tension. Gas-liquid flows possess an inherently complex hydrodynamics which includes: interactions among the interphase forces, relative motion between the phases, changes in the turbulence properties of the liquid phase due to the presence of bubbles, and radial separation and redistribution of bubbles.

The distribution of gas volume fraction across the pipe changes depending on the bubble size and is determined by the interaction between non-drag forces. The non-drag forces, such as lift, wall, and turbulent dispersion, which act perpendicular to the flow direction, are responsible for the lateral movement of bubbles inside a pipe. The lift force causes smaller and larger bubbles to move towards the wall and centre of the pipe, respectively. The wall force tends to move the bubbles away from the wall, while the turbulent dispersion force represents the smoothing of the gas volume fraction profile due to the turbulence in the liquid phase.

Generally, bubbly flows with a lower gas volume fraction, contain smaller bubbles that accumulate near the pipe wall causing a gas volume fraction distribution with a peak value near the wall. In contrast, larger bubbles, which occur for a relatively higher gas content, move to the centre of the pipe resulting in a gas volume fraction profile with a peak value near the centre of the pipe. These two cases are characterized by a wall-peak and center-peak gas volume fraction profile, respectively.

Most bubbly flows are turbulent in nature. The turbulence in the liquid phase becomes more complicated due to the presence of the gas phase, which can modify the turbulence properties as well as the mean flow properties.

Gas-liquid flow can be classified as either mono-disperse or poly-disperse based on the number of bubble sizes present. For mono-disperse bubbly flow, bubbles are characterized by a single bubble diameter. In contrast, poly-disperse bubbly flow consists of bubbles with different diameters. For poly-disperse flow, bubbles can be classified into a number of groups based on the size known as

bubble group. Bubbles of the same size can move with the same velocity, while bubbles of different size move with a distinct velocity.

The gas-liquid bubbly flow structure inside the pipe is also determined by the process of bubble coalescence and breakup. Bubbles can collide with each other mostly due to the effects of turbulence and interaction between the non-drag forces. Moreover, a bubble can break up due to the effects of destroying and restoring stresses. A destroying stress could be due to the effect of turbulence, while surface tension provides a restoring stress. The bubble breakup and coalescence process modifies the volume fraction of different bubble groups due to the exchange of gas fraction between bubble groups. The bubble breakup rate increases as the size of the bubble increases and the coalescence rate increases with the number of bubbles.

1.1 Motivation and research challenges

It is essential to develop a predictive model based on an understanding of the bubbly flow behaviour within a pipe because of its widespread industrial applications. Computational fluid dynamics (CFD) has demonstrated itself capable of providing realistic predictions of many single-phase flows based on the RANS equations. The RANS equations, which represents the time-averaged equations of motion for fluid flow, are widely used to describe turbulent flow. Recently, RANS modelling is being used successfully and is gaining more attention to formulate predictive tools for gas-liquid flow analysis (Colombo and Fairweather, 2015). However, the CFD analysis of bubbly flow using a RANS formulation remains an important issue.

CFD analysis of some multiphase flow uses different interface tracking techniques, such as the volume of fluid (VOF) method, the level-set method (LSM), and front tracking (FT) method, to follow the temporal and spatial development of gas-liquid interfaces. These tracking methods, within the RANS formulation, use a Lagrangian frame of reference to describe the motion of the gas phase based on the dynamics of all the bubbles in the system. Therefore, these methods require large computational resources, especially when a large number of bubbles are present in the flow domain.

The two-fluid model is an alternative approach, which represents an average formulation of gas and liquid phase. The two-fluid model treats both phases as interpenetrating continua, and uses the local volume fraction of each phase to characterize the temporal and spatial distribution of the two phases in an Eulerian framework. For gas-liquid flow, the two-fluid approach is appropriate when the gas bubbles are finely dispersed in the liquid phase. The liquid and gas phases have similar conservation equations for mass and momentum. However, the coupling between the gas and liquid phase is achieved through the pressure and interphase transfer terms in the momentum equations. The drag force is often considered to be the dominant interfacial force and is responsible for the transfer of the mean kinetic energy from the liquid to the gas.

The developed model considers gas bubbles with a spherical shape, and uses the concept of gas volume fraction profile rather than considering bubbles to reflect the distribution of gas in the liquid. The modelling of gas-liquid turbulent flow remains a challenging task which includes: effects of bubble diameter on the gas volume fraction distribution across the pipe, effects of the dispersed gas phase on the continuous liquid phase turbulence, and separation and redistribution of the gas bubbles considering bubble coalescence and breakup processes.

Experimental measurements of gas-liquid flow are especially challenging, which is reflected in the scarcity of data. For a three-dimensional pipe flow configuration, the main challenge lies in measuring the flow properties near the wall. The essential flow parameters such as volume fraction, gas and liquid phase velocity, Reynolds stress, and turbulence kinetic energy are required for the complete assessment of a numerical model. However, the available experiments fall short in documenting these flow properties. Therefore, the limited experimental data imposes another challenge for the validation of a computational model. Recently, the results obtained from direct numerical simulation (DNS) are gaining attention to provide insight related to this kind of flows.

1.2 Objectives

This thesis considers the case of fully developed turbulent gas-liquid upward flow in a vertical pipe. The challenges are addressed using the following three specific objectives.

1. **Develop and implement the two-fluid model to predict the gas volume fraction:** A computational model is implemented based on the two-fluid model to predict the gas volume fraction distribution. The effects of bubble size on the radial forces are investigated to understand the development of either a centre-peak or a wall-peak profile. The contribution of the turbulence induced by bubbles compared to the shear induced turbulence is also explored.
2. **A comprehensive assessment of turbulence modulation including a budget analysis:** The effect of bubbles on the liquid phase turbulence is evaluated. The performance of a specific turbulence modulation model is assessed thoroughly by comparing the predicted gas volume fraction, mean phasic velocities, and turbulence properties to the available experimental data. A budget analysis for the turbulence transport equations is also performed to understand the contribution of the turbulence modulation.
3. **A model for the bubble coalescence and breakup process is investigated for the poly-disperse distribution of bubbles:** A poly-disperse distribution of bubbles is analyzed using the so-called iMUSIG approach with a bubble coalescence and breakup model. The bubble coalescence and breakup model redistributes the gas volume fraction among the different bubble groups. The turbulence modulation for poly-disperse and mono-disperse bubbly flow is also compared.

An in-house one-dimensional model is developed in order to achieve the objectives. The governing two-fluid transport equations are discretized using the finite volume method and a low Reynolds number $k-\varepsilon$ model is used to predict the turbulence field for the liquid phase. The predicted results pertain to the case of fully developed gas-liquid bubbly upward flow in a vertical pipe. The gas volume fraction is predicted using a radial force balance for the bubble phase. The model is used to predict the mean velocity for both phases as well as the turbulent viscosity in the liquid based on the turbulence kinetic energy and its dissipation rate. One important aspect of this thesis is that it mostly used models available in the literature and implemented small modifications to improve their performance. A contribution of the thesis is the selection of experimental studies that can be used to validate the results in each objective. Finally, the thesis looked at a relatively small set of bubble groups for the analysis of poly-disperse flow. Objectives 1, 2 and 3 are addressed sequentially in Chapters 2, 3 and 4 of this dissertation since it adopts a manuscript-style format.

1.3 Literature Review

Gas-liquid flow analysis can be divided into two categories: experimental studies and numerical simulations. A brief discussion of each category relevant to this thesis is described in this section. The experimental studies were used to validate the predicted results while the numerical studies documented some of the model formulations adopted in the present thesis.

1.3.1 Experimental studies

Only a limited number of researchers have conducted experimental measurements of air-water flow within a vertical pipe and documented the properties of the flow.

Liu (1997, 1998) conducted an experiment using a flush-mounted hot film anemometer probe to investigate the effect of bubble size on the wall shear stress for air-water bubbly flow in a vertical channel. The experimental flow conditions covered both the wall- and centre-peak volume fraction distributions. Measurements were performed for the void fraction profile, bubble size distribution, liquid phase velocity, and axial liquid phase turbulence intensity. In addition, the mean and time-varying fluctuation properties of the wall shear stress were documented in their study. The liquid phase superficial velocity and the presence of smaller bubbles were found to be the dominant parameters for determining the magnitude and fluctuation intensity of the wall shear stress.

The transition in flow regime for gas-liquid flow in a large vertical pipe was experimentally examined by Ohnuki and Akimoto (2000). They studied the gas volume fraction profile, bubble distribution, axial gas and liquid phase velocity, and velocity fluctuations for both phases. The churn flow regime was found to be dominant in a large vertical pipe, whereas a smaller pipe exhibits slug flow for the same flow conditions. It was also reported that the flow conditions at which bubble coalescence begins for large scale pipes is similar to that for small scale pipes.

Hibiki *et al.* (2001) performed an experimental study of air-water upward flow in a vertical tube using a double-sensor probe and hot film probe. Their study considered flow regimes from bubbly to slug flow in order to capture both the wall-peak and centre-peak volume fraction distributions. For various liquid and gas superficial velocities, measurements were carried out for the gas volume

fraction profile, interfacial area concentration, bubble size distribution, interfacial velocity, and liquid phase velocity as well as turbulence intensity.

Experimental measurements of the radial gas volume fraction and bubble size distribution were performed by Lucas *et al.* (2005) using a wire-mesh sensor technique. The gas volume fraction profiles were decomposed for specific bubble sizes. The measurement was conducted for the bubbly and slug flow regimes within a vertical pipe. It was reported that small bubbles are likely to be found near the wall region, while larger bubbles tend to concentrate in the centre region of the pipe. The sign of the lift force changes depending on the bubble size, which was confirmed by the measurements.

Prasser *et al.* (2007) experimentally investigated the development of gas-liquid flow structure for a vertical pipe with a larger diameter compared to the experiment of Liu (1997, 1998), Hibiki *et al.* (2001), and Lucas *et al.* (2005). The measurement considered bubbly to churn flow regimes with an improved wire-mesh sensor compared to that used by Lucas *et al.* (2005). The measurements include the distribution of gas volume fraction, gas velocity, and bubble size distributions. In addition, it examined the influence of the physical properties of the fluid phase by comparing the results of the standard air-water mixture to steam-water. Their study documented the evolution of the bubble-size distributions and the associated bubble coalescence and breakup process.

Shawkat *et al.* (2008) experimentally analyzed air-water bubbly flow for a vertical pipe. The gas phase characteristics were measured using a dual optical probe and the liquid-phase turbulence properties were measured with hot-film anemometry. The measurements included gas volume fraction, bubble size distribution, gas and liquid phase mean velocity, axial and radial turbulence intensity, and Reynolds shear stress for the liquid phase. The gas volume fraction and superficial velocity of both phases were smaller compared to other experimental studies (Lucas *et al.*, 2005; Prasser *et al.*, 2007). The change from a wall-peak to a centre-peak gas volume fraction profile occurs as the volume fraction and bubble size was increased, which was consistent with the findings of other experiments. The liquid phase mean velocity and turbulence intensities were less uniform in the core region of the pipe as the gas volume fraction profile changed from a wall to a centre peak case. It was observed that the Reynolds shear stress increases near the wall region as

the gas and liquid superficial velocities increase. Generally, the level of turbulence intensity increases for gas-liquid flow, with respect to single-phase flow, due to the presence of bubbles in the flow. Interestingly, for a low gas volume fraction with high liquid superficial velocity, turbulence suppression was observed close to the pipe wall compared to single-phase flow. The reason for the change in turbulence intensity was found to be consistent with the measured relative velocity between the phases. The relative velocity tends to decrease toward the pipe wall at low liquid superficial velocity. As liquid superficial velocity is increased, the profiles become uniform and then increase toward the pipe wall indicating higher turbulence in that region.

Hosokawa and Tomiyama (2009) experimentally investigated bubbly pipe flow using an image processing method and laser Doppler velocimetry. Measurements were performed for mean flow parameters such as the gas volume fraction distribution, bubble size distribution, mean phasic velocities, and turbulence kinetic energy for the liquid phase. Enhancement and suppression of the turbulence kinetic energy profile was found for lower and higher liquid superficial velocities, respectively, which was consistent with the observation of Shawkat *et al.* (2008).

With respect to turbulence modulation, the effect of bubbles on the liquid phase turbulence was not clearly documented in the experimental studies of Liu (1997, 1998), Lucas *et al.* (2005), and Prasser *et al.* (2007). Turbulence enhancement and suppression due to the presence of bubbles was noted in the experimental measurements of Shawkat *et al.* (2008), and Hosokawa and Tomiyama (2009). Overall, the experimental data available for the assessment of models for turbulent gas-liquid flow is insufficient and inconclusive.

1.3.2 Numerical analysis

Gas-liquid flows are classified as either mono-disperse or poly-disperse depending on the gas bubble size. Bubbles are characterized by a single bubble diameter in mono-disperse flow, whereas, poly-disperse flow contains bubbles of different diameters. The first part of this section describes the studies related to mono-disperse flow, while the second part considers the case of poly-disperse flow.

1.3.2.1 Mono-disperse gas-liquid flow

Lucas *et al.* (2001) performed a numerical simulation to predict gas-liquid flow in a pipe. For their one-dimensional model formulation, the gas volume fraction was evaluated based on a radial force balance on the bubbles. The radial forces, also known as the non-drag forces, such as lift, wall or lubrication and turbulent dispersion, act on the bubbles perpendicular to the flow direction and the magnitude of these forces depends on bubble size.

Vitankar *et al.* (2002) predicted the gas volume fraction and liquid phase mean velocity profiles for a bubble column using the two-fluid model. A low Reynolds number $k-\varepsilon$ model was used to describe the liquid phase turbulence, and the characteristics of the flow were investigated, especially in the near-wall region. An iterative procedure was described for the numerical simulation using a drift-flux model for the calculation of the gas volume fraction. They extended the one-dimensional model to predict the pressure drop of the gas-liquid flow.

As reported by Krepper *et al.* (2005), the lift and wall forces play the most important role in determining the gas volume fraction profile. Their model prediction includes gas volume fraction, bubble size distribution, gas and liquid phase velocity, distributions of the non-drag forces, and turbulence properties. The drag force dominates the momentum exchange in the flow direction, and the lift force strongly influences the radial distribution of bubbles.

Ekambara *et al.* (2005) carried out CFD simulations for the prediction of bubbly flow in cylindrical bubble column reactors. One-dimensional (1D), two-dimensional (2D), and three-dimensional (3D) formulations of the two-fluid model were implemented with a two-equation turbulence model. The predicted results include gas volume fraction, liquid phase velocity, turbulence kinetic energy, dissipation rate of turbulence kinetic energy, eddy viscosity, and Reynolds shear stress. The 3D results for the gas volume fraction and liquid phase velocity were observed to be in good agreement with the experimental data.

Lucas *et al.* (2007) performed numerical simulation of gas-liquid flow using a one-dimensional (1D) solver. The available correlation of bubble forces, e.g. lift, wall, and turbulent dispersion were thoroughly assessed based on the detailed experimental database for vertical pipe flow. The simulated results include the gas volume fraction and turbulence kinetic energy profiles. They

concluded that the correlations of Tomiyama lift and wall force, Favre averaged turbulent dispersion force was found to provide the best agreement with the experimental data.

Dhotre *et al.* (2007) performed 3D simulations for gas-liquid flow in a vertical pipe using the two-fluid formulation. The predicted results include gas volume fraction distribution, gas and liquid phase velocity, and turbulence kinetic energy. Turbulence modulation was implemented in the turbulence transport equations to include the effects of bubbles. The use of an isotropic turbulence model, i.e. an eddy viscosity model, may have an adverse effect for flow predictions where the turbulence structure is anisotropic.

Monahan and Fox (2009) presented a two-fluid simulation of a pseudo-2D bubble column considering an extensive set of interphase force terms. The simulated results include gas volume fraction, and gas and liquid phase velocity profiles. The qualitative and quantitative comparisons between the experimental data and simulated results were found to be satisfactory. However, in some cases, the predicted results differed from the experimental data. They concluded that changing the liquid velocity boundary condition from zero stress to zero slip leads to a small improvement in their simulated results.

Rzehak and Krepper (2013) performed a numerical simulation for gas-liquid flow using the two-fluid method. The simulated results include gas volume fraction, bubble size distribution, liquid phase velocity, turbulent viscosity, and turbulence kinetic energy. They provided a detailed description of the modelling of the bubble induced turbulence in the turbulence transport equations. They proposed use of a time scale that adopts the bubble size as the length scale for the bubble induced turbulence model.

1.3.2.2 Poly-disperse gas-liquid flow

The following section describes numerical studies of poly-disperse flow, which contains bubbles of different diameter. A poly-disperse distribution of gas bubbles in a bubbly flow is typically described through the so-called multiple size group (MUSIG) approach. Generally, poly-disperse flow analysis includes a coalescence and breakup model to incorporate the exchange of gas volume fraction among the bubble groups due to bubble coalescence and breakup events.

Both a MUSIG and average bubble number density (ABND) model were used for the prediction of the bubble size distribution of a poly-disperse bubbly flow by Cheung *et al.* (2007). Coalescence and breakup was evaluated based on the local flow parameters such as gas volume fraction, mean bubble diameter, interfacial area concentration, and mean velocity for both phases. It was concluded that a reasonable bubble size distribution of poly-disperse flow can be achieved with the MUSIG model, which requires less computational time than the ABND model. The gas volume fraction was found to be over-predicted by the ABND approach.

Krepper *et al.* (2008) developed a generalized iMUSIG model for the simulation of poly-disperse flow. To account for bubble coalescence and breakup events, their model used the Prince and Blanch (1990) model for coalescence and the Luo and Svendsen (1996) model for breakup. The model was implemented into the commercial CFD code ANSYS CFX, which enables the subdivision of the dispersed phase into a number of different size groups. Their model shows the capability of describing poly-disperse bubbly flows, especially for the separation of bubbles. The ability to capture the separation phenomena of small and large bubbles was found to be the strength of their model. Specification of the coalescence and breakup coefficients was a weakness of their model that warrants further investigation.

A one-dimensional model for poly-disperse bubbly upward flow was implemented by Issa and Lucas (2009). The predicted results included gas volume fraction, gas and liquid phase velocity, turbulent viscosity, and turbulence kinetic energy and its dissipation rate. The improved agreement of their model with the experimental data was attributed to a more reliable evaluation of coalescence and breakup rates. A drawback of their model related to the source term coefficients for the turbulence equations that vary with the pipe diameter.

Sattar *et al.* (2013) performed 3D numerical simulations based on the two-fluid formulation with bubble coalescence and breakup processes. Simulated results in terms of gas volume fraction, mean bubble diameter, mean phasic velocities were found to be in good agreement with the experimental data. The obtained result shows that the radial distributions of smaller size bubbles are more than larger size bubbles in terms of number. A suggestion to change in the source term coefficient for bubble breakup and coalescence approach was made in order to better predict the number density of bubbles.

A baseline closure model (BSL) with bubble coalescence and breakup was developed and implemented in ANSYS CFX for simulation of adiabatic poly-disperse bubbly flow by Liao *et al.* (2015). The predicted results in terms of bubble size distribution, gas volume fraction, and gas velocity profiles were in good agreement with the experimentally measured data. The mechanisms related to the bubble-bubble collision and bubble breakup events were discussed in their study. Their model represents the current state of the art in terms of modelling bubble coalescence and breakup and the associated redistribution of gas volume fraction among the different bubble groups.

Overall, the two-fluid model needs further development related to the inherent challenges in the prediction of gas-liquid flow. In particular, the numerical simulation of poly-disperse bubbly flow with bubble coalescence and breakup is still relatively new and has not yet been explored in-depth.

1.4 Thesis Organization

This thesis documents a numerical study of turbulent gas-liquid flow within a pipe using the popular two-fluid model. The layout of this dissertation consists of five chapters that include three journal manuscripts. The research motivation and challenges, objectives and a brief summary of the literature are presented in the first chapter. Three original research articles that address the first, second, and third objectives of the thesis are documented in Chapters 2, 3, and 4, respectively. A numerical prediction of the radial gas volume fraction profiles for mono-disperse bubbly flow is presented in Chapter 2. Modeling of the turbulence modulation for gas-liquid bubbly flow is reported in Chapter 3. Numerical simulation of the radial gas volume fraction profiles for poly-disperse bubbly flow with a bubble coalescence and breakup model is described in Chapter 4. Finally, Chapter 5 presents the thesis summary, conclusions and research contributions, and an outline of future work based on the current study.

Chapter 2

Prediction of mono-disperse gas-liquid turbulent flow in a vertical pipe

A similar version of this chapter has been published as:

A. S. M. Atiqul Islam, N. A. Adoo, D. J. Bergstrom. Prediction of mono-disperse gas-liquid turbulent flow in a vertical pipe. International Journal of Multiphase Flow 85 (2016) 236–244.

- The first author conducted the simulations for centre-peak as well as wall-peak case of gas volume fraction, post-processed and analyzed the results, and prepared the first draft of the manuscript. However, the first co-author contributed in conducting the simulations only for the centre-peak case. The first author then worked with the second co-author to discuss the results and finalize the content and form of the manuscript.

Abstract

A two-fluid model in the Eulerian-Eulerian framework has been implemented for the prediction of gas volume fraction, mean phasic velocities, and the liquid phase turbulence properties for gas-liquid upward flow in a vertical pipe. The governing two-fluid transport equations are discretized using the finite volume method and a low Reynolds number $k-\varepsilon$ model is used to predict the turbulence field for the continuous liquid phase. In the present analysis, a fully developed one-dimensional flow is considered where the gas volume fraction profile is predicted using the radial force balance for the bubble phase. The current study investigates: 1) the turbulence modulation terms which represent the effect of bubbles on the liquid phase turbulence in the k-ε transport equations; 2) the role of the bubble induced turbulent viscosity compared to turbulence generated by shear; and 3) the effect of bubble size on the radial forces which results in either a centre-peak or a wall-peak in the gas volume fraction profiles. The results obtained from the current simulation are generally in good agreement with the experimental data, and somewhat improved over the predictions of some previous numerical studies.

2.1 Introduction

Two-phase flow, where one component is distributed as droplets, bubbles or particles throughout a continuous phase, is relevant to many engineering applications. In particular, gas-liquid flow occurs in many industrial applications within the petrochemical, chemical and nuclear industries. For example, bubble columns, where the flow of bubbles is driven by buoyancy, are often used to facilitate reactions in chemical engineering applications. Gas-liquid flow in a pipe is of special interest within the nuclear industry due to the boiling heat transfer which takes place within reactor systems. It encompasses different flow regimes, such as bubbly, slug, churn and annular flow, which depend on the operating and flow conditions. Each of these flow regimes can be characterized by their corresponding gas-phase volume fraction (Shaikh and Al-Dahhan, 2007). Among the different gas-liquid flow regimes, the bubbly flow regime is most widely encountered in industrial applications including the nuclear industry. From a design viewpoint, it would be advantageous for engineers to have access to computational tools capable of predicting the behavior of such flows.

Computational fluid dynamics (CFD) is currently able to provide realistic predictions for many single-phase flows. Recently, it has been applied to multiphase flows by using the volume of fluid or level-set method to track the temporal and spatial development of the gas-liquid interface. However, these techniques require relatively large computational resources and are often impractical for modeling large industrial systems. An alternative approach is provided by the Eulerian-Eulerian two-fluid model, which requires significantly less computational effort than interface-tracking methods, since it represents both phases as inter-penetrating continua with the local composition defined by the volume fraction field. Most importantly, it avoids having to resolve the details of the local interface and its complex evolution in time and space. The two-fluid model has been successfully applied to multiphase flows as a tool for predicting the spatial- and time-average flow properties (Monahan and Fox, 2009). Although it shows significant promise, application of the two-fluid model to gas-liquid flows also includes some on-going challenges, such as modeling the effect of the dispersed gas-phase on the continuous liquid-phase turbulence, the development of appropriate interphase momentum exchange correlations and improved wall treatments for the liquid phase.

Limited experimental data is available for validating computational models of gas-liquid flow in a vertical pipe. Lucas *et al.* (2005) measured the gas volume fraction and bubble size distributions for bubbly flow in a vertical pipe for air-water flow using a high resolution wire-mesh sensor. In addition to studying the transition from the wall-peaking to the centre-peaking case for the bubbly flow regime, they also measured the gas volume fraction profile for the slug flow regime. Their database is useful for the validation of computational models which account for the various forces acting on the bubbles, as well as bubble coalescence and breakup. The evolution of gas-liquid flow structure in a large vertical pipe was investigated by Prasser *et al.* (2007) using a high resolution wire-mesh sensor for the bubbly, slug and churn turbulent flow regimes. They also studied the influence of the physical properties of the fluid by comparing results for experiments of air-water to steam-water mixtures at high pressure. Ohnuki and Akimoto (2000) investigated the transition characteristics of upward air-water flow in a large vertical pipe to examine the dependency on the pipe size. They found the flow conditions at which bubble coalescence begins are almost the same as for small-scale pipes, and that churn flow is dominant in large vertical pipes for the conditions where small-scale pipes exhibit slug flow. Whereas drag forces dominate the momentum exchange in the flow direction, the lift force strongly influences the radial distribution of bubbles and changes

sign depending on the bubble diameter resulting in the radial separation of small and large bubbles (Krepper *et al.*, 2005).

A number of computational studies have also considered the case of gas-liquid flow. Vitankar and Joshi (2002) predicted the gas volume fraction and liquid phase mean velocity profiles for bubble columns with a centre-peak volume fraction profile using an iterative procedure with a low Reynolds number $k-\varepsilon$ model. They prescribed a general form and also used a drift-flux model for prediction of the gas volume fraction profile, also known as the hold-up profile. They extended their one-dimensional (1D) model for the prediction of pressure drop for the case of two-phase gas-liquid flow in bubble columns. One benefit of a 1D analysis is that it readily facilitates an assessment of the effects of individual models, both for the turbulence and multiphase transport, using experimental data compared to a fully three-dimensional flow where the measurements are both more complicated and difficult to obtain. Although a number of 1D models are documented in the literature, some critical modeling issues remain such as: the appropriate closure model for the turbulent and interphase correlation terms, modelling of the radial movement of bubbles, and the overall interphase momentum and energy balances, as noted by Vitankar and Joshi (2002). Ekambara *et al.* (2005) performed simulations to predict the flow pattern in cylindrical bubble column reactors for one-, two- and three-dimensional flows using a *k-ε* model, and observed good agreement with experimental measurements for the axial liquid phase velocity and gas volume fraction profiles, especially for the three-dimensional flow. For the fully developed flow case in a vertical pipe, the non-drag forces, i.e. the lift, wall or lubrication, and turbulent dispersion forces act on the gas bubbles perpendicular to the flow direction and determine the gas volume fraction profile (Lucas *et al.*, 2001). These forces are also responsible for the bubble coalescence or bubble breakup (Lucas *et al.*, 2005). The lift and wall force plays the dominant roles in determining the gas volume fraction profile as noted by Krepper *et al.* (2005).

The present study focuses on modeling mono-disperse gas-liquid turbulent bubbly flow in a vertical pipe using the Eulerian two-fluid model. For this fully developed flow scenario, a 1D computational model is used to predict the volume fraction profiles, mean phasic velocities, and turbulence properties based on a two-equation eddy viscosity model. The analysis implements a bubble induced turbulence model together with a conventional eddy viscosity model. Results are presented for the case of flow patterns characterized by both centre-peak and wall-peak gas volume

fraction profiles. The remainder of the paper documents the computational method, discusses the simulated results and presents some conclusions related to the underlying models which are relevant for future studies.

2.2 Computational Method

2.2.1 Two-fluid model

The governing Reynolds-Averaged Navier–Stokes (RANS) equations for the mean velocity fields are obtained by averaging the conservation of mass and momentum equations for each phase, resulting in a so called Eulerian-Eulerian formulation. The two-fluid model treats both the gas and liquid phases as interpenetrating continua, and uses the local volume fraction of each phase to characterize the spatial distribution of the two phases. Coupling between the two phases is achieved through the pressure and interfacial transfer terms in the momentum equations. The two-fluid model is most appropriate when the dispersed phase is finely distributed in the corresponding continuous phase. For a turbulent gas-liquid flow, the relative motion between the phases is important in terms of interfacial energy and mass transfer, and the turbulence induced in the liquid phase by the dispersed gas bubbles can also be significant.

2.2.2 Mathematical formulation

For steady, fully developed pipe flow, the momentum equations for the mean axial velocity components using cylindrical coordinates are given below for the liquid and gas phase, respectively:

$$0 = -\alpha_l \frac{dP}{dz} + \alpha_l \frac{1}{r}\frac{d}{dr}\left(r\left(\mu_{eff}\frac{du_z}{dr}\right)\right) + \alpha_l \rho_l g - F^D \qquad (2.1a)$$

$$0 = -\alpha_g \frac{dP}{dz} + \alpha_g \frac{1}{r}\frac{d}{dr}\left(r\left(\mu_g \frac{dv_z}{dr}\right)\right) + \alpha_g \rho_g g + F^D \qquad (2.1b)$$

The orientation of the pipe is vertical and the flow is upward. The left hand side of each momentum equation, which represents the acceleration in the axial direction, is zero. The terms on the right hand side of each equation represent the pressure gradient, effective stress model, body force, and

interphase momentum exchange, respectively. Mass transfer due to bubble coalescence and breakup is not considered here. The model parameters used to solve Eqs. (2.1a) and (2.1b) are given in Table 2.1. Note that for the liquid phase, the effective stress term is modelled using an eddy viscosity model, which includes contributions from both the fluid turbulence and the so called bubble induced turbulence based on the model of Sato and Sekoguchi (1975). In this case, the interphase momentum exchange term is modelled solely by the fluid drag term.

Table 2.1 Model relations for the phasic axial momentum equations.

Volume fraction, $\alpha_g + \alpha_l = 1$
Effective viscosity, $\mu_{eff} = \mu_l + \mu_t + \mu_{BIT}$
Bubble induced turbulent viscosity of Sato and Sekoguchi (1975),
$\mu_{BIT} = C_{\mu,BIT}\alpha_g\rho_l d_b\lvert v_z - u_z\rvert$
where $C_{\mu,BIT} = 0.60$
Drag force of Monahan and Fox (2009),
$F^D = \frac{3}{4}\alpha_g\alpha_l\rho_l\frac{C_D}{d_b}\lvert v_z - u_z\rvert(v_z - u_z)$, $Re_b = \frac{\rho_l\lvert v_z - u_z\rvert d_b}{\mu_l}$
where $C_D = \frac{24}{Re_b} + \frac{6}{1+\sqrt{Re_b}}$

A variety of different turbulence model closures are available in the literature (Masood and Delgado, 2014) for modelling gas-liquid duct flows. In this case, the eddy viscosity of the liquid phase turbulence was modelled using a two-equation turbulence model closure. The low Reynolds number $k-\varepsilon$ model of Myong and Kasagi (1990) was implemented to include the damping of turbulence near the wall. The effect of the bubbles on the liquid phase turbulence was modeled by additional source terms, i.e. the turbulence modulation terms developed by Dhotre *et al.* (2007). The form of the transport equations for k and ε for steady, fully developed pipe flow are given as follows:

$$0 = \frac{1}{r}\frac{d}{dr}\left(r\alpha_l\left(\left(\mu_l + \frac{\mu_t}{\sigma_k}\right)\frac{dk}{dr}\right)\right) + \alpha_l\mu_t\left(\frac{du_z}{dr}\right)^2 - \alpha_l\rho_l\varepsilon + C_{k1}C_f\alpha_g\alpha_l\rho_l k \qquad (2.2a)$$

$$0 = \frac{1}{r}\frac{d}{dr}\left(r\alpha_l\left(\left(\mu_l + \frac{\mu_t}{\sigma_\varepsilon}\right)\frac{d\varepsilon}{dr}\right)\right) + C_1 f_1\alpha_l\frac{\varepsilon}{k}\mu_t\left(\frac{du_z}{dr}\right)^2 - C_2 f_2\alpha_l\rho_l\frac{\varepsilon^2}{k} + C_{k2}C_f\alpha_g\alpha_l\rho_l\varepsilon \qquad (2.2b)$$

The turbulence model expressions used in these equations are given in Table 2.2. The values of the model coefficients are the same as specified by Myong and Kasagi (1990) for the case of single-phase flow, except for C_{k1} and C_{k2}, which are discussed later in the paper.

Table 2.2 Model relations for the low Reynolds number *k*-ε turbulence closure.

Turbulent viscosity, $\mu_t = \frac{C_\mu f_\mu \rho_l k^2}{\varepsilon}$,	$f_1 = 1$
$f_2 = \left(1 - \frac{2}{9}\exp\left(-\frac{R_T}{6}\right)^2\right)\left(1 - \exp(-\frac{y^+}{5})\right)^2$,	$f_\mu = \left(1 - \exp(-\frac{y^+}{70})\right)\left(1 + \frac{3.45}{\sqrt{R_T}}\right)$
$y^+ = \frac{\rho_l u_\tau (R-r)}{\mu_l}$,	$R_T = \frac{\rho_l k^2}{\mu_l \varepsilon}$
$u_\tau = \sqrt{\frac{\tau_w}{\rho}}$,	$C_f = \frac{3}{4}\left(\frac{C_D}{d_b}\right)(\lvert v_z - u_z \rvert)$

Model constants:

$C_1 = 1.40 \quad C_2 = 1.80 \quad C_\mu = 0.09 \quad C_{k1} = 0.15 \quad C_{k2} = 0.20 \quad \sigma_k = 1.40 \quad \sigma_\varepsilon = 1.30$

2.2.3 Volume fraction prediction

For the case of 1D flow, the most challenging task in a gas-liquid flow analysis is the prediction of the gas volume fraction profile in the radial direction, since the continuity equation is eliminated by the fully-developed flow assumption. In this case, Lucas *et al.* (2001) have shown that the volume fraction distribution is governed by the balance of the non-drag forces acting on the bubbles in the radial direction. The non-drag forces include the lift, wall, and turbulent dispersion force (including a term based on the Eötvös number) following Lucas *et al.* (2001). The lift force acting on the bubbles causes coalescence of the smaller bubbles near the wall of the pipe, and these in turn drift towards the centre of the pipe due to the wall force (Tomiyama, 1998). The turbulent dispersion force represents the smoothing of the gas volume fraction profile due to the turbulence in the liquid phase. For vertical upward pipe flow, smaller bubbles tend to move towards the wall, while larger bubbles accumulate at the centre of the pipe (Lucas *et al.*, 2005). These two cases are characterized by wall-peak and centre-peak gas volume fraction profiles, respectively.

Lucas *et al.* (2001) used the following radial force balance to predict the local gas volume fraction α_g for both centre- and wall-peak cases:

$$F^{\mathrm{L}} + F^{\mathrm{W}} + F^{\mathrm{TD}} + F^{\mathrm{TD,Eo}} = 0 \tag{2.3}$$

where the correlations for the lift and wall force are adopted from Tomiyama (1998) and documented together with the correlations for the turbulent dispersion force in Table 2.3. Alternative approaches for the turbulent dispersion force are also available in the literature, e.g. (Burns *et al.* 2004), however the model formulation of Lahey *et al.* (1993) was used in the present study. Substituting the various model relations from Table 2.3 into Eq. (2.3) and rearranging gives the following first-order differential relation for the gas volume fraction:

$$\left(0.1k + C_{D,Eo}(Eo - 1)\right)\frac{d\alpha_g}{dr} + \left(C_L(v_z - u_z)\frac{du_z}{dr} + C_W\left(\frac{d_b}{2}\right)(v_z - u_z)^2\left(\frac{1}{(R-r)^2} - \frac{1}{(R+r)^2}\right)\right)\alpha_g = 0 \tag{2.4}$$

The values of select model coefficients given in Table 2.3 were slightly modified in the present study to obtain improved agreement with the experimental results. The modified values are documented in the discussion of the results given below.

Table 2.3 Model relations for the radial force components acting on the gas phase.

Lift force of Zun (1980) reported by Lucas *et al.* (2001), $F^L = -C_L \alpha_g \rho_l (v_z - u_z) \frac{du_z}{dr}$
Wall force of Tomiyama *et al.* (1995) reported by Lucas *et al.* (2001), $F^W = -C_W \alpha_g \rho_l \left(\frac{d_b}{2}\right) (v_z - u_z)^2 \left(\frac{1}{(R-r)^2} - \frac{1}{(R+r)^2}\right)$
Turbulent dispersion force of Lahey *et al.* (1993) reported by Lucas *et al.* (2001), $F^{TD} = -C_{TD} \rho_l k \frac{d\alpha_g}{dr}$, where $C_{TD} = 0.10$
Turbulent dispersion force based on Eötvös number (Lucas *et al.*, 2001), $F^{TD,Eo} = -C_{D,Eo} \rho_l (Eo - 1) \frac{d\alpha_g}{dr}$, where $C_{D,Eo} = 0.0015\ \mathrm{m^2 \cdot s^{-2}}$
The Tomiyama (1998) lift force coefficient reported by Shi *et al.* (2004) $C_L = \begin{cases} \min[0.288 \tanh(0.121 Re_b), f(Eo_d)] & Eo_d < 4 \\ f(Eo_d) = 0.00105 Eo_d^3 - 0.0159 Eo_d^2 - 0.0204 Eo_d + 0.474 & 4 \le Eo_d \le 10 \\ -0.29 & Eo_d > 10 \end{cases}$
where Eo_d is the Eötvös number based on the long axis d_H of a deformable bubble, and $Eo_d = \frac{(\rho_l - \rho_g) g d_H^2}{\sigma}, \quad d_H = d_b (1 + 0.163 Eo^{0.757})^{1/3}, \quad Eo = \frac{(\rho_l - \rho_g) g d_b^2}{\sigma}$
The Tomiyama (1998) wall force coefficient reported by Shi *et al.* (2004) $C_W = \begin{cases} \exp(-0.933 Eo + 0.179) & 1 \le Eo \le 5 \\ 0.007 Eo + 0.04 & 5 < Eo \le 33 \end{cases}$

2.2.4 Boundary conditions

As noted above, the geometry corresponds to a circular pipe oriented in the vertical direction. For the 1D symmetric flow considered, the computational domain consisted of a thin wedge of arbitrary azimuthal angle bounded by the pipe centreline and the wall. The boundary conditions for the phasic mean axial velocities and turbulence quantities are given in Table 2.4. No-slip boundary conditions were used at the wall and symmetry boundary conditions were applied at the centreline of the pipe. For the low Reynolds number model adopted, the dissipation rate at the

wall was balanced by the diffusion of turbulence kinetic energy to the wall. Finally, the value of the gas volume fraction was set to zero at the wall.

Table 2.4 Numerical boundary conditions.

At the centre:	$\frac{du_z}{dr} = 0,$	$\frac{dv_z}{dr} = 0,$	$\frac{dk}{dr} = 0,$	$\frac{d\varepsilon}{dr} = 0,$	$\frac{d\alpha_g}{dr} = 0$
At the wall:	$u_z = 0,$	$v_z = 0,$	$k = 0,$	$\varepsilon = \nu\left(\frac{d^2k}{dr^2}\right),$	$\alpha_g = 0$

2.2.5 Numerical method

The governing equations for the gas-liquid flow were discretized using the cell-centered implicit finite volume method developed by Patankar (1980), and the set of coupled discrete equations (including boundary conditions) was solved using a tri-diagonal matrix algorithm. The iterative solution was judged to be converged when the normalized difference in the field variables for two consecutive iterations was less than 0.0001. As an example, the normalized convergence criterion for the prediction of gas volume fraction is given by $\left|\frac{\alpha_{i+1}-\alpha_i}{\alpha_{i+1}}\right| < 0.0001$, where, α_i is the gas volume fraction at iteration i and α_{i+1} is the gas volume fraction at iteration $i+1$. Each flow used a non-uniform grid, which was refined in the near-wall region to accommodate the low Reynolds number $k-\varepsilon$ model. The centre-peak case used a grid consisting of 80 control volumes with the first computational node at the wall located at $y^+ = 0.80$. The wall-peak case used a grid of 100 control volumes with the first computational node at the wall located at $y^+ = 0.40$. The difference in grid size was due to the higher Reynolds number used for the wall-peak case. The grid size was justified based on a grid independence study, e.g. for the wall-peak case, increasing the number of control volumes from 100 to 120 only changed the value of the gas volume fraction by 0.20 %.

Table 2.5 Experimental flow conditions (centre-peak case).

Parameters	**Experimental (Lucas *et al.*, 2005)**
Superficial liquid velocity, [m/s]	1.0170
Superficial gas velocity, [m/s]	0.2190
Pipe diameter (D), [m]	0.0512
Bubble (mean) diameter (d_b), [m]	0.0060

Table 2.6 Experimental flow conditions (wall-peak case).

Parameters	Experimental (Lucas *et al.*, 2005)
Superficial liquid velocity, [m/s]	1.6110
Superficial gas velocity, [m/s]	0.0574
Pipe diameter (D), [m]	0.0512
Bubble (mean) diameter (d_b), [m]	0.0040

2.3 Results and discussion

Initially, two test cases from the MTLoop experiment (Lucas *et al.*, 2005) database were selected for the present study, test case 118 and 086 representing two-phase air-water flow in the bubbly flow regime with centre-peak and wall-peak gas volume fraction profiles, respectively. The simulations were performed for the experimental flow conditions given in Tables 2.5 (for test case 118) and 2.6 (for test case 086). From the experimental data for the centre-peak case, the average gas volume fraction was estimated to be $\bar{\alpha}_g = 0.20$, and the average liquid velocity estimated to be $\bar{u}_z = 1.27$ m/s, giving a bulk Reynolds number of $Re = 65{,}000$ for the liquid phase. For the wall peak case, the estimated average gas volume fraction was $\bar{\alpha}_g = 0.045$, while the corresponding bulk liquid velocity and bulk Reynolds number for the liquid phase were $\bar{u}_z = 1.687$ m/s and $Re = 86{,}200$, respectively. In the present simulations, the axial pressure gradient was adjusted to obtain the same value for the bulk Reynolds number for the liquid phase as in the experiment. An axial pressure gradient of $\frac{\mathrm{dP}}{\mathrm{dZ}} = 10450$ (N/m^3) and $\frac{\mathrm{dP}}{\mathrm{dZ}} = 10510$ (N/m^3) was used for simulation of experimental flow conditions documented in Table 2.5 and Table 2.6, respectively. The numerical model was used to predict the gas volume fraction and mean phasic velocity profiles, as well as the turbulence properties. The simulation results were compared to both the experimental measurements of Lucas *et al.* (2005) and the numerical prediction of Lucas *et al.* (2001). Finally, two additional test cases for each category i.e. centre-peak and wall peak, from the MTLoop experiment were also simulated and documented in terms of the volume fraction prediction in order to demonstrate the versatility of the current model.

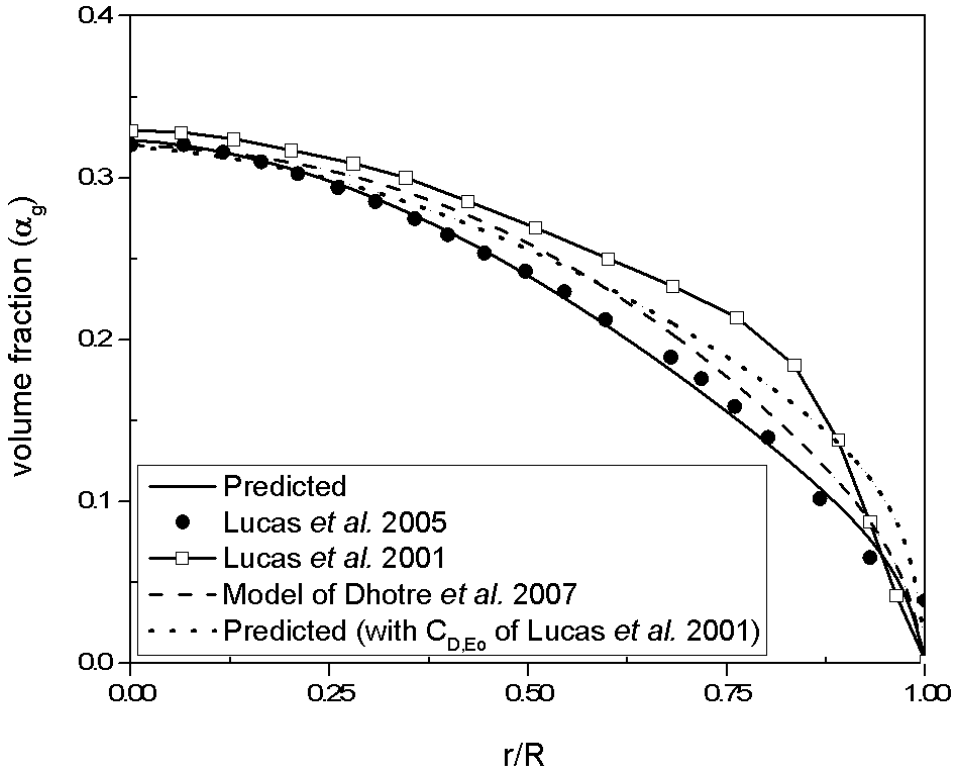

Fig. 2.1 Comparison of predicted gas volume fraction profiles (centre-peak case) to other experimental and numerical data.

From Fig. 2.1, the predicted gas volume fraction is observed to be in good agreement with the experimental measurements of Lucas *et al.* (2005) and performs somewhat better than the numerical model of Lucas *et al.* (2001). Note that for this bubble size ($d_b = 0.006$ m), the gas volume fraction peaks at the centre of the pipe, which can be attributed to the process whereby smaller bubbles detach from the wall, coalesce into larger bubbles and drift towards the centre of the pipe due to the interaction between the lift, wall and turbulent dispersion forces. As shown in the figure, the improved prediction is partly due to the modified values of the source term coefficients used in the k and ε equations compared to the values recommended by Dhotre *et al.* (2007). The other reason for the improvement was the modified value of the coefficient for the dispersion force: the present simulation used $C_{D,Eo} = 0.001$ compared to the original value of $C_{D,Eo} = 0.0015$ used by Lucas *et al.* (2001). Simulations for flow conditions corresponding to other values of the average gas volume fraction and the same bubble diameter (not shown) also predicted centre-peak profiles with a similar characteristic shape.

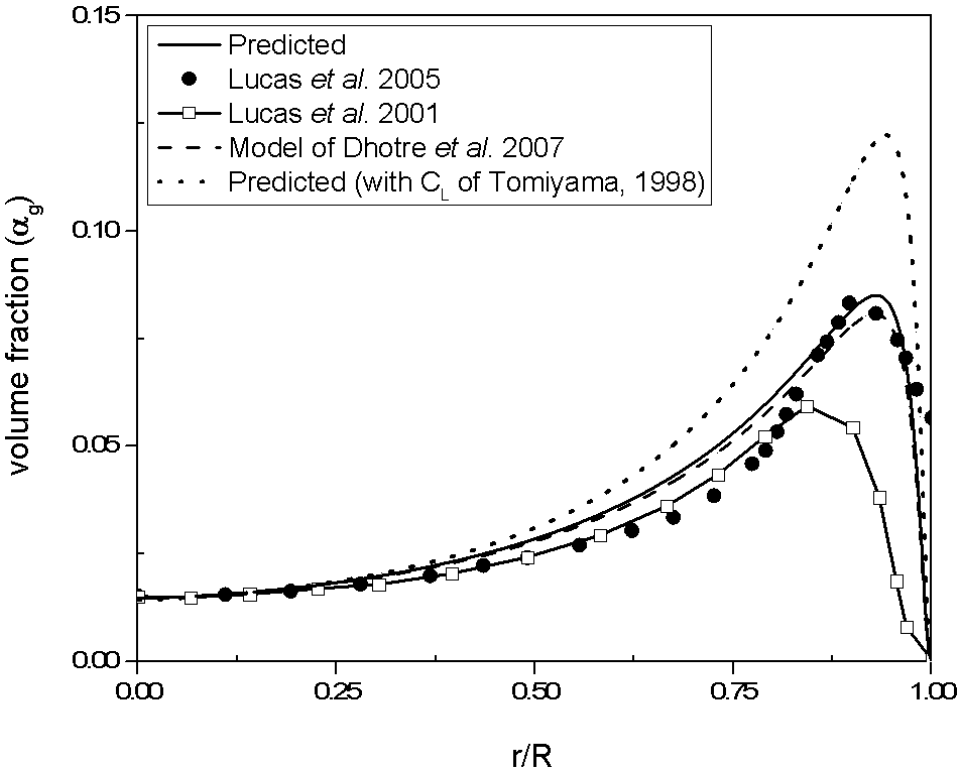

Fig. 2.2 Comparison of predicted gas volume fraction profiles (wall-peak case) to other experimental and numerical studies.

Fig. 2.2 considers the case of a smaller bubble size of $d_b = 0.004$ m. For this bubble size, the gas volume fraction peaks near the wall of the pipe, which can be attributed to the process whereby smaller bubbles move towards the wall from the centre-line due to the transverse lift force (Lucas *et al.*, 2005). The predicted profile for the gas volume fraction is in good agreement with the experimental measurements of Lucas *et al.* (2005), and the current model better resolves the peak than the model of Lucas *et al.* (2001). In this case, the same modified values of the source term coefficients were used in the k and ε equations to improve the agreement between the predicted and experimental data, compared to the coefficient values used by Dhotre *et al* (2007). In addition, the value of the Tomiyama lift force coefficient was modified to be $C_L = \min[\,0.250\tanh(0.121Re_b), f(Eo_d)]$ for the range $Eo_d < 4$, and the value of the turbulent dispersion coefficient was modified to be $C_{D,Eo} = 0.015$ compared to the value of $C_{D,Eo} = 0.0015$ used by Lucas *et al.* (2001). The model formulation of Rzehak and Krepper (2013) for the source terms was also assessed in terms of its prediction for the volume fraction profile: the results (not

shown) were in good agreement with the experimental data for the centre-peak case, but less so for the wall-peak case.

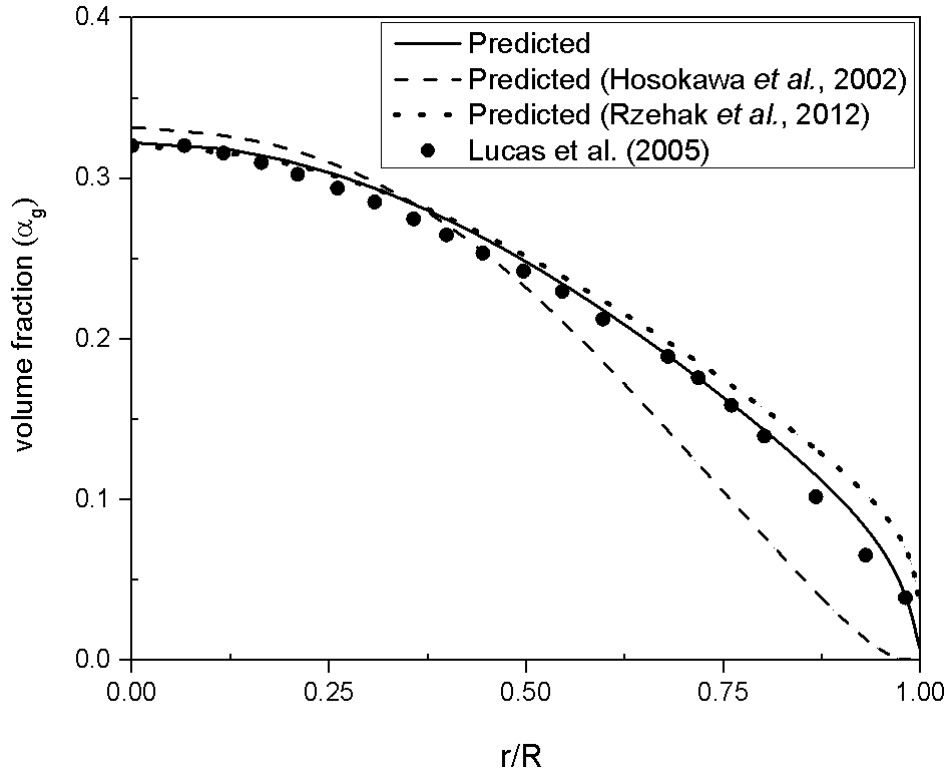

Fig. 2.3 Comparison of volume fraction profiles for centre-peak case using different wall force models.

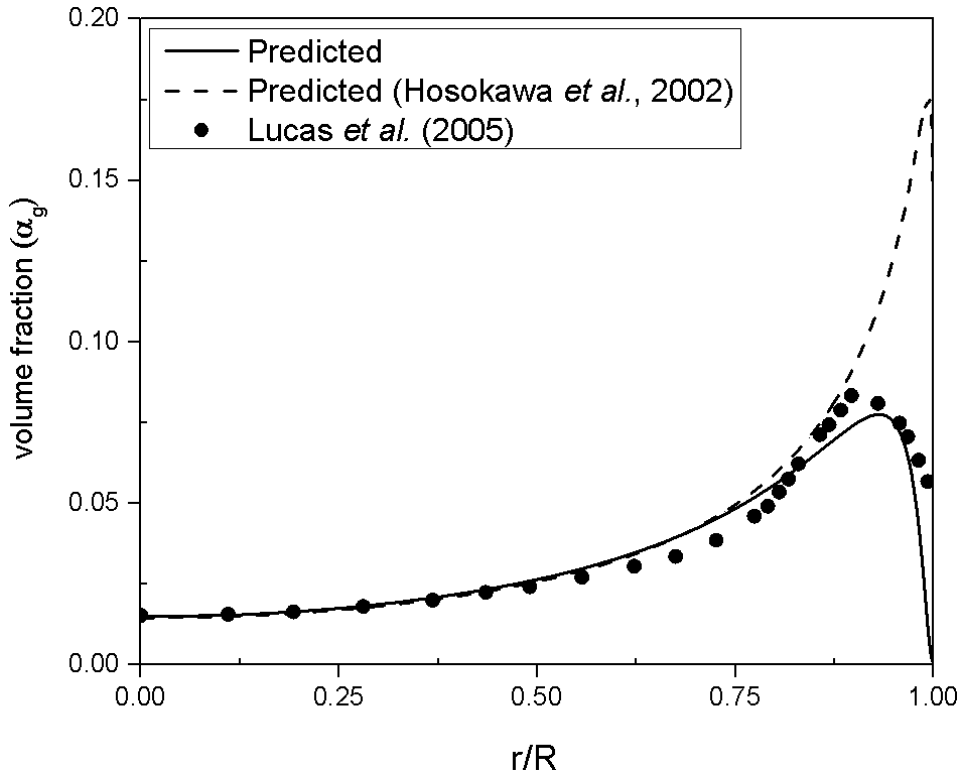

Fig. 2.4 Comparison of volume fraction profiles for wall-peak case using different wall force models.

Apart from the Tomiyama (1998) wall force correlation used for the results presented above, different wall models are also available in the literature. The wall force model formulations of Hosokawa *et al.* (2002) and Rzehak *et al.* (2012) were also evaluated in the present study. It can be seen from Fig. 2.3 that the predicted gas volume fraction profile using the wall force correlation of Tomiyama *et al.* (1998) matches the experimental result for the centre-peak case. On the other hand, the gas volume fraction is poorly predicted using the wall force correlation developed by Hosokawa *et al.* (2002), especially in the near wall region. A small over prediction is observed for the volume fraction profile in the wall region using the correlation reported by Rzehak *et al.* (2012). Fig. 2.4 shows that the predicted volume fraction profile using the wall force correlation of Tomiyama *et al.* (1998) closely matches the experimental data for the wall-peak case. In contrast, the gas volume fraction is over predicted using the wall force correlation of Hosokawa *et al.* (2002) in the near wall region. The model of Rzehak *et al.* (2012) did not yield a converged solution for the wall-peak case. Based on the predicted results In Fig. 2.3 and 2.4, it can be concluded that the Tomiyama (1998) wall force correlation performs better than the other models.

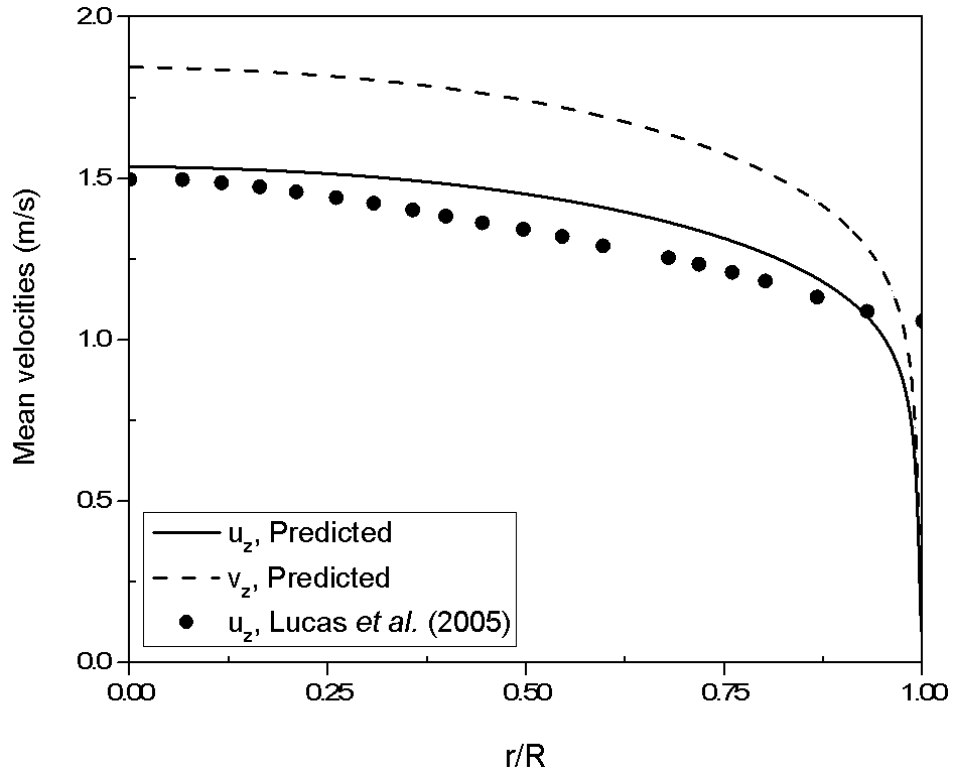

Fig. 2.5 Comparison of liquid (u_Z) and gas (v_Z) mean velocity profiles for centre-peak case.

Fig. 2.5 presents the predictions for the phasic velocity profiles for a centre-peak case for which experimental data is available for comparison. It is evident from the Fig. 2.5 that the mean velocity predicted for the liquid phase is in good agreement with the experimental data of Lucas *et al.* (2005), although the model slightly over-predicts the experimental values away from the wall. For this upward flow, the gas velocity is greater than the liquid velocity, as would be expected. The two-fluid model predicted a superficial gas velocity of 0.254 m/s, whereas the experimental measurement was 0.219 m/s. As such, the model over-predicted the value of the superficial gas velocity by approximately 16%. The slip velocity was predicted to be a maximum at the centre-line and decreased towards the wall for both the centre-peak and wall-peak case (results not shown).

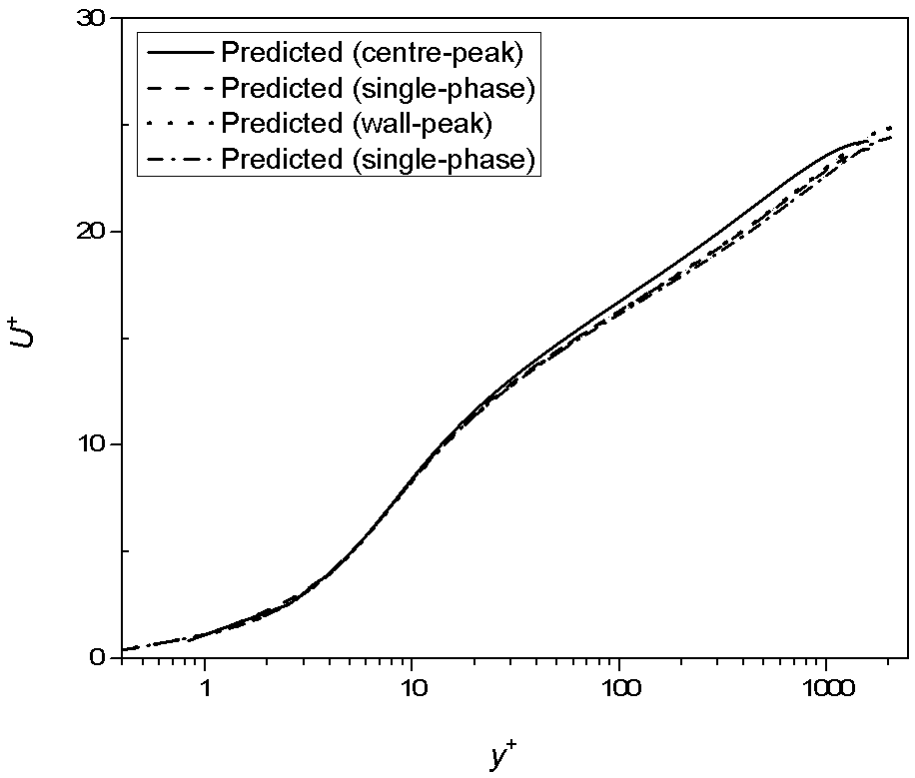

Fig. 2.6 Comparison of mean liquid velocity profiles for gas-liquid and single phase flows.

Fig. 2.6 compares the dimensionless mean liquid velocity ($u^+ = \frac{u_z}{u_\tau}$) profile for each gas-liquid flow case to a single-phase flow profile at the same bulk Reynolds number. The figure uses a semi-log plot for which the over-lap region, characterized by a logarithmic profile, is represented by a straight line. All velocity profiles are very close to each other, indicating that the effect of the gas phase on the liquid velocity profile is minimal, even for the case of a bulk gas volume fraction as high as 20 percent (the centre-peak case). Notwithstanding this observation, a detailed analysis of the turbulence field given below shows significant differences between the gas-liquid and single phase flow.

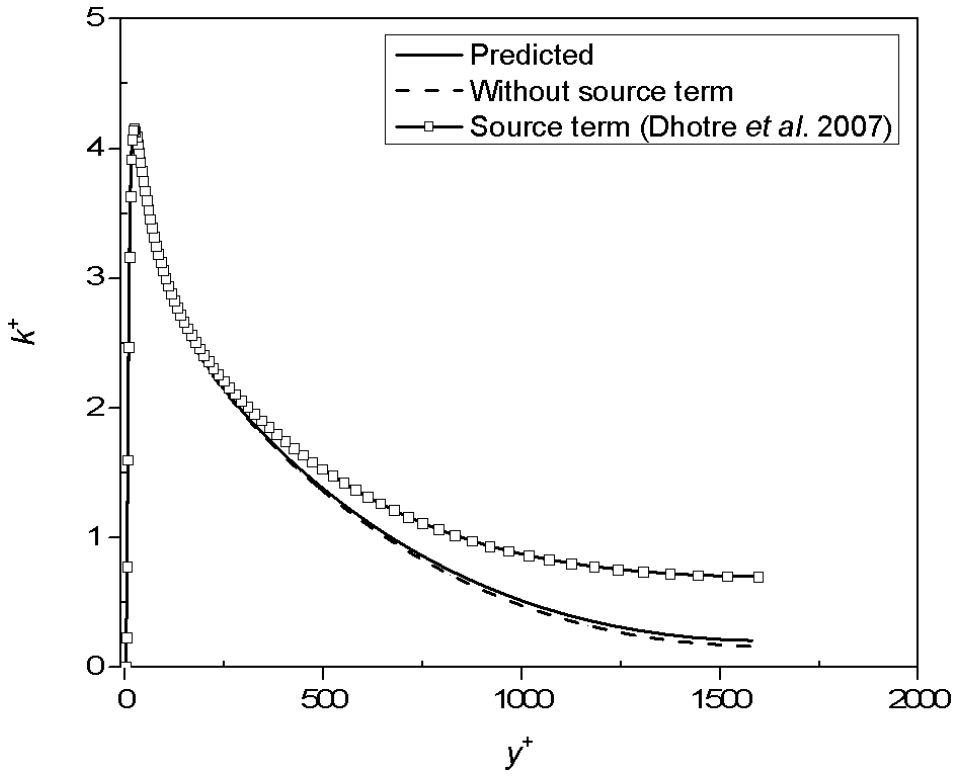

Fig. 2.7 Comparison of dimensionless turbulence kinetic energy profiles for centre-peak case.

Fig. 2.7 considers the case of the centre-peak volume fraction profile and shows the profile for the dimensionless turbulence kinetic energy ($k^+ = \frac{k}{u_\tau{}^2}$) of the liquid phase as a function of dimensionless wall normal distance $y^+ = \frac{yu_\tau}{\nu}$ for different values of the turbulence modulation terms in the k and ε equations, as well as the case of no turbulence modulation term. All the predicted profiles include a sharp near-wall peak, which is characteristic of wall bounded turbulent flow. It can be seen from the predicted profiles that the source term has negligible effect in the near-wall region where the shear production is dominant. Generally, the effect of the gas phase is to enhance the level of the turbulence kinetic energy near the centre of the pipe where the gas volume fraction is highest. The predicted results using the modified values for the source term coefficients, i.e., $C_{k1} = 0.15$ and $C_{k2} = 0.20$, in the k and ε equations, respectively, resulted in a relatively small increase in the level of the turbulence kinetic energy compared to the case with no source term modulation. In contrast, the prediction using the values for the model coefficients ($C_{k1} = 0.75$ and $C_{k2} = 0.60$) recommended by Dhotre *et al.* (2007) results in a significant change in the turbulence kinetic energy, with an enhanced value at the centreline. It appears that the source term coefficients used by Dhotre *et al.* (2007) are not universal and may depend on the

bubble diameter; this issue warrants further investigation as indicated by Sheng and Irons (1993). Note that in the present two-fluid model formulation, the turbulence kinetic energy was also used to determine the turbulent dispersion force in the force balance profiles, so that an incorrect prediction for the turbulence field would also affect the radial force balance on the bubbles.

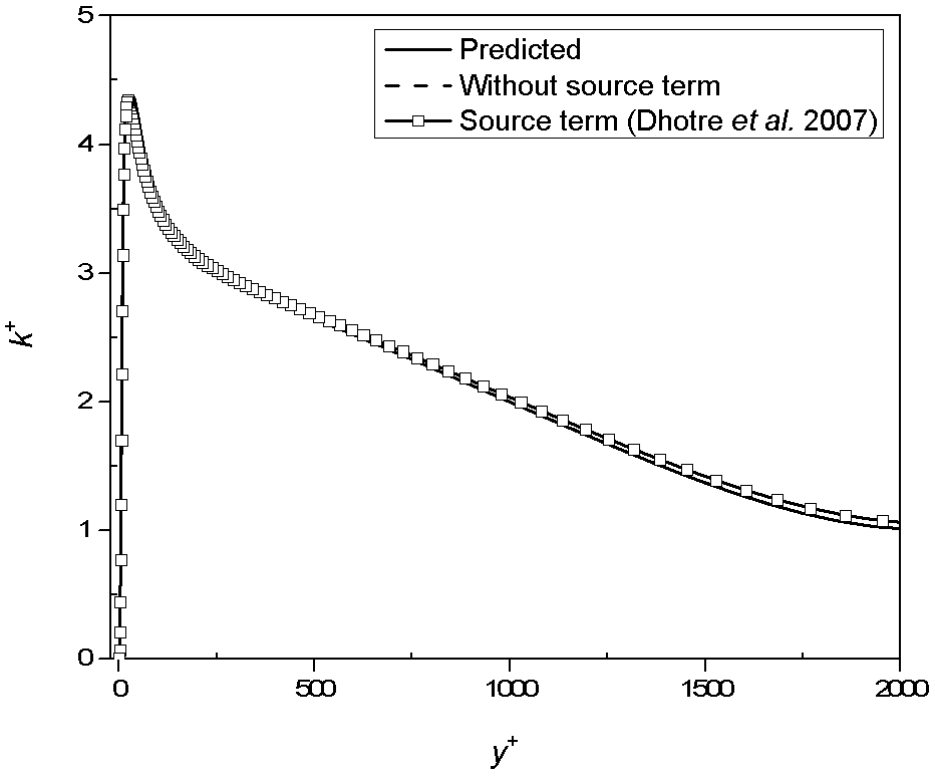

Fig. 2.8 Comparison of dimensionless turbulence kinetic energy profiles for wall-peak case.

Fig. 2.8 presents the corresponding predictions for the turbulence kinetic energy for the wall-peak case based on a smaller bubble diameter. All of the profiles for the turbulence kinetic energy are very similar, with a strong near-wall peak and a slightly enhanced level in the centre of the pipe due to the gas phase. In this case, the values of the modulation coefficients recommended by Dhotre *et al.* (2007) only result in a modest increase in the level of the turbulence kinetic energy, which is very different from the centre-peak case. This can be explained by the fact that the source term is proportional to the gas volume fraction, which is relatively small except near the wall for this bubble size. For the modified values of the source term coefficients used in the present study, the overall effect of the modulation terms on the value of the turbulence kinetic energy is almost negligible.

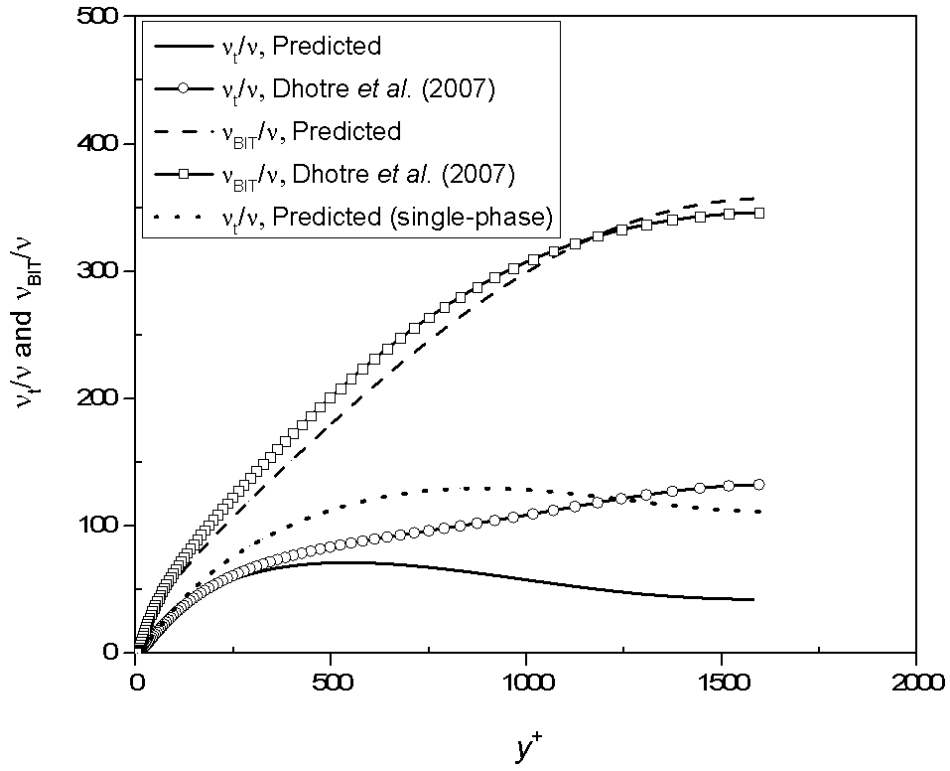

Fig. 2.9 Comparison of eddy and bubble-induced turbulent viscosity profiles for centre-peak case.

Fig. 2.9 examines the contribution of the liquid shear and bubble induced turbulence to the overall turbulent transport for the centre-peak case. The profiles for the shear and bubble induced turbulence components of the effective viscosity indicate that both are approximately the same order of magnitude; however, the bubble induced turbulence is the dominant contribution for the present flow conditions. Although some studies have neglected including a separate turbulence model for the liquid phase in specific applications, e.g. Monahan and Fox (2009), in this case the shear-driven turbulence in the liquid phase is not negligible. Note that the prediction for the shear-driven turbulence based on the model of Dhotre *et al.* (2007) is quite different. The relatively high value of the turbulence kinetic energy (refer to the Fig. 2.7) predicted by the model of Dhotre *et al.* (2007) results in high value for the shear-driven turbulent viscosity. For the model used in the present study, the viscosity due to the bubble induced turbulence was largest near the centre of the pipe where the gas volume fraction is a maximum. It is generally recognised that for a turbulent gas-liquid flow, the presence of dispersed gas bubbles with diameter greater than a critical value

will enhance the turbulence due to the wake effects in the carrier liquid phase (Sato and Sekoguchi, 1975).

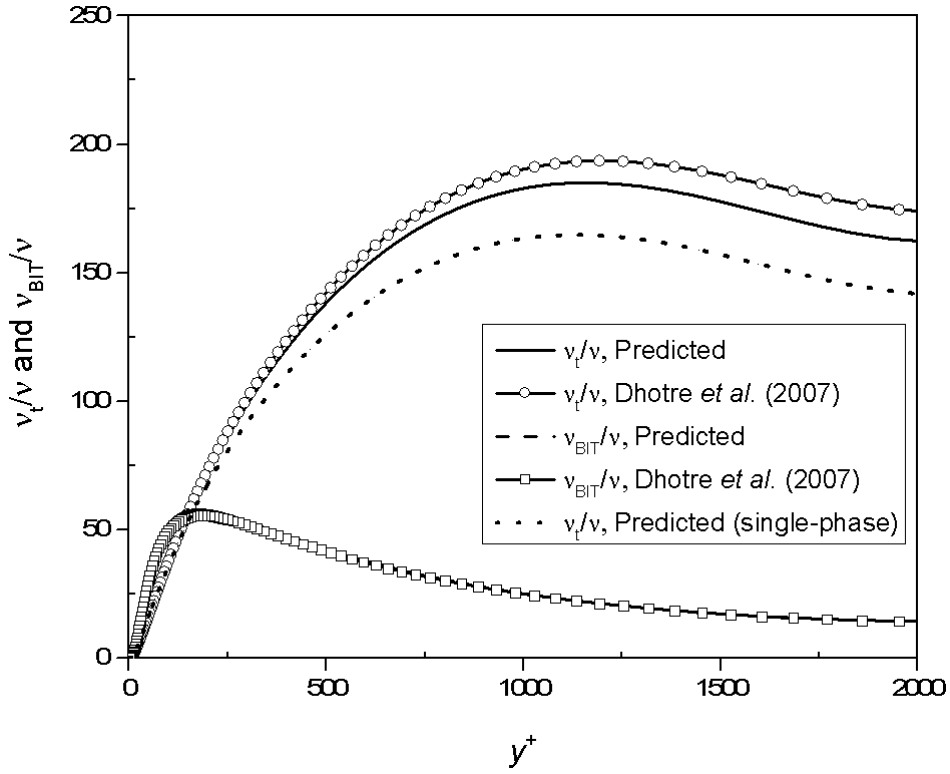

Fig. 2.10 Comparison of eddy and bubble-induced turbulent viscosity profiles for wall-peak case.

Fig. 2.10 presents the corresponding results for the wall-peak case. For this flow, the bubble induced turbulence is smaller than the shear induced turbulence, mostly due to the fact that the volume fraction of the gas phase was much lower throughout most of the pipe than for the centre-peak case. This behaviour is also consistent with the observation that for bubbles with a diameter smaller than a critical value, the turbulence is attenuated in the corresponding liquid phase. Note that the model for the bubble induced turbulent viscosity is directly proportional to the bubble diameter. For the wall-peak case, the viscosity due to the bubble induced turbulence peaks near the wall of the pipe where the gas volume fraction is a maximum. Finally, the model used by Dhotre *et al.* (2007) results in similar profiles for the two turbulent viscosity components for the

wall-peak case, since the predictions for the turbulence kinetic energy and gas volume fraction are much closer to those of the present model.

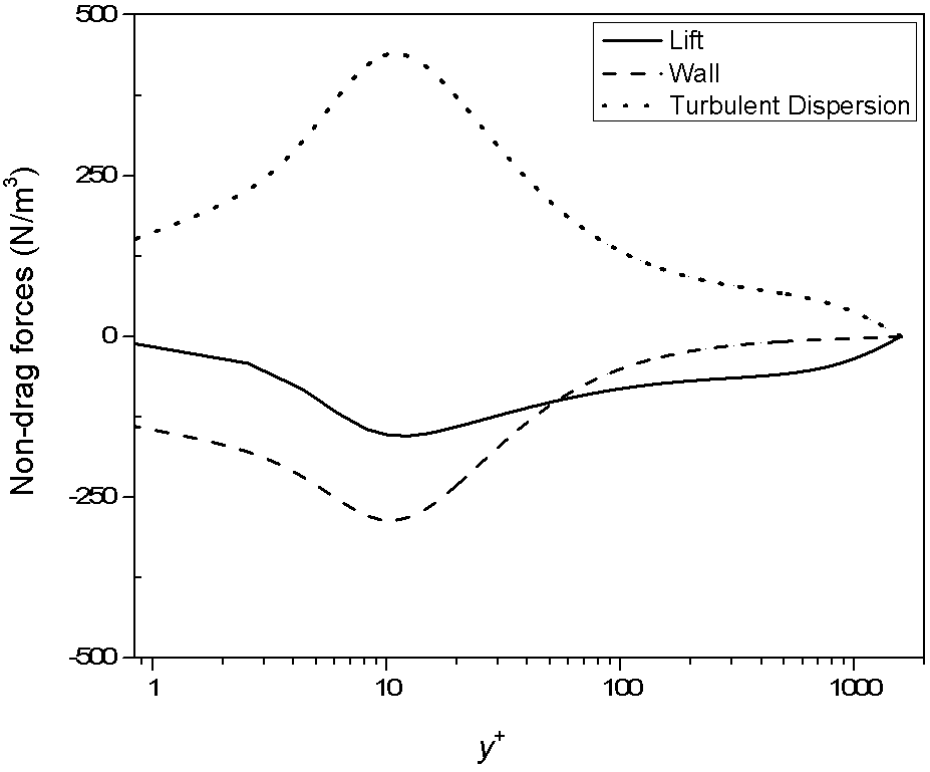

Fig. 2.11 Radial force balance for gas-phase (centre-peak case).

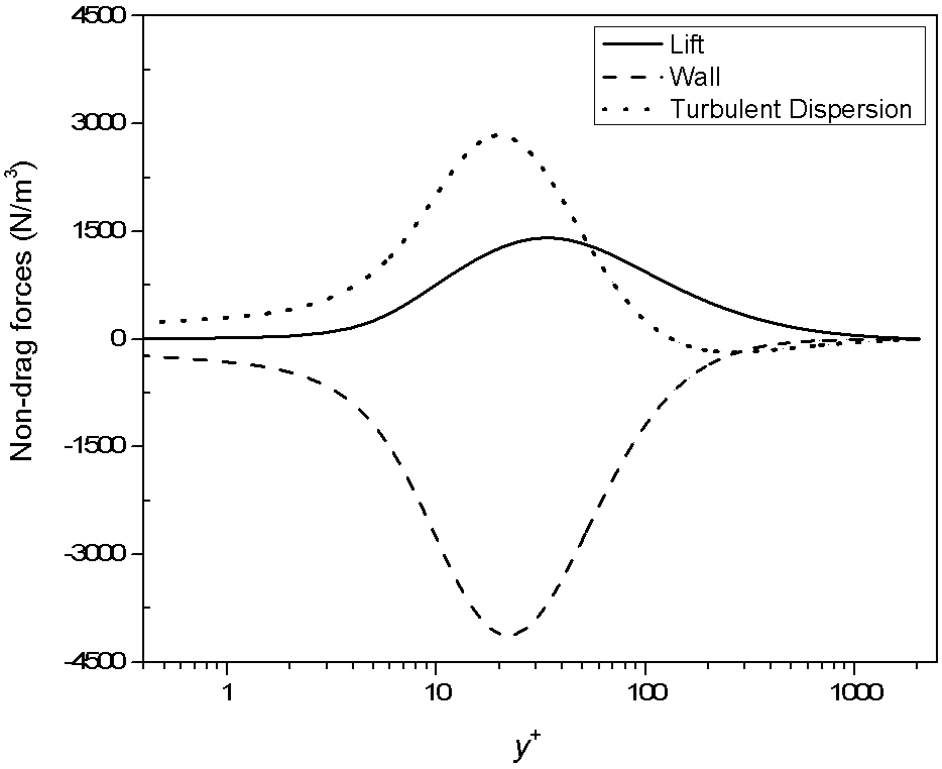

Fig. 2.12 Radial force balance for gas-phase (wall-peak case).

Figs. 2.11 and 2.12 present the radial force balance across the pipe in terms of the lift, wall and total dispersion force components acting on the gas phase for the centre-peak and wall-peak cases, respectively. Note that although the forces are plotted in terms of the dimensionless wall normal distance y^+, the forces are defined in terms of the radial direction, so that a positive radial force is directed away from the centre of the pipe and towards the wall. Also, a logarithmic scale is used in these figures on the horizontal axis to highlight the peak values which occur very close to the wall. For both cases, the dispersion force tends to oppose the wall force, which directs bubbles toward the centre of the pipe. The effect of the lift force is opposite for the two flows considered, based on the critical bubble diameter of 5.80 mm given by Tomiyama (1998). For the centre-peak case which considers a bubble larger than the critical diameter, the lift force has a negative value and directs bubbles towards the centre of the pipe, while for the wall-peak case which considers a bubble smaller than the critical diameter, the lift force has a positive value and directs bubbles towards the pipe wall. Note that the peak values of the forces are typically one order of magnitude greater for the wall-peak case shown in Fig. 2.12 compared to the centre-peak case given in Fig.

2.11. This can be attributed to the dependence of the model forces on the Eötvös number, which in term depends on the square of the bubble diameter.

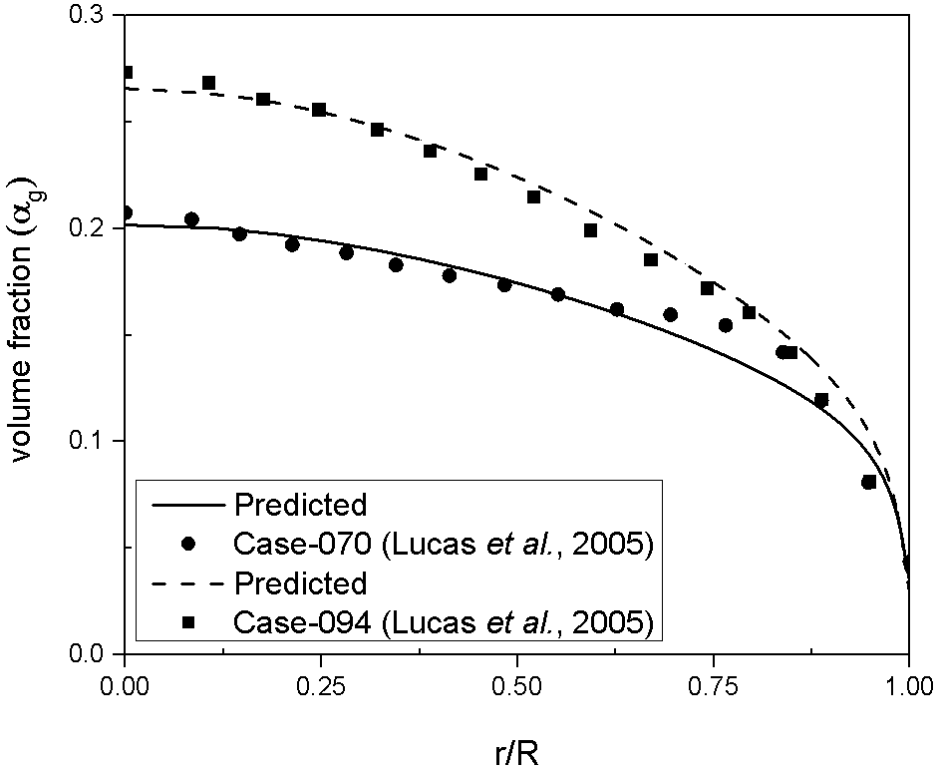

Fig. 2.13 Comparison of volume fraction profiles (centre-peak case) for different test condition.

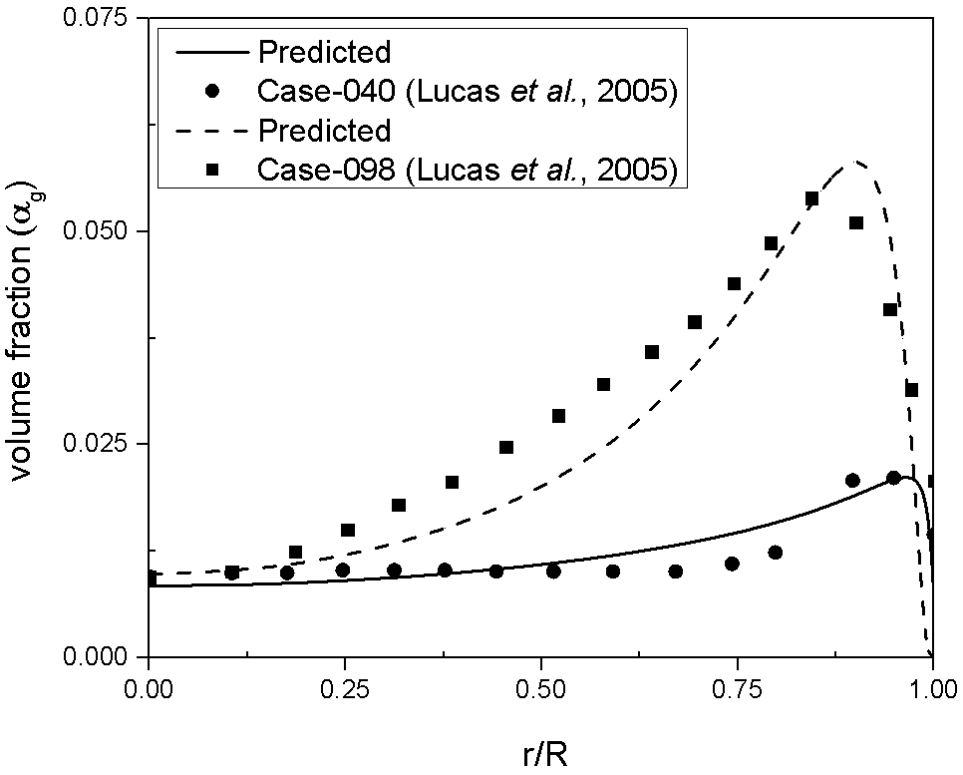

Fig. 2.14 Comparison of volume fraction profiles (wall-peak case) for different test condition.

Finally, two additional test cases for each type of flow, i.e. centre-peak (test case 070 and 094) and wall-peak (test case 040 and 098), taken from the MTLoop experiment (Lucas *et al.*, 2005) were selected for predicting the volume fraction profiles using the present model. Average volume fraction values (approximately) of $\bar{\alpha}_g = 0.16$ and $\bar{\alpha}_g = 0.18$ were used for test case 070 and 094, respectively, and the mean bubble diameter was $d_b = 0.006$ m for both cases. Average volume fraction values (approximately) of $\bar{\alpha}_g = 0.0120$ and $\bar{\alpha}_g = 0.03$, and mean bubble diameters of $d_b = 0.005$ m and $d_b = 0.0035$ m were used for test cases 040 and 098, respectively. For all four test cases, the predicted profiles given in Figs. 2.13 and 2.14 generally show good agreement with the experimental data. For the wall-peak case 098, the value of the volume fraction is somewhat under-predicted the region away from the wall compared to the experimental data.

2.4 Conclusions

A one-dimensional two-fluid model has been successfully implemented for the prediction of fully developed upward gas-liquid flow in a vertical pipe. The study considers turbulent, bubbly flow characterized by a single bubble diameter. The computational model includes contributions from both the shear-driven and bubble induced turbulence. The gas volume fraction profile was predicted using the radial momentum balance for the bubble phase and the present model was able to successfully predict both the centre-peak and wall-peak gas volume fraction profiles. For the computational model adopted, the change in the location of the peak value of the gas volume fraction was determined by the change in sign- and hence direction- of the lift force, following the model proposed by Tomiyama (1998). Modifying the source term coefficients in the k and ε equations resulted in an improved prediction for the gas volume fraction profile and a more realistic profile for the turbulence kinetic energy compared to predictions based on the source term coefficients recommended by Dhotre *et al.* (2007). For the centre-peak case, the bubble induced turbulence was greater than the shear driven turbulence, whereas for the wall-peak case the bubble induced turbulence was smaller than the shear driven turbulence. Overall, the computational model demonstrated the capability to predict the significantly different bubble physics and turbulence properties associated with the centre-peak and wall-peak flows. The 1D model documented in the present study should prove useful in the further assessment of both turbulence and two-fluid models for multiphase flow applications, especially in the nuclear industry. At the same time, the model critically depends on force model relations that are highly empirical; hence, the ability of the model to predict more general flows requires additional testing.

2.5 Acknowledgements

The authors are grateful to the Canadian Nuclear Laboratories (formerly Atomic Energy Canada Limited) and the Natural Sciences and Engineering Research Council of Canada (NSERC) for providing financial assistance for this research project.

Chapter 3

Modelling bubble induced turbulence for gas-liquid bubbly flow in a vertical pipe

A similar version of this chapter has been published as:

A. S. M. Atiqul Islam and D. J. Bergstrom. Modelling bubble induced turbulence for gas-liquid bubbly flow in a vertical pipe. Chemical Engineering Science 197 (2019) 159–171.

- The first author conducted the simulations, post-processed and analyzed the results, and prepared the first draft of the manuscript. The first author then worked with the co-author to discuss the results and finalize the content and form of the manuscript.

Abstract

A two-fluid model in the Eulerian-Eulerian framework has been implemented for the turbulent gas-liquid bubbly upward flow in a vertical pipe. The transport equations, i.e. Reynolds-Averaged Navier-Stokes equations for the two-fluid model, are discretized using the finite volume method. The effect of the disperse gas phase on the liquid phase turbulence, referred to as turbulence modulation, was accounted for through source terms in the transport equations for a low Reynolds number $k-\varepsilon$ turbulence closure. The model was used to predict the turbulence kinetic energy and its dissipation rate, mean phasic velocities and volume fraction distribution for a set of test cases selected from the available literature. The focus of the present study was on assessing the model predictions using measurements of the turbulence kinetic energy of the liquid phase. A relatively novel aspect of the present analysis is the use of the budgets of the transport equations for the turbulence kinetic energy and dissipation rate to assess the effect of the turbulence modulation on the liquid turbulence field. Although the present model formulation is shown to adequately predict the effect of bubbles in some flows and perform better than some of the other model formulations, the overall conclusion is that the present approaches for incorporating turbulence modulation are at best partially successful and still need further development.

3.1 Introduction

Computational fluid dynamics (CFD) has been applied to investigate the hydrodynamics of complex two-phase flows. Given the increase of computational power it has begun to provide an alternative and/or complement to experimental studies. Two-phase flow, specifically gas-liquid flow, in a pipe is an active area of research and has applications in many engineering fields such as the oil and gas, chemical and nuclear industries. Depending on the operating and flow conditions different flow regimes, for example bubbly, slug, churn, annular and disperse, can be observed for gas-liquid flow within a pipe (Brennen, 2005). The bubbly flow regime, where the gas (bubble) and liquid are treated as the dispersed and continuous phase, respectively, is the most common flow regime in industrial applications.

Most gas-liquid flows are also turbulent in nature. Generally, turbulence for the gas phase is neglected for bubbly flows as the density of air is negligible compared to the liquid phase.

Modeling the turbulence for single phase flow itself is a complex process, which is further complicated for two-phase flow since the presence of the second phase, i.e. gas, modifies the turbulence of the continuous liquid phase. To include the effect of the gas phase on the turbulence of the liquid phase, which is referred to as turbulence modulation, adds an additional level of complexity to the turbulence analysis. Depending on the level of the turbulence modulation, this may have a corresponding effect on the mean flow parameters.

For simulation of turbulent gas-liquid flow, the turbulent transport is often modeled using an eddy viscosity model. In such cases, the effect of turbulence induced by the bubbles can be accounted for in two ways: 1) using a separate viscosity correlation for bubble induced turbulence in the effective viscosity relation, and 2) adding source terms in the turbulence transport equations used to calculate the eddy viscosity. The first option often uses the bubble induced turbulence (BIT) viscosity model of Sato and Sekoguchi (1975). In the second method, a number of alternative formulations for the source terms have been proposed. In a few cases, both options have been applied together, e.g. Dhotre *et al.* (2007) and Masood and Delgado (2014). The present study focuses on the second option i.e. the use of additional source terms in the transport equations for the turbulence variables to include the effect of the bubbles on the liquid phase turbulence. Vitankar *et al.* (2002) introduced an approach to account for the interphase energy transfer between gas and liquid for two-phase flow in bubble columns. At the gas-liquid interface, energy released during the rise of a bubble is first converted to turbulence in the liquid phase.

Some of the turbulence modulation models available in the literature for mono-disperse flow include those of Troshko and Hassan (2001), Pfleger and Becker (2001), Yao and Morel (2004), and Rzehak and Krepper (2013). The basic difference among these approaches is in the calculation of the characteristic time scale used in formulating the source terms. The time scale can be based on the turbulence scales, in this case the turbulence kinetic energy and its dissipation rate, or include additional scales introduced by the gas phase, e.g. the bubble diameter. It is not yet clear which approach best captures the physics of the turbulence modulation process.

The experimental data available for air-water bubbly upward flow in a vertical pipe is limited, and in some cases the results appear to be inconsistent with each other. The following section summarizes some of the relevant studies, especially with respect to any observations relating to

the effect of the bubble/gas phase on the liquid phase turbulence. Liu (1997, 1998) conducted an experiment to investigate the effects of bubble size on the wall shear stress for air-water upward bubbly flow in a vertical channel. Measurement of radial profiles for void fraction, bubble size distribution, liquid phase mean velocity and axial liquid turbulence intensity were performed for a channel with an aspect ratio of 60. In addition to the change in volume fraction from wall-peak to centre-peak depending on bubble size, it was found that that smaller diameter bubbles result in a higher wall shear stress. Radial profiles of void fraction, interfacial area concentration, interfacial velocity, bubble size, liquid velocity and turbulence intensity were experimentally measured by Hibiki *et al.* (2001). Measurements were performed for a vertical upflow of air and water using a double-sensor probe and hot film anemometry to measure the gas and liquid velocity, respectively. Their analysis covered the flow regimes from bubbly to slug transition to capture both the wall-peak and centre-peak volume fraction profiles. The gas volume fraction and bubble size distributions for air-water bubbly and slug flow regimes in a vertical pipe were experimentally measured by Lucas *et al.* (2005). The transition from wall-peak to core-peak gas volume fraction profile, and the change in sign of the lift force with bubble size was confirmed by their measurements, which supports the findings of Tomiyama (1998). Using an improved measurement technique, Prasser *et al.* (2007) investigated the development of gas-liquid flow in a large vertical pipe for the bubbly, slug and churn flow regimes. Apart from the measurement of gas volume fraction profiles and bubble size distributions, they also explored the influence of the physical properties of the fluid by comparing the results of standard air-water to steam-water at high pressure. The turbulence characteristics of air-water bubbly flow were analyzed experimentally by Shawkat *et al.* (2008) for a large diameter pipe in a vertical orientation. In general, they observed that the level of turbulence intensity increases due to the presence of bubbles. Their values of the superficial velocities and average gas volume fraction were smaller compared to the studies of Lucas *et al.* (2005) and Prasser *et al.* (2007). For flow at low void fraction, the radial volume fraction profile showed a wall-peak which changed to a centre-peak as the volume fraction and bubble size were increased. Turbulence suppression was observed near the wall of the pipe in terms of the axial and radial turbulence intensity, and Reynolds shear stress relative to single-phase flow for a low void fraction with high liquid superficial velocities. The turbulence enhancement or suppression was related to the relative velocity between the gas and liquid phase. For low superficial velocities with smaller bubbles and low void fraction, the shear stress increases

compared to single-phase flow. The shear stress decreases when the superficial velocities are increased. Hosokawa and Tomiyama (2009) measured the radial distribution of void fraction, bubble size distribution, mean phasic velocities and turbulence kinetic energy for a limited number of flow conditions. The measurements were conducted for a small diameter pipe and low average gas volume fraction, and the turbulence kinetic energy was found to be augmented and suppressed for the low and high liquid superficial velocities, respectively. The researchers also developed a numerical model and compared the results against their own experimental data set. For a low gas volume fraction, as the liquid superficial velocity increases a noticeable effect of turbulence modulation on the turbulence kinetic energy is observed. In contrast, the gas superficial velocity has minimal effect on the turbulence.

In summarizing the experimental results above, the effect of bubbles on the liquid phase turbulence is not clearly addressed in the studies of Liu (1997, 1998), Lucas *et al.* (2005), and Prasser *et al.* (2007). Both turbulence enhancement and suppression due to the presence of bubbles has been reported in the experiments of Shawkat *et al.* (2008), and Hosokawa and Tomiyama (2009). Finally, it is possible for both turbulence enhancement and suppression to occur at different locations in the same flow, e.g. Hosokawa and Tomiyama (2009). Overall, the database available for evaluating turbulence modulation in gas-liquid bubbly flow is incomplete and the experimental results are not yet conclusive.

In terms of numerical studies, the paper of Rzehak and Krepper (2013) is especially significant in that it reports a benchmark and relatively comprehensive computational study of upward gas-liquid bubbly flow in a pipe that compares different models for the turbulence modulation. They used ANSYS-CFX to predict the radial distribution of gas volume fraction, liquid velocity, turbulent viscosity and turbulence kinetic energy, and made comparisons to select experimental data. They introduced a new characteristic time scale in their turbulence modulation model which appeared to yield better results for select test cases. Numerical simulation of polydisperse bubbly flow in bubble columns using the inhomogeneous multi-size-group (iMUSIG) model was performed by Ziegenhein *et al.* (2013) using a three dimensional (3D) Eulerian two-fluid method. They used the BIT model of Rzehak and Krepper (2013) and the possible influence of the swarm effects of bubbles on the non-drag forces was investigated. Ziegenhein *et al.* (2015) also used the same BIT model of Rzehak and Krepper (2013) in the context of an unsteady Reynolds Averaged Navier-

Stokes (URANS) formulation for predicting transient flow in a bubble column. They explored the effect of the bubble induced turbulence on the flow structure and also found that the virtual mass force was not negligible as is often assumed. Transient simulations based on the URANS approach were conducted for both uniform and nonuniform flows in bubble columns by Ziegenhein *et al.* (2017). The BIT model of Rzehak and Krepper (2013) was used for the turbulence modelling of the continuous liquid phase. The presence and absence of larger-scale flow structures was captured by the URANS approach for the non-uniform and uniform bubbly flow cases, respectively. The study of Ma *et al.* (2017) proposed a new time scale, i.e. $\frac{d_p}{u_r}$, where d_p is the bubble diameter and u_r is the relative velocity, and model relations for the coefficients for the bubble induced turbulence (BIT) source terms in the turbulence kinetic energy and dissipation rate equations based on a DNS study of a bubbly flow in a vertical channel. A previous study by Santarelli *et al.* (2016) had performed a comprehensive assessment of the turbulence kinetic energy budget based on the same DNS study, and evaluated the performance of some existing closures for predicting the interfacial transport term.

The present study builds on the results of Rzehak and Krepper (2013) and aims to provide additional insight. One difference between the present study and that of Rzehak and Krepper (2013) is that they used the shear stress transport (SST) turbulence model whereas the current study uses the standard $k-\varepsilon$ two-equation closure. For the turbulence modulation, based on dimensional analysis, Rzehak and Krepper (2013) developed and tested a new time scale, i.e. $\frac{d_b}{\sqrt{k}}$, based on the bubble diameter d_b. In contrast, the present study uses a turbulence modulation model based on the conventional turbulence time scale given by $\tau = \frac{k}{\varepsilon}$. The present study specifically focuses on a comparison of the turbulence quantities for single-phase and two-phase flow working with the limited experimental results available in the literature. This analysis was not included in the paper of Rzehak and Krepper (2013). A comparison of the time scale profiles and an assessment of the turbulence modulation term in the context of the turbulence kinetic energy budget are also novel contributions of the present paper.

In summary, the principal objective of the present paper is to document an analysis of available turbulence modulation models and their ability to predict the effects of bubbles for gas-liquid

turbulent flow. The performance of select turbulence modulation models in terms of predictions for the turbulence kinetic energy, mean axial liquid and gas velocity, gas volume fraction and other turbulence properties for air-water bubbly flow in a vertical pipe is carefully documented. The computational model is described in section 3.2, which includes the two-fluid model equations, interphase force balance between phases, the turbulence closure, and the turbulence modulation models. The predicted results for select experimental conditions based on the present model are presented in section 3.3 and finally, a brief conclusion relevant to the present model is outlined in section 3.4.

3.2 Computational Model

3.2.1 Two-fluid model

In the present study, the two-fluid model (TFM), which treats both the gas and liquid phase as interpenetrating continua (Drew and Passman, 1998), was used to treat the two phases. The essence of the Eulerian-Eulerian two-fluid model is that it characterizes the spatial distribution of the two phases using their corresponding local volume fraction values. The governing Reynolds-Averaged Navier-Stokes (RANS) equations for the mean velocity fields are obtained by the ensemble averaging of the continuity and momentum equations for each phase. The two phases are coupled through the pressure and interphase transfer terms in the momentum equations. The flow in the current study is considered to be steady, adiabatic and fully developed in the streamwise direction. The flow is axisymmetric, and the geometry is that of a vertical cylindrical pipe of radius R. The governing two-fluid transport equations, for the mean velocity components in cylindrical coordinate system are given below for the liquid and gas phase, respectively:

$$0 = -\alpha_l \frac{dP}{dz} + \alpha_l \frac{1}{r}\frac{d}{dr}\left(r\left(\mu_{eff}\frac{du_z}{dr}\right)\right) + \alpha_l \rho_l g - F^D \tag{3.1}$$

$$0 = -\alpha_g \frac{dP}{dz} + \alpha_g \frac{1}{r}\frac{d}{dr}\left(r\left(\mu_g \frac{dv_z}{dr}\right)\right) + \alpha_g \rho_g g + F^D \tag{3.2}$$

The left hand side of each governing equation, representing the temporal and convective acceleration, is zero due to the assumption of steady state and fully developed flow. The continuity equations under the assumption of fully developed flow require the mean radial velocity component of each phase to be zero. The parameters on the right hand side of Eqs. (3.1) and (3.2) represents the pressure gradient, effective stress model, body force due to gravity and interphase momentum exchange, respectively. The gas and liquid phases are characterized by their corresponding volume fractions, which at each location satisfy the constraint $\alpha_g + \alpha_l = 1.0$, and the net interphase momentum exchange is zero. The turbulent viscosity for the liquid phase is modelled using a two-equation eddy viscosity model, which includes contributions from both the shear induced turbulence and the so called bubble induced turbulence. It is to be noted that the drag force is the only interphase force considered in the streamwise momentum balance. The interphase forces and the eddy viscosity model including the turbulence modulation are briefly described in the following section. With the mono-disperse assumption, the bubbles are characterized by a single bubble diameter, so that the exchange of gas volume fraction due to the bubble coalescence and breakup is not considered. The flow parameters along with the necessary correlations used to solve Eqs. (3.1) and (3.2) are given in Table 3.1.

Table 3.1 Model correlations for the mean axial momentum equations.

Effective viscosity, $\mu_{eff} = \mu_l + \mu_t$
Drag force of Monahan and Fox (2009), $F^D = \frac{3}{4}\alpha_g\alpha_l\rho_l\frac{C_D}{d_b}\lvert v_z - u_z\rvert(v_z - u_z)$, $Re_b = \frac{\rho_l\lvert v_z - u_z\rvert d_b}{\mu_l}$ where $C_D = \frac{24}{Re_b} + \frac{6}{1+\sqrt{Re_b}}$

3.2.2 The interphase forces and radial force balance

The interphase forces (expressed per unit volume) due to the momentum exchange between gas bubbles and liquid while flowing coaxially in a pipe consist of both drag and non-drag forces. The lift, wall and turbulent dispersion forces are the most commonly used non-drag forces (Lucas *et*

al., 2001; Krepper *et al.*, 2005; Lucas *et al.*, 2007; Frank *et al.*, 2008; Rzehak *et al.*, 2012; Rzehak and Krepper, 2013; Masood and Delgado, 2014; Colombo and Fairweather, 2015). The virtual mass force is also considered as a non-drag force by some researchers (Ekambara *et al.*, 2005; Dhotre *et al.*, 2007; Monahan and Fox, 2009; Ziegenhein *et al.*, 2015). However, the virtual mass force has not been considered in the present analysis because of its negligible contribution compared to the other non-drag forces.

The drag force was already discussed in the previous section. A summary description of each of the interfacial forces relating to the radial direction will be presented below. Note that the bubble size (d_b) used in the following interphase force models is based on the assumption of a fixed mono-disperse size distribution with an average bubble size taken from the corresponding experimental data (Rzehak and Krepper, 2013) for both the centre-peak and wall-peak case.

A shear-induced force due to the interaction of bubbles with the deformation-rate field of the liquid phase is referred to as the lift force (Lucas *et al.*, 2001). The lift force was introduced by Zun (1980) and is defined as:

$$F^{\mathrm{L}} = -C_L \alpha_g \rho_l (v_z - u_z) \frac{du_z}{dr} \tag{3.3}$$

where, the lift force coefficient (C_L) correlation with experimentally determined (Tomiyama, 1998) values is given below:

$$C_{\mathrm{L}} = \begin{cases} \min[0.288\tanh(0.121\mathrm{Re_b}), \mathrm{f(Eo_d)}] & \mathrm{Eo_d} < 4 \\ \mathrm{f(Eo_d)} = 0.00105\mathrm{Eo_d^3} - 0.0159\mathrm{Eo_d^2} - 0.0204\mathrm{Eo_d} + 0.474 & 4 \le \mathrm{Eo_d} \le 10 \\ -0.29 & \mathrm{Eo_d} > 10 \end{cases} \tag{3.4}$$

For better agreement with the experimental data, the expression above of Tomiyama (1998) was modified (Islam *et al.*, 2016) so that the lift force expression used a value of 0.25 instead of the value of 0.288 in the range of $\mathrm{Eo_d} < 4$ for the wall-peak case.

The lift force acting on the bubbles can be either positive or negative depending on the bubble size. Considering the radial movement of the gas bubbles, a positive lift force is directed towards the pipe wall. The lift force experienced by bubbles is calculated from a correlation that changes sign

with the bubble size. The bubble diameter at which the lift force coefficient changes the sign is known as the critical diameter. The value of the critical bubble diameter is 5.80 mm as documented by Tomiyama (1998). The lift force coefficient is plotted against the bubble diameter in Fig. 3.1. Based on the above correlation, the lift coefficient changes sign at $d_b = 5.80$ mm.

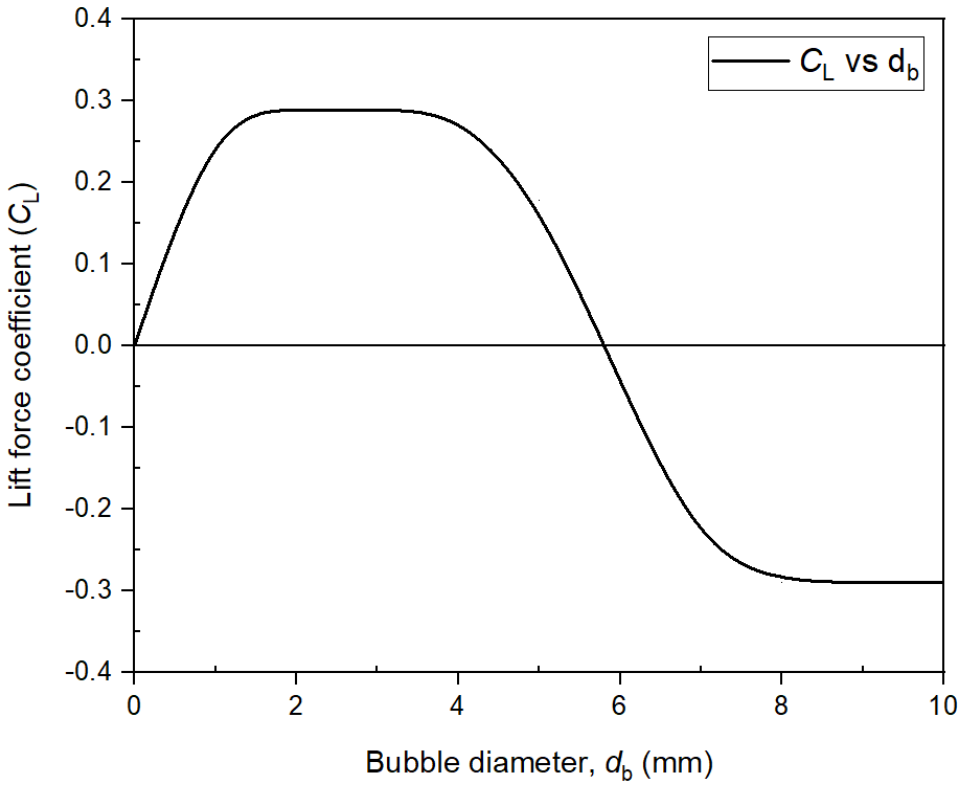

Fig. 3.1 Lift force coefficient (C_L) vs bubble diameter (d_b)

The critical bubble diameter mainly depends on the Eötvös number ($Eo_d = \frac{(\rho_l - \rho_g) g d_H^2}{\sigma}$), which is calculated based on the properties of air and water, as well as the surface tension of the air-water interface (Tomiyama, 1998; Prasser *et al.*, 2007). As noted above for an air-water system of atmospheric pressure and room temperature, the critical bubble diameter is 5.80 mm (Prasser et al., 2007). For higher temperatures and pressures, the surface tension of water becomes smaller. Therefore, the critical bubble diameter decreases with increasing saturation pressure. For example, the critical bubble diameter is found to be 3.50 mm at 6.5 MPa (Prasser *et al.*, 2007).

A number of studies have noted the change in sign of the lift force (Zun, 1986; Auton, 1987; Drew and Lahey, 1987; Kariyasaki, 1987; Zun, 1987; Tomiyama *et al.*, 1993; Tomiyama *et al.*, 1995; Lucas *et al.*, 2001; Troshko and Hassan, 2001; Tomiyama *et al.*, 2002; Politano *et al.*, 2003; Yao and Morel, 2004; Ekambara *et al.*, 2005; Krepper *et al.*, 2005; Cheung *et al.*, 2007; Dhotre *et al.*, 2007; Lucas *et al.*, 2007; Frank *et al.*, 2008; Issa and Lucas, 2009; Hosokawa and Tomiyama, 2009; Monahan and Fox, 2009; Duan *et al.*, 2011; Rzehak *et al.*, 2012; Rzehak and Krepper, 2013; Liao *et al.*, 2015). Interestingly, none of these studies has given the specific reason for this phenomenon. The following discussion on the effect of bubble size on the sign of the lift force is drawn from the study of Tomiyama (1998).

For bubbly upward flow in a pipe, the smaller bubbles are likely to maintain a spherical shape because of the high surface tension. The smaller bubbles are likely to migrate in the direction of the lower liquid velocity, i.e. toward the pipe wall. In other words, the smaller bubbles tend to move towards the pipe wall due to the shear-induced lift force. When a bubble grows above a certain diameter, the spherical shape of the bubble deforms into a wing shape due to the complex interaction between the vortex behind the bubble and the liquid phase velocity field (Tomiyama, 1998). The effect of the shape deformation for the larger size bubble results in an asymmetric liquid velocity distribution around the bubble. In a shear flow field, the vortex behind the deformed bubble tilts, which causes the larger bubble to migrate towards the region of low shear and higher liquid velocity, i.e. towards the pipe centre line. Therefore, the complex velocity field resulting from the interaction between the bubble wake and external shear field determines the direction of lateral migration of larger bubbles.

The lift force coefficient above depends on the Eötvös number (Eo) and the bubble Reynolds number (Re_b). The symbol Eo_d refers to the Eötvös number based on the long axis d_H of a deformable bubble (Wellek *et al.*, 1966) and is defined as:

$$Eo_d = \frac{(\rho_l - \rho_g) g d_H^2}{\sigma}, \qquad d_H = d_b(1 + 0.163 Eo^{0.757})^{1/3}, \qquad Eo = \frac{(\rho_l - \rho_g) g d_b^2}{\sigma} \tag{3.5}$$

The force which is responsible for driving the bubbles away from the pipe wall is known as the wall or lubrication force and was introduced by Antal *et al.* (1991). Here, the following modified version of the wall force by Tomiyama *et al.* (1995) is used for the calculation:

$$F^W = -C_W \alpha_g \rho_l \left(\frac{d_b}{2}\right)(v_z - u_z)^2 \left(\frac{1}{(R-r)^2} - \frac{1}{(R+r)^2}\right) \quad (3.6)$$

where the wall force coefficient C_W is calculated following Tomiyama (1998):

$$C_W = \begin{cases} \exp(-0.933Eo + 0.179) & 1 \leq Eo \leq 5 \\ 0.007Eo + 0.04 & 5 < Eo \leq 33 \end{cases} \quad (3.7)$$

The current model does not consider individual bubbles, but instead the radial distribution of gas volume fraction throughout the pipe. In addition to the drag, lift and wall forces, the turbulent dispersion force also plays an important role in the development of the gas-liquid flow structure in a pipe. It accounts for the turbulent mixing of bubbles and acts to smooth the radial gas volume fraction distribution due to the turbulence (Lucas *et al.*, 2001). Here, the following turbulent dispersion force expression of Lahey *et al.* (1993) is used for the calculation:

$$F^{TD} = -C_{TD} \rho_l k \frac{d\alpha_g}{dr}, \text{ where } C_{TD} = 0.10 \quad (3.8)$$

For the present analysis an additional term, known as the turbulent dispersion force based on the Eötvös number (Eo), is included as a part of the total dispersion force. Zun (1986) documented that the magnitude of the intrinsic fluctuating motion of bubbles increases with an increase in bubble size, which was consistent with the observation of Tomiyama *et al.* (1993). These fluctuating motions of the bubbles require an additional smoothing of the profiles. Hence, a second dispersion force depending on the bubble size is included in the present study. However, the second dispersion force (based on the Eötvös number) is only applicable when the value of the Eötvös number is greater than unity. The turbulent dispersion force based on the Eötvös number (Lucas *et al.*, 2001) is defined as follows:

$$F^{TD,Eo} = -C_{D,Eo} \rho_l (Eo - 1) \frac{d\alpha_g}{dr}, \text{ where } C_{D,Eo} = 0.0015 \text{ m}^2 \cdot \text{s}^{-2} \quad (3.9)$$

In the present study, the value of $C_{D,Eo}$ was adjusted to 0.001 and 0.015 for the centre- and wall-peak case, respectively, to improve the agreement with the experimental data.

For fully developed duct flow, one of the most challenging aspects of gas-liquid flow analysis is the prediction of the gas volume fraction distribution. Lucas *et al.* (2001) implemented a calculation method based on the balance of the non-drag forces acting on the bubbles in the radial direction. The non-drag forces include the lift, wall, and turbulent dispersion force including the term based on the modified Eötvös number as described in the above section. In this paper, the method of Lucas *et al.* (2001) was applied to predict the gas volume fraction distribution, i.e.

$$F^L + F^W + F^{TD} + F^{TD,Eo} = 0 \tag{3.10}$$

Substituting the model correlations for the non-drag forces into the Eq. (3.10) and rearranging gives the following first-order differential equation for the local gas volume fraction profile:

$$\left(0.1k + C_{D,Eo}(Eo - 1)\right)\frac{d\alpha_g}{dr} + \left(C_L(v_z - u_z)\frac{du_z}{dr} + C_W\left(\frac{d_b}{2}\right)(v_z - u_z)^2\left(\frac{1}{(R-r)^2} - \frac{1}{(R+r)^2}\right)\right)\alpha_g = 0 \tag{3.11}$$

Solution of this balance equation based on the mean and turbulence fields, yields the gas volume fraction profile. Note that the direction of the lift force changes such that bubbles smaller than a critical bubble size tend to move towards the pipe wall, while bubbles larger than critical bubble size move towards the centre of the pipe (Lucas *et al.*, 2005). These two cases are identified as wall-peak and centre-peak gas volume fraction profiles, respectively. A more complete description of the radial forces is given in the previous study (Islam *et al.*, 2016).

3.2.3 Low Reynolds number $k-\varepsilon$ model

For turbulence modelling of gas-liquid pipe flow, a number of different turbulence closures are available in the literature (Masood and Delgado, 2014). The present calculation uses an eddy viscosity model formulation for the liquid phase based on the two-equation turbulence closure of Myong and Kasagi (1990). This model uses a low Reynolds number formulation which allows the turbulence field to be calculated throughout the pipe, including the near-wall regions where damping occurs. To apply the model of Myong and Kasagi (1990) to gas-liquid flow, the single phase equations were multiplied by the liquid phase volume fraction, and the effect of the gas phase on the liquid phase turbulence was included via additional source terms in the k and ε equations. The transport equations for the turbulence kinetic energy (k) and dissipation rate of energy (ε) considering steady, fully developed pipe flow with the additional source terms for representing the turbulence modulation, are given as follows:

$$0=\frac{1}{r}\frac{d}{dr}\left(r\alpha_l\left(\left(\mu_l+\frac{\mu_t}{\sigma_k}\right)\frac{dk}{dr}\right)\right)+\alpha_l\mu_t\left(\frac{du_z}{dr}\right)^2-\alpha_l\rho_l\varepsilon+\varphi_K \tag{3.12}$$

$$0=\frac{1}{r}\frac{d}{dr}\left(r\alpha_l\left(\left(\mu_l+\frac{\mu_t}{\sigma_\varepsilon}\right)\frac{d\varepsilon}{dr}\right)\right)+C_1f_1\alpha_l\frac{\varepsilon}{k}\mu_t\left(\frac{du_z}{dr}\right)^2-C_2f_2\alpha_l\rho_l\frac{\varepsilon^2}{k}+\varphi_\varepsilon \tag{3.13}$$

The terms on the right hand side each equation represent: turbulent transport due to diffusion, production, dissipation and turbulence modulation, respectively. The values of the coefficients for the single phase were also used for the two-phase flow. The turbulence model expressions for Eqs. (3.12) and (3.13) are recorded in Table 3.2. Expressions for the turbulence modulation terms for k and ε equations i.e. φ_k and φ_ε are discussed in the next section.

Table 3.2 Model correlations for the low Reynolds number $k-\varepsilon$ turbulence closure.

Turbulent viscosity, $\mu_t = \frac{C_\mu f_\mu \rho_l k^2}{\varepsilon}$,	$f_1 = 1$
$f_2 = \left(1 - \frac{2}{9}\exp\left(-\frac{R_T}{6}\right)^2\right)\left(1 - \exp(-\frac{y^+}{5})\right)^2$,	$f_\mu = \left(1 - \exp(-\frac{y^+}{70})\right)\left(1 + \frac{3.45}{\sqrt{R_T}}\right)$
$y^+ = \frac{\rho_l u_\tau (R-r)}{\mu_l}$,	$R_T = \frac{\rho_l k^2}{\mu_l \varepsilon}$
$u_\tau = \sqrt{\frac{\tau_w}{\rho}}$,	$C_f = \frac{3}{4}\left(\frac{C_D}{d_b}\right)(\lvert v_z - u_z \rvert)$

Model constants:

$C_1 = 1.40,\ \ C_2 = 1.80,\ \ C_\mu = 0.09,\ \ \sigma_k = 1.40,\ \ \sigma_\varepsilon = 1.30$

3.2.4 Turbulence modulation models

In the present simulation, the turbulence modulation (TM) is implemented via source terms in the k and ε equations, denoted φ_k and φ_ε, respectively. They account for the effect of the dispersed gas phase on the continuous liquid phase turbulence. A reasonable approximation for the source term in the k equation is obtained by assuming that all the energy lost by the bubble due to the drag is transformed into the turbulence kinetic energy of the liquid phase (Rzehak and Krepper, 2013; Colombo and Fairweather, 2015). Using this approach, the k source term becomes

$$\varphi_K = C_k\, F^D\, (v_z - u_z) \tag{3.14}$$

In this case, only the drag force is considered since it is the main source of energy input. However, other researchers, e.g. Troshko and Hassan (2001), have also included the virtual mass force in addition to the drag force. For the ε source term, a similar rationale is adopted which assumes that the ε source term is proportional to the k source term divided by a characteristic time scale (τ) of the bubble induced turbulence, which can be expressed as follows:

$$\varphi_\varepsilon = C_\varepsilon\, \frac{\varphi_K}{\tau} \tag{3.15}$$

Turbulence modulation models available in the literature include those of Troshko and Hassan (2001), Yao and Morel (2004), and Rzehak and Krepper (2013). The fundamental difference among the various models relates to the calculation of the characteristic time scale. For the single phase turbulent flow, the characteristic time scale based on k and ε is given by $\tau = \frac{k}{\varepsilon}$, which represents the life span of a turbulent eddy before it breaks up into smaller eddies. For gas-liquid flow, four different time scales are possible based on the two length scales (the bubble size, d_b and eddy size, ℓ) and two velocity scales (relative velocity, u_{rel} and the square root of the turbulence kinetic energy, $\sqrt{k}$) as reported by Rzehak and Krepper (2013). Different turbulence modulation models will use different time-scales as discussed below.

For the present study, an improved version of turbulence modulation model has been developed starting from the existing formulation of Dhotre *et al.* (2007). The k source term used in the present model is:

$$\varphi_K = C_k \frac{F^D}{(v_z - u_z)} k \tag{3.16}$$

If this relation is rewritten to use the general form given in Eq. (3.14), i.e.

$$\varphi_K = C_k F^D (v_z - u_z)(k/(v_z - u_z)^2) \tag{3.17}$$

then it introduces an additional factor that is the ratio of the turbulence kinetic energy to the slip-velocity squared, which represents the ratio of the turbulence and mean energy based on the slip velocity. Note that based on consideration of the total energy balance as discussed by Ma *et al.* (2017), the implied coefficient should be constrained to be less than or equal to unity, i.e. $C_k\,(k/(v_z - u_z)^2) \leq 1$. Although this condition was met by all the simulations presented in the present paper, it may not hold for different flow conditions.

The model adopted for the ε source term is:

$$\varphi_\varepsilon = C_\varepsilon \frac{\varphi_K}{\tau} = C_\varepsilon \frac{F^D}{(v_z - u_z)} \varepsilon \tag{3.18}$$

which uses the characteristic time scale, $\tau = \frac{k}{\varepsilon}$ (3.19)

The values used for the model constants are $C_k = 0.65$ and $C_\varepsilon = 1.0$, compared to the values of $C_k = 0.75$ and $C_\varepsilon = 0.60$ recommended by Dhotre *et al.* (2007). The new values were selected to provide better overall agreement with the experimental data sets selected for evaluating the turbulence modulation.

In their study, Rzehak and Krepper (2013) used a so called mixed time scale, i.e.

$$\tau = \frac{d_b}{\sqrt{k}} \tag{3.20}$$

with the source term formulations for the k and ε equations given by Eqs. (3.14) and (3.15), respectively. They used a value of 1.0 for both model constants C_k and C_ε. The motivation for using d_b for the turbulence modulation time scale was that the bubble size is a different estimate of the size of the turbulent eddy.

The source terms for k and ε equations given in Eqs. (3.14) and (3.15), respectively, was also used in the model of Yao and Morel (2004). They also introduced the bubble size, but combined it with the dissipation rate of turbulence kinetic energy to obtain the following expression:

$$\tau = \left(\frac{{d_b}^2}{\varepsilon}\right)^{1/3} \tag{3.21}$$

The authors considered that the wake region behind a bubble is almost the same size as the bubble and the larger the wake the longer will be the time period for its energy to cascade to the smallest eddy before it is completely dissipated (Liao, 2013). They used a value of 1.0 for both model constants C_k and C_ε.

Troshko and Hassan (2001) also adopted the standard form of the source terms given in Eqs. (3.14) and (3.15). They proposed a new expression for the time scale, known as the bubble time scale, based on the both the bubble diameter and the coefficient of the virtual mass force (C_{VM}), i.e.

$$\tau = \frac{2\, C_{VM}\, d_b}{3\, C_D\, |v_z - u_z|} \tag{3.22}$$

It can be seen from the above expression that the time scale is no longer a function of the dissipation rate. The values of the model constants were $C_k = 1.0$, $C_\varepsilon = 0.45$ and $C_{VM} = 0.50$.

In summary, Eqs. (3.16) and (3.18) together with the corresponding time scale given in Eq. (3.19) will be used for the bubble-induced source terms in the present simulations. Limited comparisons will also be made to some of the other turbulence modulation formulations considered, specifically those of Rzehak and Krepper (2013) and Yao and Morel (2004), both of which adopt different turbulence time scales.

3.2.5 Boundary conditions and discrete solution procedure

No-slip and symmetry boundary conditions were implemented for the present numerical method at the wall and centerline of the pipe, respectively for both phases i.e.

At the centre: $\frac{du_z}{dr} = 0, \quad \frac{dv_z}{dr} = 0, \quad \frac{dk}{dr} = 0, \quad \frac{d\varepsilon}{dr} = 0, \quad \frac{d\alpha_g}{dr} = 0$ (3.23)

At the wall: $u_z = 0, \quad v_z = 0, \quad k = 0, \quad \varepsilon = \nu\left(\frac{d^2k}{dr^2}\right), \quad \alpha_g = 0$ (3.24)

For the present simulation, the no-slip boundary condition at the wall implemented for both phases is consistent with Ekambara *et al.* (2005) and Dhotre *et al.* (2007). The transport equations were discretized using a cell-centered finite volume method (Patankar, 1980). The set of coupled discrete equations (Eqs. (3.1), (3.2), (3.11), (3.12) and (3.13)) including boundary conditions (Eqs. (3.23) and (3.24)) were solved iteratively using a tri-diagonal matrix algorithm. The numerical simulation employed a non-uniform grid to refine the grid in the wall region where the gradients in the flow properties were highest. The solution of the iterative procedure was considered to be converged when the normalized difference in the field variables for two successive iterations was less than 0.0001. For all of the test cases, a grid of 100 control volumes was used with the first numerical node located at $y^+ = 0.20$ (approximately) near the wall. A grid sensitivity study was conducted in order to justify the number of control volumes. More specifically, the predicted value of the liquid phase mean velocity changed by less than 0.10% when the number of control volume increased from 100 to 120 for the test cases.

3.3 Results and discussions

Unlike single-phase flow, there are relatively few experimental data sets available in the literature for upward bubbly gas-liquid flow in a pipe. Furthermore, not all of the experiments document the full set of flow properties including both the mean and turbulence fields. The present study investigates the effect of bubble-induced turbulence by comparing the predicted results with and without the turbulence modulation model. Since the main objective of the present study is to investigate the effect of the gas phase (bubbles) on the turbulence field of the liquid phase, the experimental studies selected for analysis were those which directly measured a turbulence quantity. The experiments of Hosokawa and Tomiyama (2009), Shawkat *et al.* (2008) and Liu (1998) include measurements of the turbulence kinetic energy, Reynolds stresses or turbulence intensities, as well as the mean velocity and volume fraction profiles. The turbulence kinetic energy and Reynolds stresses are directly influenced by the turbulence modulation model. However, the performance of the present turbulence modulation model has been assessed primarily on the basis of the prediction for the turbulence kinetic energy, since only the experiment of Shawkat *et al.* (2008) measured the Reynolds stress field. The predictions for the mean velocity and volume fraction profiles have also been included, to assess whether the turbulence modulation has any significant effect on the mean properties of the flow.

The simulations were performed for the experimental flow conditions (Hosokawa and Tomiyama, 2009; Shawkat *et al.*, 2008; Liu, 1998) for the selected test cases documented in Table 3.3. In the present study, the test cases with numbered 1, 2, 3, 4, 5, 6, 7, 8 represents the cases Ho11, Ho12, Ho21, Ho22, L21C, L22A, S21, S33 considered by Rzehak and Krepper (2013), respectively. Note that the gas volume fraction distribution peaks at the wall for all of the selected test cases taken from Rzehak and Krepper (2013), since the bubble diameters for each case is less than the critical bubble diameter. For the numerical analysis, the experimental flow conditions in terms of average gas volume fraction value and bulk Reynolds number for the liquid phase were obtained by setting the bulk volume fraction and adjusting the pressure gradient to obtain the desired Reynolds number. For the simulations, axial pressure gradients are $\frac{\mathrm{dP}}{\mathrm{dZ}} = 10000$ (N/m^3), $\frac{\mathrm{dP}}{\mathrm{dZ}} = 10000$ (N/m^3), $\frac{\mathrm{dP}}{\mathrm{dZ}} = 10100$ (N/m^3), $\frac{\mathrm{dP}}{\mathrm{dZ}} = 10100$ (N/m^3), $\frac{\mathrm{dP}}{\mathrm{dZ}} = 10390$ (N/m^3), $\frac{\mathrm{dP}}{\mathrm{dZ}} = 10390$ (N/m^3), $\frac{\mathrm{dP}}{\mathrm{dZ}} = 10550$

(N/m^3), and $\frac{dP}{dZ} = 10700$ (N/m^3) were used for test cases 1, 2, 3, 4, 5, 6, 7, and 8, respectively. Reynolds number in Table 3.3 represents the Reynolds number of the flow based on the corresponding liquid (water) phase bulk velocity, density, viscosity, and pipe diameter. The results and discussion section is divided into three parts. Section 3.1 documents a comparison of the predictions for the turbulence kinetic energy profiles for single-phase and two-phase flow. It also compares the predicted value of the turbulence kinetic energy to the experimental data. The mean flow properties for both phases are discussed in section 3.2, and the time scale profiles for different models are compared in section 3.3. Finally, the contribution of the turbulence modulation to the budget of the turbulence kinetic energy and its dissipation rate are presented in section 3.3.

Table 3.3 Experimental flow conditions for the selected test cases used in the numerical analysis.

Experiment	**Case number**	**Pipe diameter D (m)**	**J_L (m/s)**	**J_G (m/s)**	**d_b (mm)**	**α_g**	**Reynolds number**
Hosokawa and Tomiyama (2009)	Case 1	0.025	0.50	0.018	3.20	0.023	12500
	Case 2	0.025	0.50	0.025	4.25	0.04	12500
	Case 3	0.025	1.0	0.02	3.50	0.015	25000
	Case 4	0.025	1.0	0.036	3.70	0.033	25000
Liu (1998)	Case 5	0.0572	1.0	0.13	4.20	0.096	57250
	Case 6	0.0572	1.0	0.22	3.90	0.157	57250
Shawkat et al. (2008)	Case 7	0.200	0.45	0.015	4.10	0.024	90000
	Case 8	0.200	0.68	0.10	4.70	0.10	135000

3.3.1 Prediction for turbulence kinetic energy

This section discusses the predicted profiles of turbulence kinetic energy (TKE) considering both single-phase and two-phase flow in a pipe. For the single-phase flow analysis, the experimental data of Hosokwa and Tomiyama (2009) has been used for comparison due to the scarcity of single-phase measurements in two-phase experiments. The single-phase flow condition corresponding to the two-phase flow was obtained by utilizing the same liquid superficial velocity and matching the same bulk Reynolds number of the liquid phase (Table 3.3).

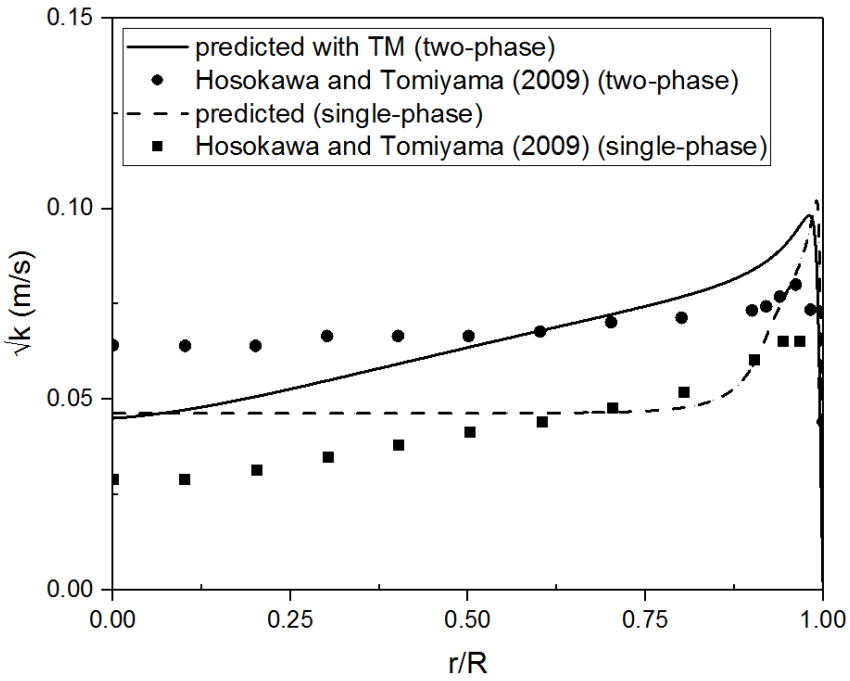

Fig. 3.2 Comparison of turbulence kinetic energy profiles for two-phase and single-phase flow (Case 2).

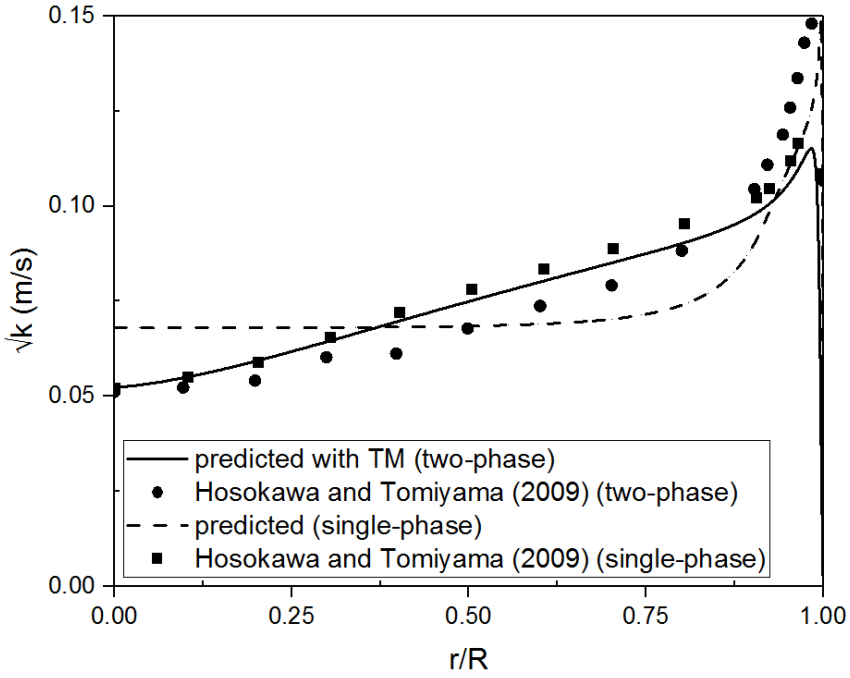

Fig. 3.3 Comparison of turbulence kinetic energy profiles between two-phase and single-phase (Case 4).

Figs. 3.2 and 3.3 illustrate the predicted profile of the turbulence kinetic energy for the liquid phase. The turbulence model adopted in the current study cannot capture the anisotropy of the turbulence field. Therefore, the square root of the turbulence kinetic energy is considered as an alternative to assess the different models following Rzehak and Krepper (2013). Note that both Case 1 and 2 share the same superficial liquid velocity, however the superficial gas velocity, bubble diameter and bulk gas volume fraction value is slightly higher for Case 2. The predicted profile of the single-phase flow is also included in the corresponding figures for comparison. It can be seen from Fig. 3.2 that the measured value of the turbulence kinetic energy is higher for the gas-liquid flow than for the single-phase flow. For both experimental profiles, the turbulence kinetic energy increases in the radial direction, and exhibits the prototypical peak value near the wall. The predicted profiles of turbulence kinetic energy for single- and two-phase flow also indicate an increase in the level of the turbulence kinetic energy due to the presence of the bubbles. One difference observed in the predicted profiles in Fig. 3.2 is the lower level of turbulence kinetic energy for the two-phase flow near the centreline of the pipe, almost the same as for single-phase flow. At the wall, the model predicts a lower peak value for the two-phase flow, which is also

located further from the wall. In general, the model predictions were close to the experimental data in the near-wall region.

Fig. 3.3 indicates a somewhat different behaviour in terms of the effect of bubbles on the liquid phase turbulence. In contrast to Fig. 3.2, the measured value of the turbulence kinetic energy is lower for the gas-liquid flow than for the single-phase flow except in the near wall region. The difference in the measured profiles is also smaller than in Fig. 3.2. The profile of turbulence kinetic energy predicted by the computational model for the two-phase flow was able to capture a similar behaviour, but only in the region near the centreline of the pipe. Elsewhere, the model predicted a small enhancement in the turbulence kinetic energy due to bubbles. The profile predicted for the two-phase flow exhibited the same characteristics as the experimental profiles, but the level was closer to that measured for the single-phase flow.

Figs. 3.2 and 3.3 consider Case 2 and 4, respectively, for which both the superficial liquid and gas velocities increase. Based on the experimental results shown in Figs. 3.2 and 3.3, as the liquid and gas superficial velocities increase (Case 4 versus Case 2), the turbulence kinetic energy is enhanced in the near-wall region. The predicted profiles exhibited the same behaviour. As such, the numerical model is able to capture the experimental trend of enhancement and suppression of the turbulence kinetic energy based on the superficial liquid and gas velocities.

The next set of figures looks specifically at the effect of the turbulence modulation model on the prediction for the two-phase flow. The predicted profiles are compared against the selected data sets from the experimental studies of Hosokwa and Tomiyama (2009), Liu (1998) and Shawkat *et al.* (2008), as well as the numerical prediction of Rzehak and Krepper (2013) for each flow case. The flow conditions corresponding to each experiment can be found in Table 3.3.

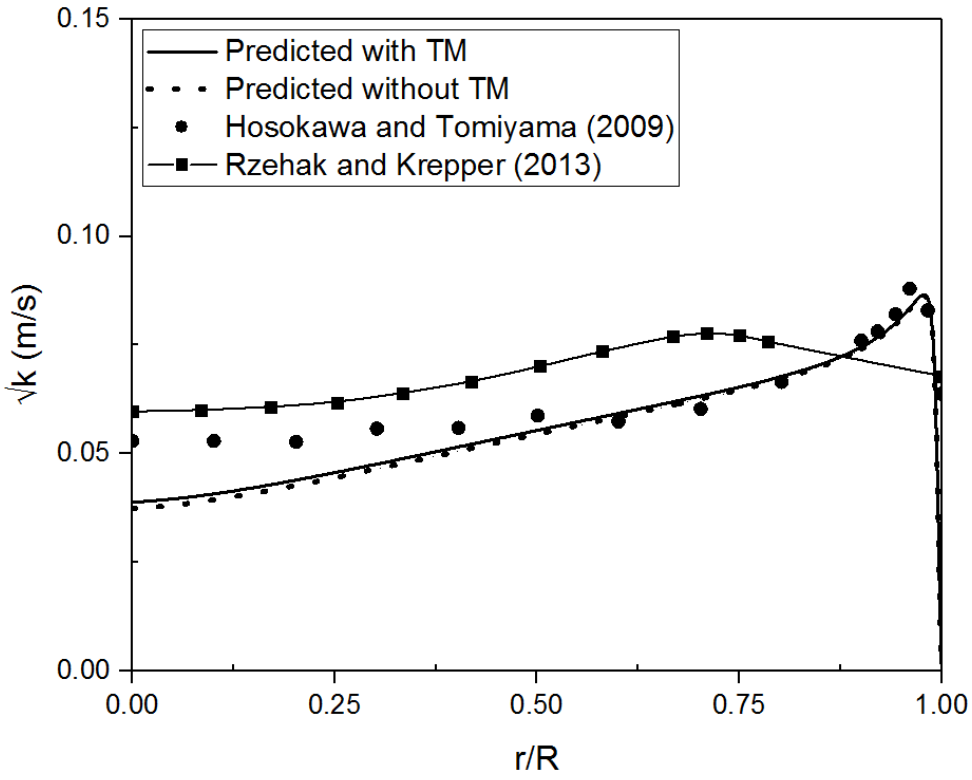

Fig. 3.4 Predicted profiles of turbulence kinetic energy (Case 1).

Fig. 3.4 compares the predicted and experimental results for Case 1. In this case the effect of the turbulence modulation in the numerical model was almost negligible. Curiously, the profile for the case of no turbulence modulation captured the experimental profile quite well in the outer region of the pipe. The predicted profile of Rzehak and Krepper (2013) was generally higher than the experimental profile, except in the near-wall region where it did not capture the peak value.

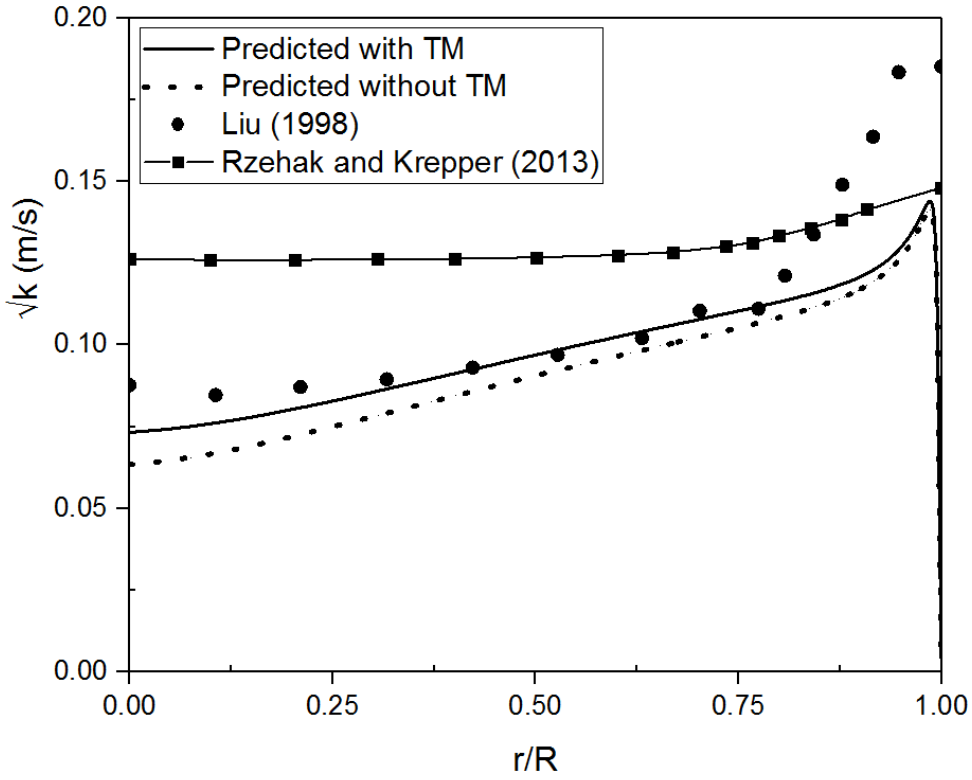

Fig. 3.5 Predicted profiles of turbulence kinetic energy (Case 6).

Fig. 3.5 compares the predicted and experimental results for Case 6. In this case the effect of the turbulence modulation in the numerical model was to modestly enhance the level of the turbulence kinetic energy. The predicted profile with turbulence modulation was close to the experimental data, except near the centreline and in the near-wall region, where it significantly under-predicted the peak value. The profile predicted by Rzehak and Krepper (2013) in general substantially over-predicted the turbulence kinetic energy, except in the near-wall region where it missed resolving the peak value.

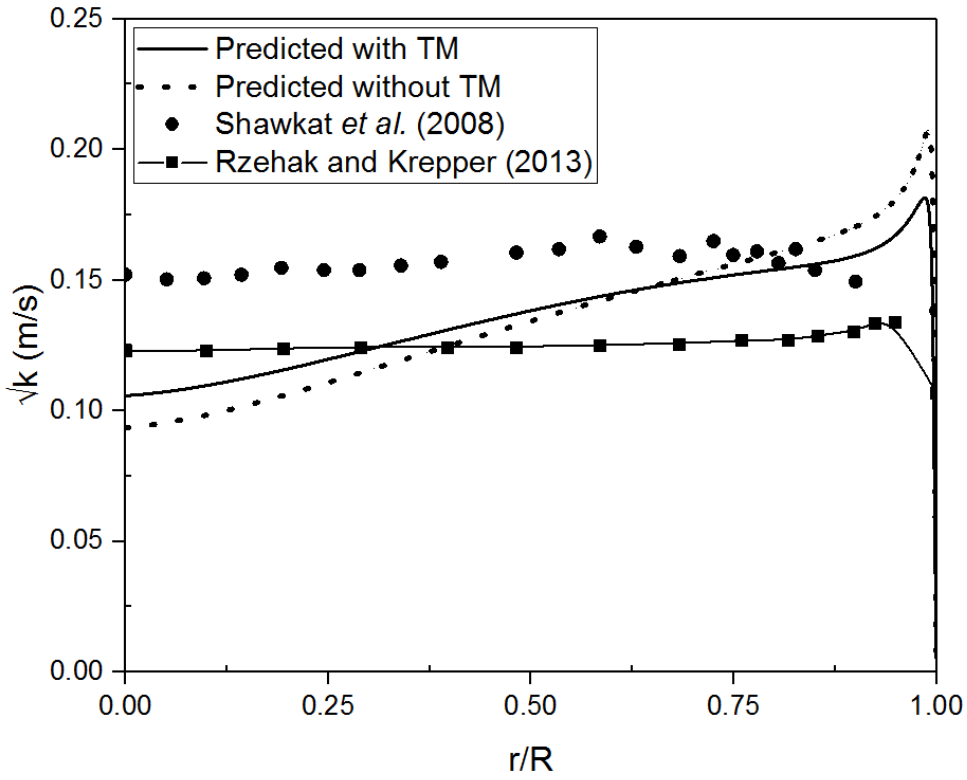

Fig. 3.6 Predicted profiles of turbulence kinetic energy (Case 8).

Fig. 3.6 compares the predicted and experimental results for Case 8. In this case the effect of the turbulence modulation in the numerical model was observed to both enhance and suppress the level of the turbulence kinetic energy in the inner and outer region of the pipe, respectively. The profile predicted for the turbulence kinetic energy including turbulent modulation consistently under-predicted the experimental data except for a small region in the outer part of the pipe. It also included a peak value near the wall that was not present in the experimental data. One effect of the turbulence modulation was to somewhat reduce the magnitude of the peak value. The model of Rzehak and Krepper (2013) also significantly under-predicted the level of the turbulence kinetic energy. However, their model did not include a strong peak near the wall, which was consistent with the experiment.

Overall, the comparisons presented in Figs. 3.4 – 3.6 illustrate the varied performance of the turbulence modulation model. Its effect can be minimal or significant; it can both enhance and suppress the level of the turbulence kinetic energy, sometimes at different locations in the same

pipe flow. This illustrates the challenge of developing a turbulence modulation model that effectively reproduces the dependence of the modulation effect on the specific flow conditions. A comparison of the performance of the present model with that of Rzehak and Krepper (2013) indicates that for the three test cases considered, the present model exhibits a more varied performance and overall yields results which are closer to the experiments.

3.3.2 Mean flow properties

This section presents the profiles predicted for the mean velocity (of both phases), volume fraction and eddy viscosity. The intent is to investigate the effect of the turbulence modulation on the mean properties of the flow. The predicted profiles are compared to select experimental data (Liu, 1998; Shawkat *et al.*, 2008) and the numerical results of Rzehak and Krepper (2013). For the mean flow properties analysis, Case 6 and 8 have been considered as these two cases shows the finite effect of turbulence modulation i.e. enhancement and suppression in the turbulence kinetic energy (Figs. 3.5 and 3.6). In comparing the results for the turbulence modulation model of Rzehak and Krepper (2013) with predictions based on the present model, it should be noted that they did not use the same bubble force model, which resulted in different profiles for the velocity and gas volume fraction profiles.

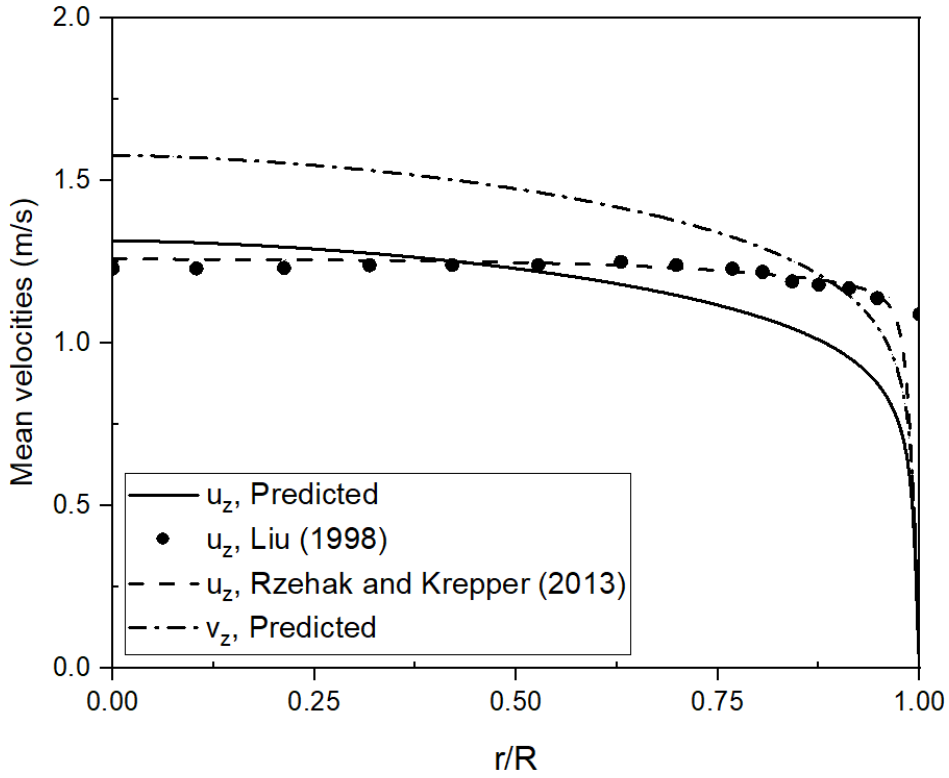

Fig. 3.7 Predicted mean velocity profiles (Case 6).

Fig. 3.7 shows the mean velocity profiles for the gas and liquid phase for Case 6. Compared to the experimental data, the present model slightly over-predicts the liquid phase velocity in the center region of the pipe, and under-predicts the liquid phase velocity in the outer region of the pipe. The experimental profile for the liquid phase velocity is relatively flat, and exhibits a finite value at the wall that is inconsistent with the no-slip condition used by the present model. The profile calculated by the model of Rzehak and Krepper (2013) is very close to the experimental data. The gas phase velocity profile predicted by the current model is generally higher than the liquid phase velocity, but follows the same shape. No experimental data were available for comparison for the gas phase.

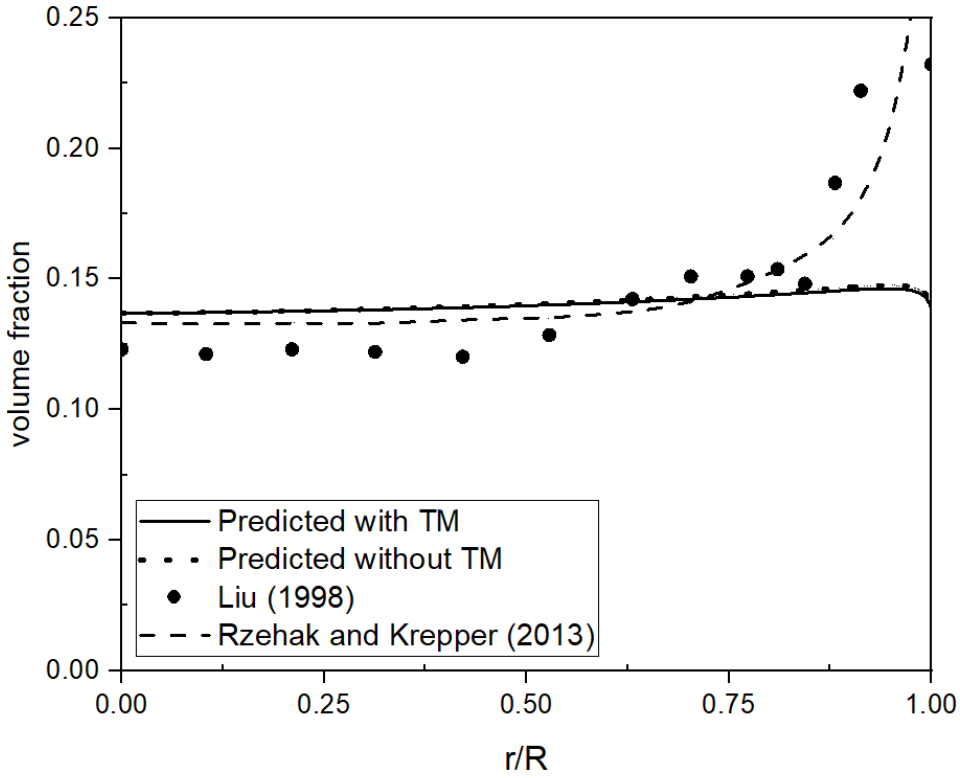

Fig. 3.8 Predicted gas volume fraction profiles (Case 6).

Fig. 3.8 shows the gas volume fraction distribution predicted by the present model for Case 6, which represents a wall-peak profile. For this flow, the effect of the turbulence modulation in the predicted profile was almost negligible. The numerical model over- and under-predicts the gas volume fraction distribution near the centerline and wall of the pipe, respectively, compared to the measured data. The predicted profiles do not capture the strong peak in gas volume fraction documented by the experiment near the wall. The simulated profile of Rzehak and Krepper (2013) does a better job of reproducing the experimental data in the centre region of the pipe. However, it predicts very high values near the wall which exceed the peak shown in the experimental data.

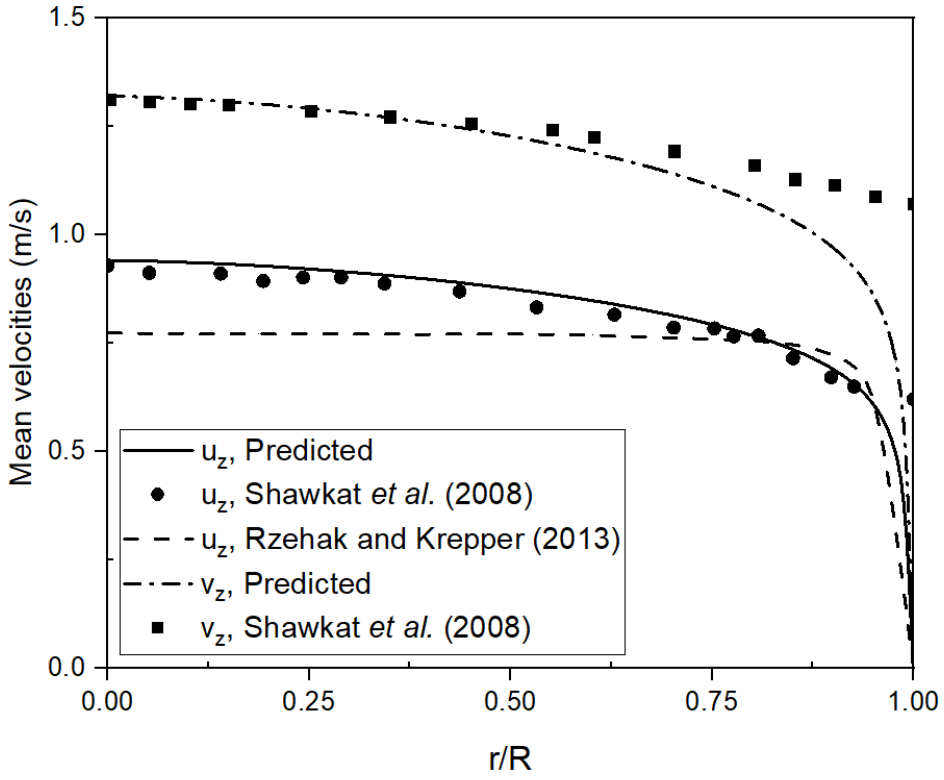

Fig. 3.9 Predicted mean velocity profiles (Case 8).

Fig. 3.9 gives the mean velocity profiles predicted for both phases for Case 8. For this flow, the present model does an excellent job of capturing the experimental profile, with the exception of the value at the wall. The present model uses a no-slip condition for the liquid velocity at the wall, whereas the measurements indicate a finite value. In contrast, the prediction of Rzehak and Krepper (2013) is almost flat, and under-predicts the experimental data over most of the pipe, with the exception of the near-wall region. The prediction of the present model for the gas phase velocity is also close to the experimental data over much of the pipe domain. However, because it uses a no-slip velocity for the gas phase at the wall, it under-predicts the experimental data in the near wall region. The present model also accurately predicts the slip-velocity between the two phases over most of the pipe domain. Although the results are not shown for Case 7, the behavior of the present model is very similar to that observed for Case 8 in Fig. 3.9.

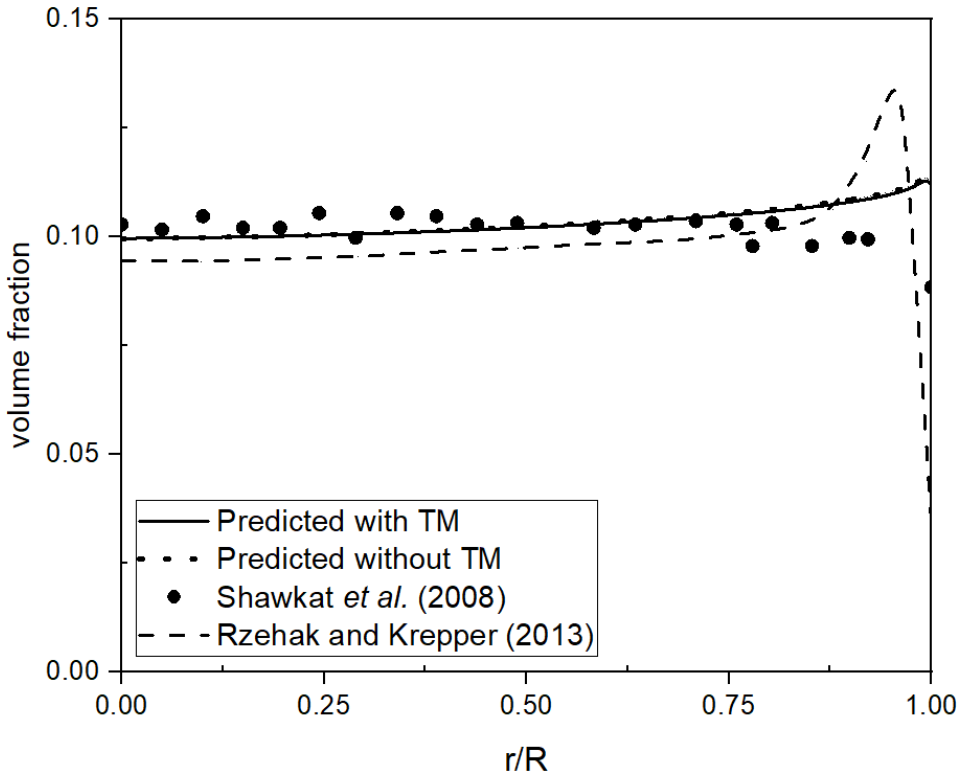

Fig. 3.10 Predicted gas volume fraction profiles (Case 8).

Fig. 3.10 depicts the gas volume fraction distribution predicted by the various model formulations for Case 8. Note that the phase distribution would be expected to exhibit a wall-peak profile, as reported by Rzehak and Krepper (2013), since the considered bubble diameter is less than the critical bubble diameter. However, the data show a profile without a definitive peak value, either at the wall or elsewhere in the pipe. Although the data show some scatter, the experimental profile is almost uniform across the pipe, with a small decrease in the value near the wall. The predicted profile captures the experimental profile better than the prediction of Rzehak and Krepper (2013) over most of the pipe domain. In contrast to the experimental profile, the predicted profiles by the present model and Rzehak and Krepper (2013) model show a small and sharp peak, respectively, in the gas volume fraction near the wall. For this flow, the turbulence modulation has negligible effect on the gas volume fraction distribution.

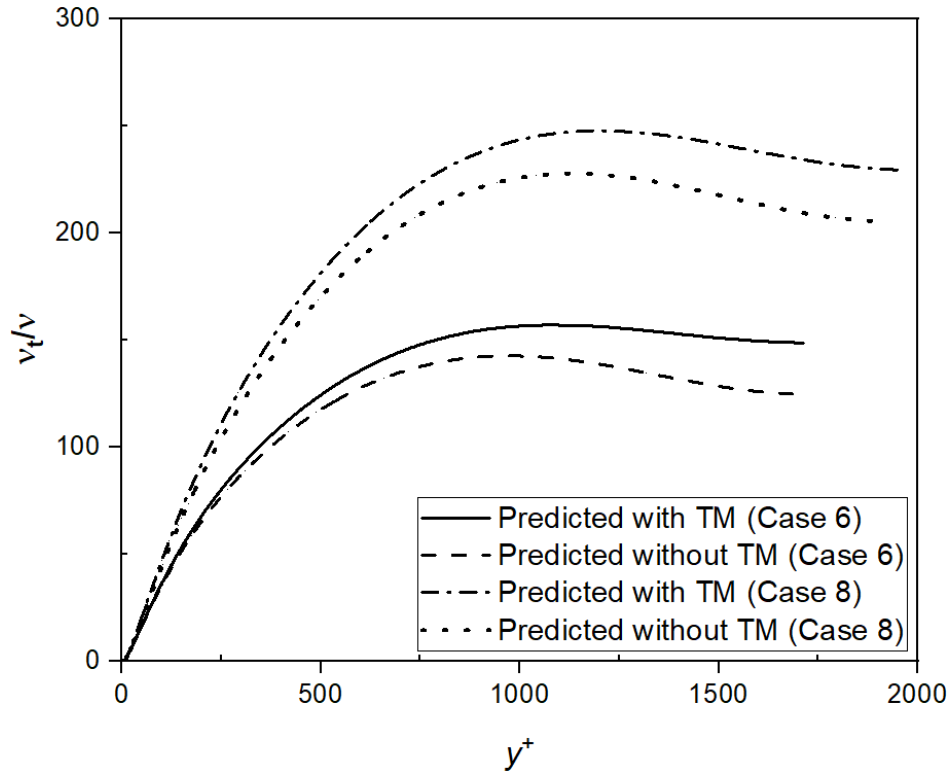

Fig. 3.11 Comparison of the predicted eddy viscosity profiles (Case 6 and 8).

Fig. 3.11 presents a comparison of the predicted turbulent or eddy viscosity profiles for Case 6 and 8 plotted against the normalized wall normal distance y^+. The turbulent viscosity profile given by the solid line corresponds to the experimental flow condition (Case 6) of Liu (1998), whereas, the dash-dot line corresponds to the experimental flow condition (Case 8) of Shawkat *et al.* (2008). Both curves have the same characteristic shape, i.e. a value of zero at the wall and a peak value in the middle region of the pipe. The turbulent viscosity for Case 8 is observed to be greater than that for Case 6, since the turbulence kinetic energy (Fig. 3.6) and bulk Reynolds number (Table 3.3) are much higher for Case 8 compared to Case 6. However, it is evident from Fig. 3.11 that there is a small but significant enhancement of the eddy viscosity profile due to the turbulence modulation which can be attributed to the change in turbulence kinetic energy (Fig. 3.6).

Overall, the effect of the turbulence modulation on the mean velocity fields and gas volume fraction appears to be minimal, even though there is a noticeable effect of the turbulence modulation on the eddy viscosity profile. Furthermore, comparison of the predictions for the mean

velocity and gas volume fraction profiles of the present model with those of Rzehak and Krepper (2013) indicates a significant variation, with neither model consistently capturing the trend of the experimental data.

3.3.3 Time scale and turbulence kinetic energy budget

This section explores the distribution of the characteristic time scales for the different turbulence modulation models. The turbulence modulation terms in the turbulence kinetic energy and dissipation rate equations are also assessed in terms of the budgets of those transport equations. For completeness, both centre-peak and wall-peak results will be considered in this section. The values of the time scale presented for Rzehak and Krepper (2013) in Figures 3.12 and 3.13 were obtained using the formulation, $\tau = \frac{d_b}{\sqrt{k}}$ in the present model. Likewise, the values of the time scale presented for Yao and Morel (2004) in Figures 3.12 and 3.13 were obtained with the expression, $\tau = \left(\frac{{d_b}^2}{\varepsilon}\right)^{1/3}$.

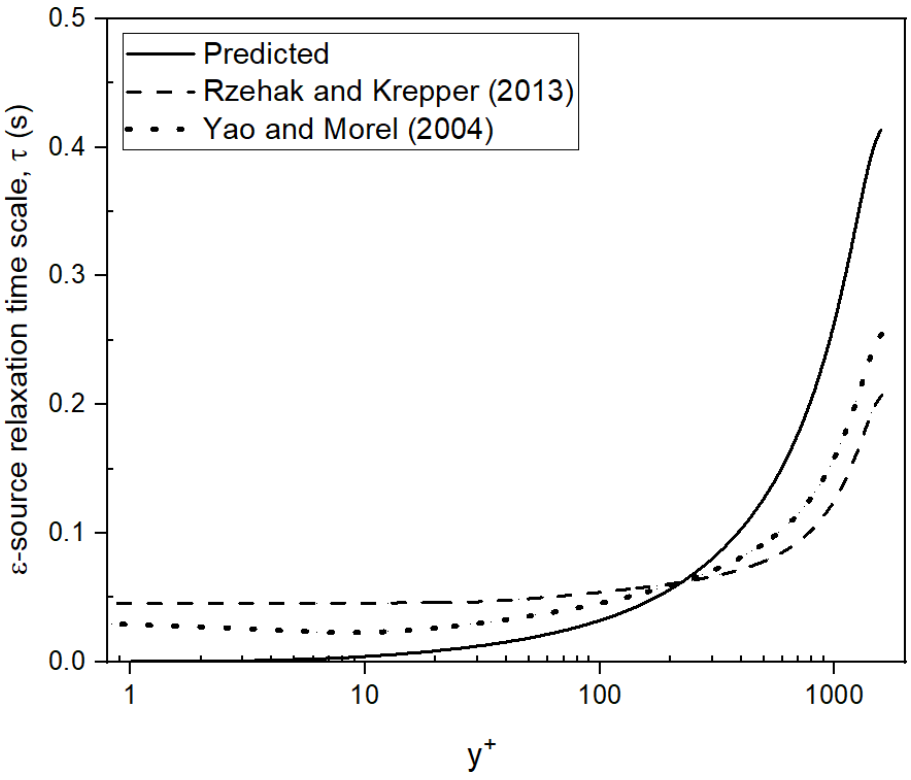

Fig. 3.12 Characteristic time scale profiles for centre-peak case.

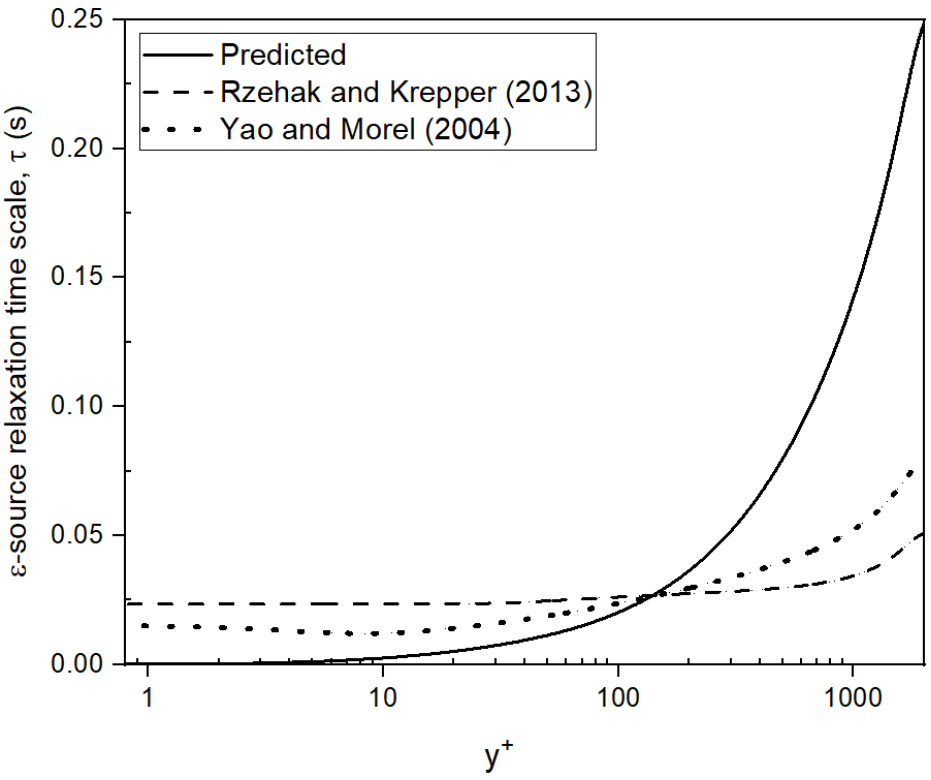

Fig. 3.13 Characteristic time scale profiles for wall-peak case.

Figs. 3.12 and 3.13 present the distributions of the characteristic time scale (τ) used in the ε-equation source term for a centre-peak ($d_b = 6.0$ mm) and wall-peak ($d_b = 4.0$ mm) case, respectively. The simulations correspond to the experimental flow conditions of test case 118 and test case 086 of Lucas *et al.* (2005). Three different characteristic time scale formulations are considered, i.e. the present model, the model of Rzehak and Krepper (2013) and the model of Yao and Morel (2004), which were described in section 3.2.4. Recall that the present model uses the turbulence kinetic energy and dissipation rate for the calculation of the time scale based on Kolmogorov's hypothesis. The bubble diameter was considered as an estimate of the size of the turbulent eddy in the expression for the time scale proposed by Rzehak and Krepper (2013) and Yao and Morel (2004). In addition to the bubble size, the turbulence kinetic energy and dissipation rate of energy was also used in the formulation of the time scale by Rzehak and Krepper (2013) and Yao and Morel (2004), respectively. In general, for both flow cases and all three model formulations the time scale profile peaks at the centre of the pipe and decreases to a minimum value near the wall of the pipe. The present model yields the smallest value near the wall, where it

goes to zero, and the largest value near the centre of the pipe. The other two models show higher and finite values near the pipe wall, and lower values near the centre of the pipe. The pattern is consistent for both flow cases, but the relative change is much greater for the wall-peak case shown in Fig. 3.13, especially in the centre region of the pipe. Overall, the use of the bubble diameter as the length scale changes the magnitude of the time scale but not its characteristic shape.

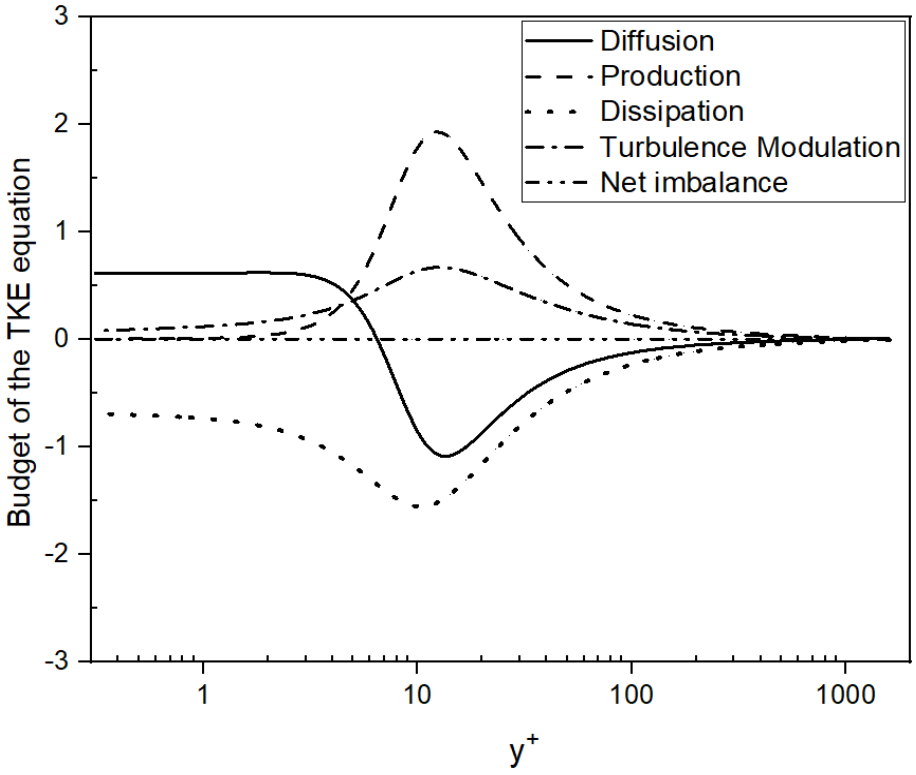

Fig. 3.14 Comparison of the diffusion, production, dissipation and turbulence modulation terms in the transport equation for turbulence kinetic energy for Case 8 using the present model.

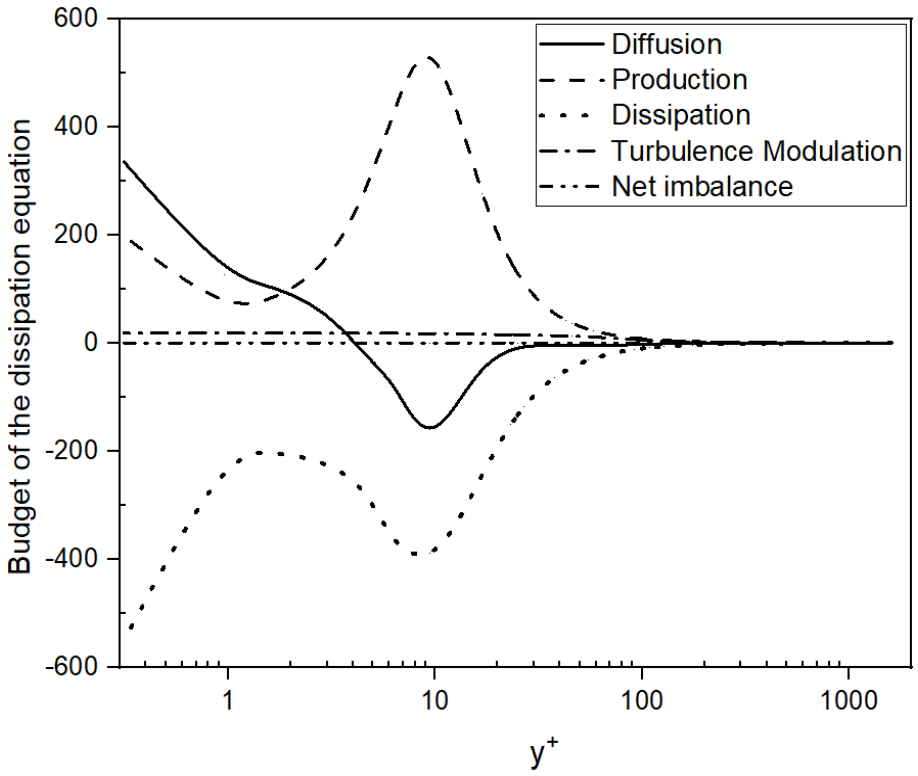

Fig. 3.15 Comparison of the diffusion, production, dissipation and turbulence modulation terms in the transport equation for the dissipation rate for Case 8 using the present model.

Figs. 3.14 and 3.15 present the budgets for the turbulence kinetic energy and its dissipation rate based on their respective transport equations for Case 8, which indicated a finite contribution from the turbulence modulation to the turbulence kinetic energy profile, see Fig. 3.6. The purpose of this analysis is to compare the turbulence modulation terms to the diffusion, production and destruction terms in these equations. For Figs. 3.14 and 3.15, the present model is used for the turbulence modulation. Typically, the shear production and dissipation are the dominant terms in the turbulence transport equations (k and ε), which also holds true for the present bubbly flow analysis. From Fig. 3.14 for the turbulence kinetic energy equation, the maximum value of the production and dissipation is observed to be at $y^+ = 10$, i.e. $1 - \frac{r}{R} = 0.007$ as expected. The peak value of turbulence modulation occurs at almost the same wall-normal location, and is approximately one-third of the peak value of the shear production. Note that for this flow the volume fraction profile of the gas phase peaks near the wall. From Fig. 3.14, the contribution of

the turbulence modulation is significant compared to the shear production and occurs very close to the wall. However, from Fig. 3.6, the turbulence kinetic energy is observed to be reduced by the turbulence modulation in the near-wall region, which trend is correct based on the experimental data. In their DNS study of bubbly flow in a vertical channel, Santarelli *et al.* (2016) showed that in the budget of the turbulence kinetic energy, the interfacial term balanced the dissipation rate over most of the inner extent of the channel. For the present pipe flow simulation, the turbulence modulation term becomes similar in magnitude to the production term in the inner region of the pipe, and both balance the dissipation rate (note that this is not clear in Fig. 3.14, which uses a log scale on the y^+axis to expand the near-wall region). However, unlike the channel flow simulation, both the net production and dissipation terms are relatively small in the center region of the pipe. The difference between the two flows may pertain to the flow geometry and flow conditions.

For the dissipation rate equation, the peak value of the production also occurs at about $y^+ = 10$, as shown in Fig. 3.15. In comparison to this term, the turbulence modulation term is relatively small and almost uniform in the region $y^+ < 100$, and negligible beyond. This behavior is partly explained by the fact that the time scale becomes much larger in the pipe region away from the wall (Figs. 3.12 and 3.13), which then reduces the turbulence modulation term. Overall Fig. 3.15 suggests that for the present turbulence modulation model, the effect on the dissipation rate is almost negligible. For a fully developed pipe flow, the net imbalance represents the summation of the production, dissipation, diffusion and turbulence modulation terms.

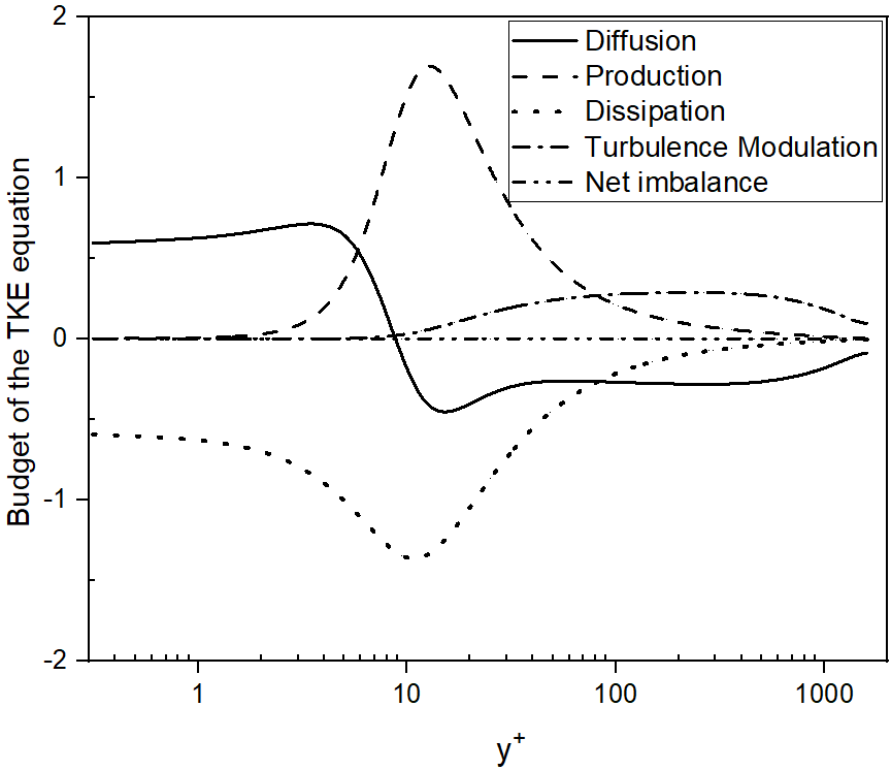

Fig. 3.16 Comparison of the diffusion, production, dissipation and turbulence modulation terms in the transport equation for the turbulence kinetic energy for Case 8 using the model of Rzehak and Krepper (2013).

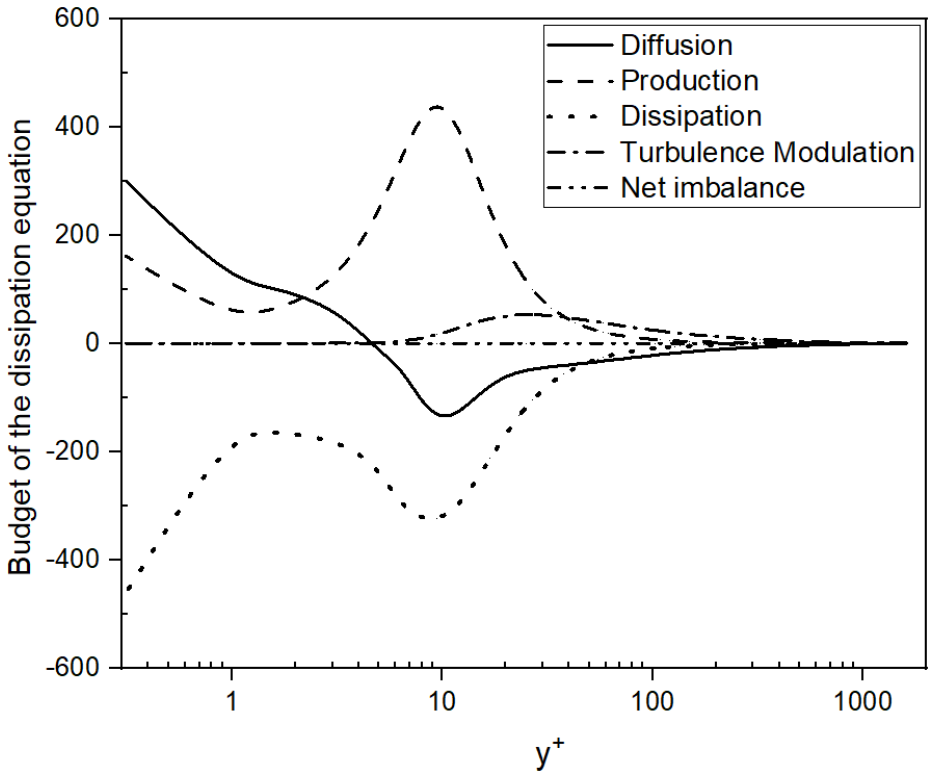

Fig. 3.17 Comparison of the diffusion, production, dissipation and turbulence modulation terms in the transport equation for the dissipation rate for Case 8 based on the model of Rzehak and Krepper (2013)

Figs. 3.16 and 3.17 examine the balance of the turbulence kinetic energy (TKE) and dissipation rate transport equations, respectively, for the turbulence modulation model of Rzehak and Krepper (2013) implemented in the present code. From Fig. 3.16, the turbulence modulation term is shifted toward the outer region of the flow, i.e. the peak value is beyond $y^+ = 100$, i.e. $1 - \frac{r}{R} = 0.065$ and it is the dominant generation term in the core region of the pipe where it balances the diffusion term. Although the level of the turbulence modulation is reduced compared to the present model, the extent of the pipe domain affected by the turbulence modulation is much greater.

For the dissipation rate budget shown in Fig. 3.17, the peak value of the turbulence modulation is also shifted outward to around $y^+ = 25$, i.e. $1 - \frac{r}{R} = 0.017$. The relative value of the turbulence modulation remains relatively small compared to the production term, however, it is significant in the core region of the pipe.

The analysis above demonstrates the usefulness of the budgets of the transport equations for the turbulence kinetic energy and dissipation rate in assessing the contribution of the turbulence modulation model. They also show that changing the time scale formulation can influence both the relative magnitude of the turbulence modulation term and also the region of the pipe where it is significant.

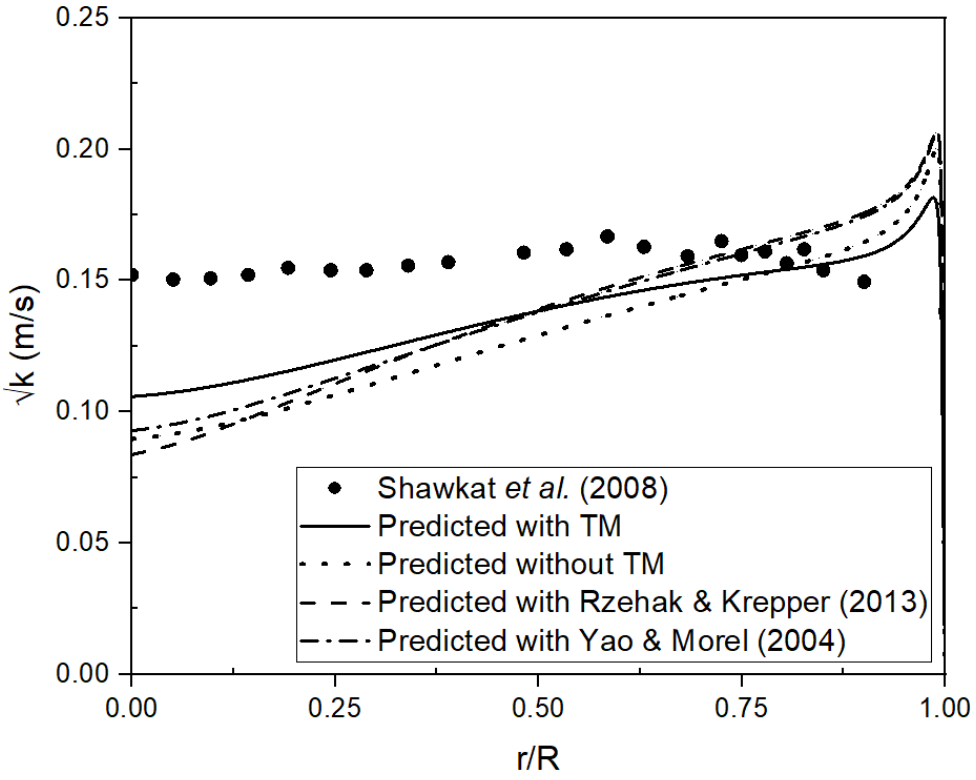

Fig. 3.18 Predicted profiles of turbulence kinetic energy for Case 8 using different turbulence modulation models.

To complete this section, Fig. 3.18 documents the effect of the turbulence modulation model on the prediction for the turbulence kinetic energy profile of the liquid phase for Case 8. More specifically, it compares the predictions for the turbulence kinetic energy using the present code and three different turbulence modulation models, i.e. the present model, and those of Rzehak and Krepper (2013), and Yao and Morel (2004). The predicted profile considering no turbulence modulation is also incorporated in the same figure. As noted previously, the effect of the turbulence modulation for the present model is mixed: it enhances the turbulence kinetic energy in the inner

region of the pipe and decreases the value near the wall. Curiously, the effect of the other two models is opposite, i.e. a suppression of the turbulence kinetic energy in the core region of the pipe and an enhancement in the outer region. Although the level of the experimental data is in general higher than all of the predicted values, it supports the trend of the present turbulence modulation model, i.e. enhancement near the centerline and suppression near the wall.

3.4 Conclusions

The present study explores the effect of the turbulence modulation on a two-fluid model prediction of fully developed turbulent bubbly upward flow in a vertical pipe. The focus of this study was on evaluating the effect of the gas phase on the turbulence of the liquid phase. All of the data available for comparison pertained to flows with a wall-peak volume fraction distribution. Some conclusions based on the comparisons documented in the paper are presented below. Firstly, the limited experimental data available show both enhancement and suppression of turbulence by the bubbles, sometimes in different regions of the same pipe flow. In some cases the turbulence modulation reproduced the experimental trend, while in other cases, the effect of the turbulence modulation on the turbulence quantities was negligible. Furthermore, in some cases where the turbulence quantities are modified by the bubbles, the effect on the mean flow properties is minimal. None of the models tested was able to consistently predict the turbulence modulation effects for the full set of tests cases considered. Although each model formulation had short comings, overall the present model, which uses source terms in the turbulence transport equations, performed as well and in some cases better than the other models tested. For the source term in the dissipation rate equation, the choice of time scale can modify the magnitude and distribution of the turbulence modulation term. For the three time scale formulations evaluated, no formulation stood out as clearly superior to the other model formulations. The predicted results also demonstrate the effect of the superficial gas and liquid phase velocities on the turbulence modulation. For example, for low bulk gas volume fractions, as the liquid superficial velocity increases, the turbulence modulation of the turbulence kinetic energy is also observed to increase. The effect of the gas superficial velocity on the turbulence modulation was observed to be much less.

One can conclude that for a two-equation RANS closure such as the $k-\varepsilon$ model, the use of source terms in the transport equations is an effective method for incorporating the effect of the

bubbles/gas phase on the liquid phase turbulence. Two critical issues that remain are the specification of the model coefficients, which likely should be expressed as functions of specific flow conditions and perhaps local flow properties, and also the choice of time scale for the source term in the dissipation rate equation, In this regard, the recent paper of Ma *et al.* (2017) demonstrates the role of DNS studies of bubbly flows in providing highly resolved data for developing and analyzing model formulations. It is also clear that in future studies the budgets for both turbulence transport equations will continue to play an important role in the assessment of new model formulations.

To conclude, including the effect of bubbles on the continuous phase turbulence through the use of additional sources terms in the turbulence transport equations remains an important issue for RANS predictions of bubbly flows. Although good progress is being made, based on comparisons between the measured data and numerical predictions, the current turbulence modulation models are limited in their ability to reproduce the effect of bubbles on the liquid phase turbulence. All model formulations, including the present version, need further development, based on more comprehensive comparisons to experimental and DNS data. Furthermore, for prediction of more complex flows, the turbulence modulation models need to be implemented in more advanced, i.e. non-isotropic, turbulence model closures, which are not limited by use of an eddy viscosity model formulation.

3.5 Acknowledgements

The authors are grateful to the Natural Sciences and Engineering Research Council of Canada (NSERC) for providing financial assistance for this research project.

Chapter 4

Numerical simulation of poly-disperse bubbly flow in a vertical pipe with a bubble coalescence and breakup model

A similar version of this chapter has been submitted as:

A. S. M. Atiqul Islam and D. J. Bergstrom, 2019. Numerical simulation of poly-disperse bubbly flow in a vertical pipe with a bubble coalescence and breakup model. International Journal of Multiphase Flow (Under Review).

- The first author conducted the simulations, post-processed and analyzed the results, and prepared the first draft of the manuscript. The first author then worked with the co-author to discuss the results and finalize the content and form of the manuscript.

Abstract

A numerical model based on the two-fluid formulation was employed for the prediction of turbulent poly-disperse gas-liquid upward flow in a vertical pipe. A poly-disperse distribution of the gas phase was implemented using the so-called inhomogeneous multiple bubble size group model. The bubble coalescence and breakup processes were modeled to redistribute the gas phase among the different bubble groups. A low Reynolds number turbulence closure was used to predict the liquid phase turbulence, and the effect of the gas phase on the liquid phase turbulence was accounted for through the turbulence modulation terms. The objectives of the study were to: (a) investigate the ability of the present model to reproduce the bubble coalescence and breakup processes, and the associated exchange of volume fraction among the bubble groups; (b) assess the performance of the inhomogeneous multiple bubble size group model based on a comparison of the predicted profiles for the gas volume fraction distribution and mean velocity to experimental data; and (c) compare the turbulence modulation for a poly-disperse bubbly flow to that for a mono-disperse flow. The results obtained from the current analysis are compared to the experimental data available, as well as other simulated results. Overall, the model reproduces many features of a bubbly flow where the variation in bubble size is significant.

4.1 Introduction

Gas-liquid flow occurs in many industrial and environmental applications, e.g. oil and gas production and nuclear reactors. With the increase in computing power, computational fluid dynamics (CFD) has become a viable tool for the analysis of such complex multiphase flows. However, CFD prediction of gas-liquid flow still presents many modeling challenges, such as the effect of the gas phase or bubbles on the liquid phase turbulence, interphase momentum exchange, and redistribution of the gas phase due to the bubble coalescence and breakup processes.

Gas-liquid flow can be categorized as either mono-disperse or poly-disperse depending on the bubble size, which for spherical bubbles is equivalent to bubble diameter. In mono-disperse gas-liquid flow, the disperse phase is characterized by a single bubble diameter, whereas poly-disperse flow contains bubbles with different diameters. In practice, most industrial gas-liquid flows are poly-disperse. Details of the analysis of the mono-disperse case are well described in other

publications, e.g. Lucas *et al.* (2001), Krepper *et al.* (2005), Frank *et al.* (2008), Rzehak *et al.* (2012), Rzehak and Krepper (2013), and Islam *et al.* (2016). The present study considers the poly-disperse case.

Typically, poly-disperse bubbly flows are analyzed using the so-called multiple size group (MUSIG) approach in which bubbles are classified into different groups based on their size. The MUSIG approach can also be divided into homogeneous and inhomogeneous formulations. When bubbles of different size move with the same velocity, this is known as the homogeneous MUSIG model. From a simulation viewpoint, this implies that a single momentum equation is solved for the continuous liquid phase and the dispersed gas phase. On the other hand, when bubbles of different size move with a distinct velocity, this is known as the inhomogeneous multiple size group (iMUSIG) model. For the iMUSIG model, one transport equation is solved for the continuous liquid phase and multiple transport equations (one for each bubble group) are solved for the dispersed gas phase (Krepper et al., 2005).

For successful modelling of gas-liquid poly-disperse bubbly flow, a number of bubble groups, with a separate radial gas fraction profiles for each bubble group, should be considered (Krepper et al., 2005). The poly-disperse distribution of bubbles and the radial separation of small and large bubbles was well predicted by Krepper *et al.* (2008) using the iMUSIG model. In poly-disperse flow, the volume fraction profile across the pipe is calculated from a separate radial force balance for each bubble group. For poly-disperse turbulent flow, bubbles can break up and coalesce with each other, which then modifies the volume fraction values of specific bubble groups due to the exchange of gas between them. A larger bubble breaks up mainly due to the shear stresses in the flow, while smaller bubbles coalesce with each other due to the interaction of turbulence and non-drag forces. The momentum transfer between bubble groups within the gaseous phase due to bubble coalescence and breakup processes has to be included in the corresponding momentum equations.

A limited set of experimental measurements of bubbly gas-liquid flow within a vertical pipe are available in the literature for documenting the physical behavior of poly-disperse flow and also verifying the predictions of computational models. The transition characteristics of upward gas-liquid flow in a large vertical pipe were investigated by Ohnuki and Akimoto (2000). They found

that the flow conditions at which bubble coalescence begins are almost the same for large and small-scale pipes. Extensive measurements, in terms of the range of gas and liquid superficial velocities, were conducted by Lucas *et al.* (2005) of the gas volume fraction and bubble size distributions for bubbly and slug flow within a vertical pipe. They used a special wire-mesh sensor to capture high resolution gas fraction data in space and time. Using a similar but improved measuring technique, Prasser *et al.* (2007) studied the evolution of the air-water flow structure in a larger diameter vertical pipe in terms of the bubble size distributions. The bubble coalescence process was observed to be the dominant mechanism in the experiment performed by Lucas *et al.* (2005), whereas the bubble break-up process was found to be more significant in the experiment conducted by Prasser *et al.* (2007). Shawkat *et al.* (2008) analyzed the turbulence characteristics of air-water bubbly flow for a large diameter vertical pipe where the bubble characteristics were measured using a dual optical probe and the liquid phase turbulence was measured using a hot-film anemometer. Their experiment considered flow rates and average gas volume fractions that were smaller compared to the experimental studies of Lucas *et al.* (2005) and Prasser *et al.* (2007). For their experiment, the radial volume fraction profile exhibits a wall-peak profile at low void fractions and changes to a centre-peak profile as the volume fraction and bubble size are increased. The radial void fraction distribution, gas and liquid mean velocity profiles and select turbulence properties of the liquid phase were measured in upward bubbly pipe flow by Hosokawa and Tomiyama (2009). The measurements were performed using image processing and laser Doppler velocimetry. Most of their gas volume fraction measurements show wall-peak profiles, since the experiment was conducted in small diameter pipes with a relatively low gas volume fraction.

In general, the prediction of poly-disperse bubbly flow with bubble coalescence and breakup requires the solution of a population balance equation that determines the spatial distribution of gas bubbles due to coalescence and breakup. Different models for including the effects of bubble coalescence and breakup (CAB) within the context of a two-fluid model formulation can be found in the literature. Some significant bubble CAB models in the literature are: the PBLS model, which combines the Prince and Blanch (1990) model for coalescence and the Luo and Svendsen (1996) model for breakup; the Average Bubble Number Density (ABND) model of Cheung *et al.* (2007); and the baseline closure model of Liao *et al.* (2015). Shen and Hibiki (2018) recently proposed a CAB model based on the one-dimensional one-group interfacial area transport equation (IATE), that was derived from an earlier model formulation of Hibiki and Ishii (2000). The original CAB

model was improved by including the contribution of the wake effect in the coalescence mechanism, and optimizing the coefficients related to the constitutive models against experimental data sets. These different CAB models have been implemented in different numerical simulations of poly-disperse turbulent bubbly flow in a vertical pipe as described below.

The performance of the MUSIG and ABND CAB models were assessed by Cheung *et al.* (2007). They found that a range of different bubble sizes in gas-liquid flow was predicted by the MUSIG model. Although the ABND model required less computational time than the MUSIG model, it provided numerical results that grossly over-predicted the volume fraction distribution (Cheung et al., 2007). Using the commercial software ANSYS CFX, Frank *et al.* (2008) reported reasonable performance using the iMUSIG model, but further improvement was required for the bubble breakup and coalescence processes. Krepper *et al.* (2008) developed a generalized iMUSIG model considering bubble coalescence and bubble fragmentation using an Eulerian modeling approach. The model was also implemented into ANSYS CFX, and was shown to be capable of describing poly-disperse bubbly flows for higher gas volume fraction values. A one-dimensional (1D) poly-disperse bubbly flow solver using a large number of bubble classes was implemented by Issa and Lucas (2009). It also accounts for the bubble induced turbulence as a source term in the k–ε turbulence closures. The improved agreement of the new model with the experimental data was attributed to a more reliable calculation of coalescence and breakup rates. However, a drawback of their model is that the value of the source term coefficient varies with the pipe diameter. The performance of two CAB models in predicting the exchange of gas volume fraction and evolution of bubble size for two experimental data sets was numerically assessed by Duan *et al.* (2011). Better predictions were obtained using the iMUSIG approach compared to the ABND model. Liao *et al.* (2011) proposed new coalescence and breakup closures for the iMUSIG model. Based on simulated results for the experimental data of Prasser *et al.* (2007), the iMUSIG model better predicted the evolution of bubble size distributions than the standard PBLS closure model. A three-dimensional (3-D) numerical model based on the two fluid formulation was implemented by Sattar *et al.* (2013). They proposed an improved source term for the population balance equation to predict the number density of different bubble classes for turbulent bubbly flow. The simulated results, which considered bubble coalescence due to the combined effect of turbulent and laminar shear stresses, and breakup due to the effect of turbulence, were in fair agreement with the experimental data. The baseline closure model was implemented in ANSYS CFX to predict poly-

disperse bubbly upward flow in a vertical pipe by Liao *et al.* (2015). They reported reasonable agreement with the measured data for the newly developed coalescence and breakup model in terms of predictions for the bubble size distribution, gas volume fraction and mean velocity profiles for a range of flow conditions. The current study adopts the baseline closure model of Liao *et al.* (2015) for the bubble coalescence and breakup process, partly because it provided a detailed description along with a discussion of physical mechanisms. Furthermore, it demonstrates considerable progress in predictions for a poly-disperse distribution of the gas bubbles using the multiple size group approach.

The present study implements the basic CAB model of Liao *et al.* (2015) in the context of a one-dimensional simulation of fully-developed bubbly flow in a vertical pipe. The CAB model is implemented using the iMUSIG concept considering two and four bubble groups, each characterized by a specific bubble size. The paper examines the capability of the model to simulate the bubble coalescence and breakup processes such that they give the correct exchange of gas volume fraction among the bubble groups based on experimental measurements. The analysis documents the performance of the iMUSIG model based on such predicted outcomes such as the volume fraction distribution, mean velocity profiles for both phases and liquid-phase turbulence properties. The turbulence modulation is compared for the case of poly-disperse and mono-disperse bubbly flow. In terms of the organization of the paper, the mathematical models and numerical method are described in section 4.2. Section 4.3 presents the simulation results along with relevant discussions, and section 4.4 provides some concluding comments.

4.2 Methodology

4.2.1 Two-fluid model formulation

The two-fluid model (TFM), which treats both the gas and liquid phase as interpenetrating continua (Drew and Passman, 1998), is used for the mathematical model. The distribution of the two phases is characterized by their corresponding local volume fraction values. The governing Reynolds-Averaged Navier-Stokes (RANS) equations for the mean velocity fields are obtained by averaging the conservation of mass and momentum equations for each phase in an Eulerian-Eulerian framework. The two phases are coupled through the pressure and interphase transfer terms in their

corresponding momentum equations. The present simulation considers one momentum equation for the liquid phase and one momentum equation for each bubble group for the gas phase. The flow being considered is turbulent upward bubbly flow in a vertical pipe. There is no swirl so that the azimuthal velocity component for each phase is zero. Furthermore, for the case of steady fully-developed flow being considered, the radial velocity component for each phase is also zero. The phasic mean momentum equations using a cylindrical coordinate system can be written as follows for the liquid and gas phases, respectively:

$$0 = -\alpha_l \frac{dP}{dz} + \alpha_l \frac{1}{r}\frac{d}{dr}\left(r\left(\mu_{eff}\ \frac{du_z}{dr}\right)\right) + \alpha_l \rho_l g - F_l \tag{4.1}$$

$$0 = -\alpha_{g,j} \frac{dP}{dz} + \alpha_{g,j} \frac{1}{r}\frac{d}{dr}\left(r\left(\mu_g\ \frac{dv_{z,j}}{dr}\right)\right) + \alpha_{g,j} \rho_g g + F_{g,j} + S_{M,j} \tag{4.2}$$

The transport equations above include the volume fractions for each phase, which are governed by the conservation constraint $\alpha_g + \alpha_l = 1.0$, where $\alpha_g = \sum_{j=1}^{n} \alpha_{g,j}$ and the subscript $j = 1, 2 \ldots n$ refers to the n bubble groups. The acceleration terms in the streamwise direction on the left hand side of each equation are zero due to the fully developed flow assumption. The four terms on the right hand side of Eq. (4.1) represent: the pressure gradient, effective stress (viscous and turbulent), body force, and interphase momentum exchange, respectively. The five terms on the right hand side of Eq. (4.2) represent: the pressure gradient, shear stress, body force, interphase momentum exchange, and momentum transfer between the bubble groups due to the bubble coalescence and breakup processes, respectively. In these equations, $F_{g,j}$ represents the interphase (drag) force for bubble group j, and the drag force for the liquid phase is given by $F_l = \sum_{j=1}^{n} F_{g,j}$. Momentum transfer between the bubble groups due to bubble coalescence and breakup is accounted for by the source term $S_{M,j}$. The net exchange of momentum due to mass transfer between bubble groups is equal to zero, i.e. $\sum_{j=1}^{n} S_{M,j} = 0$. These source terms were evaluated using the correlations of Liao *et al*. (2015) presented in following sections. The correlation of Monahan and Fox (2009) was used for the drag force, and is given in Table 4.1.

Table 4.1 Drag force relation for the mean axial momentum equation.

Drag force of Monahan and Fox (2009):
$F_{g,j} = \left(\frac{3}{4}\alpha_{g,j}\alpha_l\rho_l\frac{C_{D,j}}{d_{b,j}}\left\|v_{z,j}-u_z\right\|\left(v_{z,j}-u_z\right)\right)$
Where $C_D = \frac{24}{Re_b} + \frac{6}{1+\sqrt{Re_b}}$, $Re_b = \frac{\rho_l\|v_{z,j}-u_z\|d_b}{\mu_l}$

In this study, the effective stress model for the liquid phase is comprised of laminar and turbulent contributions. The eddy viscosity of the liquid phase was modeled using a two-equation turbulence model. Generally, turbulence for the gas phase is neglected since the density of air is negligible compared to that of the liquid. For turbulence modelling of gas-liquid flows in a pipe, a number of different turbulence models are available in the literature (Masood and Delgado, 2014). The low Reynolds number $k-\varepsilon$ model of Myong and Kasagi (1990), originally developed for single-phase flow, was implemented in the present model. It includes specialized functions to reproduce the damping of the turbulence near the wall. The effect of the bubbles on the liquid phase turbulence was modeled by additional discrete source terms in the turbulence transport equations. This specific turbulence modulation formulation was originally developed by Dhotre *et al*. (2007), however, the model coefficients have been modified. The transport equations for the turbulence kinetic energy (k) and dissipation rate of energy (ε) considering steady, fully developed pipe flow are given as follows:

$$0 = \frac{1}{r}\frac{d}{dr}\left(r\alpha_l\left(\left(\mu_l+\frac{\mu_t}{\sigma_k}\right)\frac{dk}{dr}\right)\right) + \alpha_l\mu_t\left(\frac{du_z}{dr}\right)^2 - \alpha_l\rho_l\varepsilon + C_kC_f\alpha_g\alpha_l\rho_l k \tag{4.3}$$

$$0 = \frac{1}{r}\frac{d}{dr}\left(r\alpha_l\left(\left(\mu_l+\frac{\mu_t}{\sigma_\varepsilon}\right)\frac{d\varepsilon}{dr}\right)\right) + C_1f_1\alpha_l\frac{\varepsilon}{k}\mu_t\left(\frac{du_z}{dr}\right)^2 - C_2f_2\alpha_l\rho_l\frac{\varepsilon^2}{k} + C_\varepsilon C_f\alpha_g\alpha_l\rho_l\varepsilon \tag{4.4}$$

The turbulence model parameters used in the above equations are given in Table 4.2. The values of the model coefficients are the same as those used by Myong and Kasagi (1990), and each term is also characterized by the volume fraction value of the liquid phase. The values of 0.65 and 1.0 were used for the turbulence modulation coefficients C_k and C_ε, respectively. For more explanation of the values used for C_k and C_ε, see Islam and Bergstrom (2019). For poly-disperse flow with

multiple bubble groups, the term C_f includes a separate contribution from each bubble group, as shown in Table 4.2.

Table 4.2 Model relations for the low Reynolds number $k-\varepsilon$ turbulence closure.

Effective viscosity, $\mu_{eff} = \mu_l + \mu_t$
Turbulent viscosity, $\mu_t = \frac{C_\mu f_\mu \rho_l k^2}{\varepsilon}$, $\quad f_1 = 1$
$f_2 = \left(1 - \frac{2}{9}\exp\left(-\frac{R_T}{6}\right)^2\right)\left(1 - \exp(-\frac{y^+}{5})\right)^2$, $\quad f_\mu = \left(1 - \exp(-\frac{y^+}{70})\right)\left(1 + \frac{3.45}{\sqrt{R_T}}\right)$
$y^+ = \frac{\rho_l u_\tau (R-r)}{\mu_l}$, $\quad R_T = \frac{\rho_l k^2}{\mu_l \varepsilon}$
$u_\tau = \sqrt{\frac{\tau_w}{\rho}}$, $\quad C_f = \frac{3}{4}\left\{\sum_{j=1}^{n}\left(\frac{C_{D,j}}{d_{b,j}}\right)\left(\lvert v_{z,j} - u_z\rvert\right)\right\}$
Model constants:
$C_1 = 1.40,\ \ C_2 = 1.80,\ \ C_\mu = 0.09,\ \ \sigma_k = 1.40,\ \ \sigma_\varepsilon = 1.30,\ \ C_k = 0.65,\ \ C_\varepsilon = 1.0$

4.2.2 Volume fraction prediction

A challenging aspect of the solution strategy is the methodology used to evaluate the gas volume fraction across the pipe given that the continuity equation is inherently satisfied for the present one-dimensional model. In this case, the gas volume fraction was predicted using the radial force balance method for the gas phase as outlined by Lucas *et al* (2001). The radial forces include the lift, wall, turbulent dispersion force and turbulent dispersion force based on the modified Eötvös number (Lucas *et al*., 2001). As shown in the literature, bubbles smaller than a critical size ($d_b = 5.80$ mm) tend to move towards the pipe wall, whereas bubbles larger than the critical size move towards the centre of the pipe (Lucas *et al*., 2005), and the gas volume fraction profiles for these two cases are recognized as wall-peak and centre-peak profiles, respectively. Using the correlations for the non-drag forces (outlined in Table 3) in the radial force balance shown in Eq. (4.5)

$$F^L + F^W + F^{TD} + F^{TD,Eo} = 0 \tag{4.5}$$

results in Eq. (4.6), which can be solved to predict the gas volume fraction.

$$\left(0.1k + C_{D,Eo}(Eo - 1)\right)\frac{d\alpha_g}{dr}$$

$$+\left(C_L(v_z - u_z)\frac{du_z}{dr} + C_W\left(\frac{d_b}{2}\right)(v_z - u_z)^2\left(\frac{1}{(R-r)^2} - \frac{1}{(R+r)^2}\right)\right)\alpha_g = 0 \qquad (4.6)$$

Table 4.3 Model relations for the radial force components acting on the gas phase.

Lift force (Zun, 1980), $F^L = -C_L\alpha_g\rho_l(v_z - u_z)\frac{\partial u_z}{\partial r}$
Wall force (Tomiyama *et al*., 1995), $F^W = -C_W\alpha_g\rho_l\left(\frac{d_b}{2}\right)(v_z - u_z)^2\left(\frac{1}{(R-r)^2} - \frac{1}{(R+r)^2}\right)$
Turbulent dispersion force (Lahey *et al*., 1993), $F^{TD} = -C_{TD}\rho_l k\frac{\partial\alpha_g}{\partial r}$, where $C_{TD} = 0.10$
Turbulent dispersion force based on Eötvös number (Lucas *et al*., 2001), $F^{TD,Eo} = -C_{D,Eo}\rho_l(Eo - 1)\frac{\partial\alpha_g}{\partial r}$, where $C_{D,Eo} = 0.0015\ \mathrm{m^2 \cdot s^{-2}}$
The Tomiyama (1998) lift force coefficient, $C_L = \begin{cases} \min[0.288\tanh(0.121Re_b), f(Eo_d)] & Eo_d < 4 \\ f(Eo_d) = 0.00105Eo_d^3 - 0.0159Eo_d^2 - 0.0204Eo_d + 0.474 & 4 \le Eo_d \le 10 \\ -0.29 & Eo_d > 10 \end{cases}$ where, $Eo_d = \frac{(\rho_l - \rho_g)gd_H^2}{\sigma}$, $d_H = d_b(1 + 0.163Eo^{0.757})^{1/3}$, $Eo = \frac{(\rho_l - \rho_g)gd_b^2}{\sigma}$
The Tomiyama (1998) wall force coefficient, $C_W = \begin{cases} \exp(-0.933Eo + 0.179) & 1 \le Eo \le 5 \\ 0.007Eo + 0.04 & 5 < Eo \le 33 \end{cases}$

The wall force model of Tomiyama (1998) and the model of Lahey *et al*. (1993) for the turbulent dispersion force were used in the present study. The force model relations along with their coefficients as described in the Table 4.3 have been modified to obtain better agreement with the experimental data in mono-disperse flow (Islam *et al*., 2016; Islam and Bergstrom, 2019). Again, for the case of poly-disperse flow with multiple bubble groups, a separate force balance equation is solved to determine the volume fraction $\alpha_{g,j}$ for each bubble group.

4.2.3 Bubble coalescence and breakup mechanism

The development of the gas-liquid bubbly flow structure inside the pipe is determined by the interaction between the non-drag forces and the process of bubble coalescence and breakup (Lucas *et al*., 2001). The radial forces, which act perpendicular to the flow direction, are responsible for the lateral movement of bubbles in the pipe. A schematic of the coalescence and breakup process in a vertical pipe is shown in Fig. 4.1. Beginning from bottom of the pipe as shown in Fig. 4.1, smaller bubbles for air-water flow move towards the pipe wall due to the action of a positive lift force acting towards the wall of the pipe. The outward movement of the bubbles results in a gas volume fraction profile that has a peak value near the wall, i.e. the wall-peak case. The bubble coalescence and breakup events are in steady state at that point and a stable bubbly flow is observed (Krepper *et al*., 2008). However, as the flow develops further, the smaller bubbles accumulated near the wall coalesce with each other due to the effects of turbulence and shear stress, eventually forming larger bubbles. The lift force changes its direction depending on the bubble size, so that the negative lift force acting on the larger bubbles will drive these bubbles away from the wall towards the centre of the pipe. Experimental results (Lucas *et al*., 2005) indicate that bubbles with diameter larger than 5.80 mm (Tomiyama, 1998) are likely to be found in the centre region of the pipe. This results in an average gas volume fraction profile that shows a peak value at the centre, referred to as the centre-peak case. The bubble breakup rate increases as the size of the bubble increases and the frequency of bubble breakup also increases with the dissipation rate of turbulence kinetic energy (Luo and Svendsen, 1996). The dissipation rate of turbulence kinetic energy is higher near the wall of the pipe, so that larger bubbles near the wall break up (as shown in Fig. 4.1) due to the consequences of turbulence. Some of the larger bubbles generated by the coalescence of smaller bubbles in the wall region are also transported into the centre region of the pipe without further breakup. These bubbles then grow in size because of additional coalescence events corresponding with lower breakup rates, which is typical for the lower shear region in the centre of the pipe (Krepper *et al*., 2005). As described above, the bubble coalescence and breakup processes plays an important role in the formation of small and large bubbles, which clearly influences the development of the flow structure within the pipe. The effects of these physical mechanisms need to be included in the numerical model for predicting gas-liquid bubbly flow.

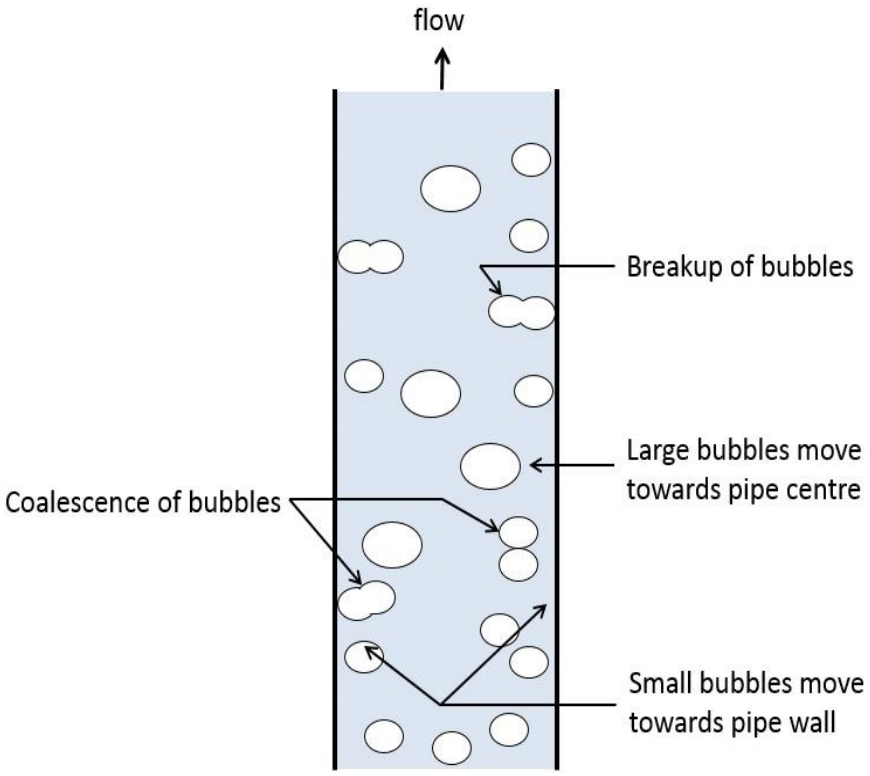

Fig. 4.1. Upward air-water flow with bubble coalescence and breakup processes (reproduced from the study of Krepper *et al.* (2008)).

4.2.4 Bubble coalescence and breakup model

For the present simulations, the baseline model of Liao *et al.* (2015) was used to evaluate the momentum source terms due to the bubble coalescence and breakup processes. The present model formulation differs from that of Liao *et al.* (2015) in that each velocity group contains only one bubble size, so that the distinction between velocity and bubble group becomes meaningless. Therefore, in the present model, we only refer to the bubble group indicated by the subscript j. The bubble diameter for each bubble group is assumed to be the Sauter mean diameter.

In order to simplify the model explanation, the description of the bubble coalescence and breakup calculation outlined in this section considers only two bubble groups, where bubble group $j = 1$ has a smaller diameter than bubble group $j = 2$. The quantity, $S_{M,j}$ which represents the source

term in the momentum equation given by Eq. (4.2) is calculated as follows for bubble group $j = 1$ and 2, respectively:

$$S_{M,1} = \max(S_1, 0)\, v_{z,2} - \max(S_2, 0)\, v_{z,1} \tag{4.7}$$

$$S_{M,2} = \max(S_2, 0)\, v_{z,1} - \max(S_1, 0)\, v_{z,2} \tag{4.8}$$

where S_j is the net volumetric mass flux for bubble group j. For the simple case of only two bubble groups, the expressions above are able to track the appropriate momentum associated with the exchange of mass between different bubble groups. For example, if the net volumetric mass exchange S_1 for bubble group $j = 1$ is positive, then that mass must be generated by the breakup of bubble group $j = 2$ and bring in specific velocity $v_{z,2}$. Note that the net volumetric mass exchange given by the sum of the mass source term for both bubble groups is equal to zero due to mass conservation, i.e. $S_1 + S_2 = 0$.

For the general case where bubble group j is interacting with multiple other bubble groups, some smaller and some larger, calculation of the net volumetric mass flux is much more complicated. The mass source term for a generic bubble group j is comprised of four parts, namely: the birth rates of bubbles in size group j caused by the breakup of larger size bubbles and coalescence of smaller size bubbles, denoted $B_{B,j}$ and $B_{C,j}$, respectively, and the death rates of bubbles in size group j due to the breakup into smaller bubbles and coalescence with other bubbles to form a larger bubble, denoted $D_{B,j}$ and $D_{C,j}$, respectively. The mass source for bubble group j can be calculated using the following population balance Eq. (4.9) of Liao *et al*. (2015), which is given by,

$$S_j = B_{B,j} - D_{B,j} + B_{C,j} - D_{C,j} \tag{4.9}$$

where

$$B_{B,j} = \alpha_{g,j}\rho_g \textstyle\sum_{i>j} \Omega(m_i, m_j) \tag{4.10}$$

$$D_{B,j} = \alpha_{g,j}\rho_g \textstyle\sum_{i<j} \Omega\left(m_j, m_i\right) \tag{4.11}$$

$$B_{C,j} = \left(\alpha_{g,j}\rho_g\right)^2 \left(\tfrac{1}{2}\textstyle\sum_{l<j}\sum_{i<j} \Gamma(m_l, m_i) X_{ilj} \frac{m_l + m_i}{m_l m_i}\right) \tag{4.12}$$

$$D_{C,j} = \left(\alpha_{g,j}\rho_g\right)^2 \left(\textstyle\sum_i \Gamma(m_j, m_i) \frac{1}{m_i}\right) \tag{4.13}$$

and m_j is the mass of bubble group j. In the equations above, $\Omega(m_i, m_j)$ is the frequency of a bubble from size group i breaking up into smaller bubbles in group j. Likewise, $\Gamma(m_l, m_i)$ is the frequency of coalescence between two bubbles from size groups l and i. The quantity X_{ilj} represents the coalescence mass matrix, which is used to determine the fraction of mass due to the coalescence between groups i and l that eventually transfers to group j. The coalescence mass matrix is evaluated in the following manner (Duan *et al*., 2011):

$$X_{ilj} = \begin{cases} 1 & if\ m_l + m_i > m_j \\ 0 & otherwise \end{cases} \tag{4.14}$$

Note that this model for the coalescence mass matrix is different from that used by Liao *et al.* (2015). Once the net volumetric mass flux for bubble group *j* is determined, it is used as the source term in the following continuity equation for each bubble group:

$$\frac{d}{dt}\left(\alpha_{g,j}\rho_g\right) = S_j \tag{4.15}$$

Eq. (4.15) is used to update the volume fraction for each bubble group. Finally, for the general case of multiple bubble groups, each contribution to the net volumetric mass flux (source term) of a specific bubble group will bring a different specific momentum with it, which then needs to be tracked in evaluating the source term in the momentum equation for each bubble group. The following subsections present brief descriptions of the expressions used for the bubble coalescence and breakup frequencies in the population balance equation following Liao *et al.* (2015).

4.2.4.1 Bubble coalescence frequency Γ

Bubble coalescence is considered to be a more complex process than bubble breakup since it involves the collision of bubbles with the surrounding liquid as well as the collision between bubbles (Liao *et al.*, 2015). In the present analysis, the coalescence effect was evaluated using the following correlation, which takes into account the most significant effects, i.e. turbulence, buoyancy and shear. It is assumed that a collision between two bubbles can lead to either a coalescence or re-separation event. For a collision, the total coalescence frequency between two bubbles of size group i and j can be calculated as follows:

$$\Gamma(m_i, m_j) = \frac{\alpha_{g,max}}{\alpha_{g,max}-\alpha_g}(\Gamma_{turb} + \Gamma_{buoy} + \Gamma_{shear}) \quad (4.16)$$

where $\alpha_{g,max} = 0.80$ represents the maximum packing limit of the bubbles (Wang *et al.*, 2005).

In general, the coalescence frequency Γ is expressed as the product of a collision frequency, h, and coalescence efficiency, λ, i.e.

$$\Gamma = h\,\lambda \quad (4.17)$$

The specific coalescence frequency expressions for turbulence, buoyancy and shear are described later in this section. The collision frequency between two bubbles is modelled based on gas kinetic theory and is approximated by the volume swept by the bubbles per unit time, i.e.

$$h = A\,u_{rel} \quad (4.18)$$

where u_{rel} is the relative approach velocity between the two bubbles and A is the effective cross-sectional area for the collision. Due to the turbulent fluctuations, bubbles can approach each other from any direction and the effective cross-sectional area for collision between two bubbles is given by:

$$A_{turb} = \frac{\pi}{4}(d_i + d_j)^2 \quad (4.19)$$

The relative velocity for two bubbles with diameters d_i and d_j can be estimated by the root mean square of the turbulent fluctuation velocity following Liao *et al.* (2015), i.e.

$$u_{rel,turb} = \left({u_{turb,i}}^2 + {u_{turb,j}}^2\right)^{1/2} \quad (4.20)$$

where the turbulent fluctuation velocity $u_{turb,i}$ for a bubble with diameter d_i is calculated as follows:

$$u_{turb,i} = \sqrt{2}(\varepsilon d_i)^{1/3} \quad (4.21)$$

based on the local dissipation rate, ε. This relation approximates the turbulent fluctuation velocity over a distance of d_i in the inertial subrange (Hinze, 975). Therefore, the coalescence frequency between two single bubbles considering turbulence induced collision is expressed as:

$$\Gamma_{turb} = \frac{\pi}{4}\left(d_i + d_j\right)^2 C_{turb}\sqrt{2}(d_i^{2/3} + d_j{}^{2/3})^{1/2}\varepsilon^{1/3}\lambda_{inertial} \quad (4.22)$$

where $\lambda_{inertial}$ represents the coalescence efficiency (given below) in the inertial collision region, i.e. for bubbles much larger than the Kolmogorov length scale (η).

For body forces such as buoyancy, a collision between bubbles in upward flow is only possible if the faster bubble comes in contact with the slower one from behind. A probability factor of 0.50 is included following Liao *et al.* (2015) for the coalescence frequency correlation due to buoyancy given below,

$$\Gamma_{buoy} = 0.5\frac{\pi}{4}\left(d_i + d_j\right)^2 C_{buoy}\left|u_{T,i} - u_{T,j}\right|\lambda_{inertial} \quad (4.23)$$

where, $\left|u_{T,i} - u_{T,j}\right|$ represents the relative velocity ($u_{rel,buoy}$) for two bubbles with diameters d_i and d_j due to buoyancy. $u_{T,i}$ is the bubble rise or terminal velocity of a bubble with diameter d_i and the inertial coalescence efficiency is used for the present case where all of the bubbles are larger than the Kolmogorov length scale. The terminal velocity ($u_{T,i}$) of a bubble with diameter d_i in equation 4.23 is calculated using the following expression, $u_{T,i} = \sqrt{\frac{4gd_{\mathrm{b,i}}}{3C_d}\left(\frac{\rho_l - \rho_g}{\rho_l}\right)}$.

For a shear-induced collision, a bubble chases and catches a preceding one in the direction of the mean velocity field from the higher velocity side. A probability factor of 0.50 is also included in this collision mechanism due to the dependence on the relative position of the bubbles (Liao *et al.*, 2015). The coalescence frequency between bubble i and bubble j caused by the mean shear is given by

$$\Gamma_{shear} = 0.5\frac{\pi}{4}\left(d_i + d_j\right)^2 C_{shear}\left[\frac{0.5}{\pi}(d_i + d_j)\dot{\gamma}_b\right]\lambda_{inertial} \quad (4.24)$$

where, $\frac{0.5}{\pi}(d_i + d_j)\dot{\gamma}_b$ is the relative velocity ($u_{rel,shear}$) for two bubbles with diameters d_i and d_j due to shear.

and $\dot{\gamma}_b$ is the shear strain rate of the bulk flow defined as

$$\dot{\gamma}_b = \sqrt{2}\left|\left(\frac{du_z}{dr}\right)\right| \quad (4.25)$$

In Eqs. (4.22), (4.23) and (4.24) above, the empirical constants C_{turb}, C_{buoy} and C_{shear} are introduced to reflect the approximate nature of the model relations. However, in the present analysis, the values of the constants were set to unity following Liao *et al.* (2015).

The coalescence efficiency $\lambda_{inertial}$, for an inertial collision is evaluated based on the collision Weber number (We), i.e.

$$\lambda_{inertial} = \exp(-C_{eff} We_{ij,max}^{0.5}) \tag{4.26}$$

where the maximum Weber number $We_{ij,max}$ is given by

$$We_{ij,max} = \frac{\rho_l d_{eq}}{\sigma} \ u_{rel}{}^2 \tag{4.27}$$

and the maximum relative velocity is computed as

$$u_{rel} = \max\left(u_{rel,turb}, u_{rel,buoy}, u_{rel,shear}\right) \tag{4.28}$$

The equivalent diameter d_{eq} of the two colliding bubbles is calculated by

$$d_{eq} = \frac{2 d_i d_j}{d_i + d_j} \tag{4.29}$$

The value of $\sigma = 0.07199$ ($\frac{N}{m}$) and the value of $C_{eff} = 5.0$ were used in the present calculations following Liao *et al.* (2015). Note that the coalescence frequency decreases as the value of the Weber number increases and vice versa (Eq. 4.26). The overall coalescence frequency is calculated from Eq. (4.16) based on the cumulative coalescence events given by Γ_{turb}, Γ_{buoy}, and Γ_{shear} based on Eqs. (4.22), (4.23), and (4.24), respectively.

4.2.4.2 Bubble breakup frequency Ω

A bubble breaks up due to destroying and restoring stresses. Generally, for a gas-liquid poly-disperse pipe flow, a bubble flowing within the liquid experiences a destroying stress τ that acts to deform and break up the gas bubble. At the same time, a restoring force is supplied by the surface tension, which also determines the critical stress τ_{crit} that is necessary for a break-up event

to take place (Liao *et al.*, 2015). A bubble will break up once the destroying stress surpasses the critical stress, i.e. $\tau > \tau_{crit}$. The destroying stress (τ) responsible for a bubble break-up event can occur due to different mechanisms, such as turbulent velocity fluctuations, turbulent shear, laminar shear and interfacial drag or friction. However, break-up by turbulent shear is not present when the Kolmogorov length scale (η) is much smaller than the bubble size. Therefore, the break-up effect was evaluated using the following correlation of Liao *et al.* (2015) considering turbulent velocity fluctuation, laminar shear force caused by the mean velocity gradient and friction effects. Finally, the break-up frequency is calculated based on the two above mentioned competing stresses, i.e. the destroying (τ) and restoring stress (τ_{crit}). As reported by Liao *et al.* (2015), the frequency of a bubble of size d_i breaking up into bubbles of size d_j has the following dependence on τ and τ_{crit}:

$$\Omega(d_i, d_j) = \begin{cases} \frac{1}{d_i}\sqrt{\frac{\tau(d_i)-\tau_{crit}(d_i,d_j)}{\rho_l}} & \tau > \tau_{crit} \\ 0 & \tau \leq \tau_{crit} \end{cases} \tag{4.30}$$

There are two different approaches available in the literature to evaluate the critical stress. One of them is based on energy ($\tau_{crit,1}$) while the second is based on forces ($\tau_{crit,2}$). In this analysis a mixed break-up constraint (τ_{crit}) is used: it is obtained as follows (Liao *et al.*, 2015):

$$\tau_{crit} = max\{\tau_{crit,1}, \tau_{crit,2}\} \tag{4.31}$$

The critical stress based on energy constraints $\tau_{crit,1}$ is obtained from the correlation of Luo and Svendsen (1996), i.e.

$$\tau_{crit,1} = E_{\sigma,j} + E_{\sigma,k} - E_{\sigma,i} = \frac{6\sigma}{d_i}\left(\left(\frac{d_j}{d_i}\right)^2 + \left(\frac{d_k}{d_i}\right)^2 - 1\right) \tag{4.32}$$

where, bubble with diameter d_i breaks into two different sized bubbles of diameter d_j and d_k as a consequence of the destroying stress. E_σ is the surface energy of a bubble and d_k is determined as follows:

$$d_k = \left(d_i^3 - d_j^3\right)^{1/3} \tag{4.33}$$

On the other hand, the critical stress based on force constraints $\tau_{crit,2}$ is determined from the capillary action of the smallest daughter bubble in the following manner:

$$\tau_{crit,2} = \frac{\sigma}{\min(d_k, d_j)} \tag{4.34}$$

The correlations for the destroying stress associated with each of the three mechanisms mentioned above are outlined below (Liao *et al.*, 2015),

1) Destroying stress caused by turbulent velocity fluctuation:

$$\tau_{turb} = B_{turb}\frac{1}{2}\rho_l u_{turb,i}^2 = B_{turb}\rho_l(\varepsilon d_i)^{2/3} \qquad (d_i > \eta) \tag{4.35}$$

2) Destroying stress because of velocity gradients in the bulk flow:

$$\tau_{shear} = B_{shear}\mu_l\dot{\gamma}_b \tag{4.36}$$

where, $\dot{\gamma}_b$ is the shear strain rate of the bulk flow defined as

$$\dot{\gamma}_b = \sqrt{2}\left|\left(\frac{du_z}{dr}\right)\right| \tag{4.37}$$

3) Destroying stress due to interfacial drag or friction:

$$\tau_{fric} = B_{fric}0.5\rho_l {u_{T,i}}^2 C_{D,i} \tag{4.38}$$

where, $C_{D,i}$ is the drag force for the bubble i. For the model adopted, the following values are used for the break-up model constants as recommended by Liao *et al.* (2015).

$$B_{turb} = B_{shear} = 1.0,\ B_{fric} = 0.25$$

Unlike the coalescence frequency mechanism, the bubble break-up frequency is determined from Eq. (4.30) based on the maximum value of the destroying stress for the three different mechanisms calculated from Eqs. (4.35), (4.36) and (4.38). The break-up frequency was then used in the population balance equation, Eq. (4.9), to determine S_1 and S_2, and subsequently in the evaluation of $S_{M,1}$ and $S_{M,2}$ from Eqs. (4.7) and (4.8), respectively.

4.2.5 Boundary conditions and numerical method

For the present numerical analysis, no-slip boundary conditions were used at the wall following the study of Ekambara *et al.* (2005) and Dhotre *et al.* (2007), and symmetry boundary conditions were applied at the centerline of the pipe for both phases, i.e.

At the centre: $\frac{du_z}{dr} = 0, \quad \frac{dv_z}{dr} = 0, \quad \frac{dk}{dr} = 0, \quad \frac{d\varepsilon}{dr} = 0, \quad \frac{d\alpha_g}{dr} = 0$ (4.39)

At the wall: $u_z = 0, \quad v_z = 0, \quad k = 0, \quad \varepsilon = \nu\left(\frac{d^2k}{dr^2}\right), \quad \alpha_g = 0$ (4.40)

The transport equations were discretized using the cell-centered finite volume method of Patankar (1980). The coupled discrete transport equations (Eqs. (4.1), (4.2), (4.3), (4.4) and (4.6)) were solved applying an iterative procedure using a tri-diagonal matrix algorithm with under-relaxation. A discrete formulation of the CAB model was implemented to redistribute the gas volume fraction among the bubble groups in the present numerical simulation. The simulation employed a non-uniform grid refined in the near-wall region where the gradients of the mean variables are very steep. The convergence criteria, i.e. the normalized difference in the value of the field variables for two successive iterations was set to 0.0001. For the selected test cases, a grid of 80 control volumes was used with the first numerical node located at $y^+ \cong 0.80$. A grid sensitivity analysis was conducted which indicated the predicted value of the gas volume fraction changed by less than 0.25% when the number of control volume was increased from 80 to 120 for all the considered test cases.

4.3 Results and discussion

The main objective of the present study is to investigate the effect of the bubble coalescence and breakup process on the predicted gas volume fraction profiles, especially with respect to the exchange of gas among the different bubble groups. Limited experimental data sets are available in the literature to describe turbulent gas-liquid poly-disperse flow within a vertical pipe. Furthermore, in those studies that do exist, the set of measured flow variables is incomplete. In this paper, the experimental study of Lucas *et al.* (2005) was selected for comparison, since it documented the measured gas volume fraction along with mean bubble size for multiple bubble

groups. The iMUSIG model was tested against the measured data along with other simulated results. Both two and four bubble groups were considered, and the gas phase mean velocity profiles of each bubble group are used to assess the model performance. The results and discussion section is divided into four parts. Section 4.1 documents a comparison of the predictions for the volume fraction profiles considering both two and four bubble groups. It specifically examines the ability of the iMUSIG model to redistribute the gas phase among different bubble groups. The mean flow properties, including comparisons to other model formulations, and sample coalescence and breakup frequency profiles are presented in section 4.2 and 4.3, respectively. Finally, the turbulence modulation and associated turbulence kinetic energy profiles are compared for mono-disperse and poly-disperse flows in section 4.4.

4.3.1 Volume fraction prediction for multiple bubble groups

This section presents the predicted gas volume fraction distribution considering two and four bubble groups, both with and without the coalescence and breakup model. For the volume fraction analysis, the experimental test case 118 of Lucas *et al.* (2005) was simulated; the prediction of Krepper *et al.* (2008) has also been included for comparison. The corresponding experimental data for the two and four bubble group cases, as documented by Krepper *et al.* (2008), are listed in the Table 4.4 and 4.5, respectively. An axial pressure gradient of $\frac{\mathrm{dP}}{\mathrm{dZ}} = 10450$ (N/m^3) was used for the simulations of the experimental flow conditions documented in Table 4.4 and 4.5. Note that each bubble group is characterized by a single bubble size, and that based on the bubble diameter, both bubble groups include wall-peak and centre-peak cases.

Table 4.4 Experimental flow conditions for two bubble groups (Lucas *et al.*, 2005)

No.	Parameters	$j = 1$	$j = 2$
1	Superficial liquid velocity, J_L [m/s]	1.017	1.017
2	Superficial gas velocity, J_G [m/s]	0.219	0.219
3	Pipe diameter, D [m]	0.0512	0.0512
4	Mean bubble diameter, d_b [m]	0.00495	0.01255
5	Average gas volume fraction, $\overline{\alpha_g}$	0.04	0.16

Table 4.5 Experimental flow conditions for four bubble groups (Lucas *et al.*, 2005)

No.	Parameters	$j = 1$	$j = 2$	$j = 3$	$j = 4$
1	Superficial liquid velocity, J_L [m/s]	1.017	1.017	1.017	1.017
2	Superficial gas velocity, J_G [m/s]	0.219	0.219	0.219	0.219
3	Pipe diameter, D [m]	0.0512	0.0512	0.0512	0.0512
4	Mean bubble diameter, d_b [m]	0.00376	0.00495	0.00610	0.01255
5	Average gas volume fraction, $\overline{\alpha_g}$	0.01	0.030	0.035	0.125

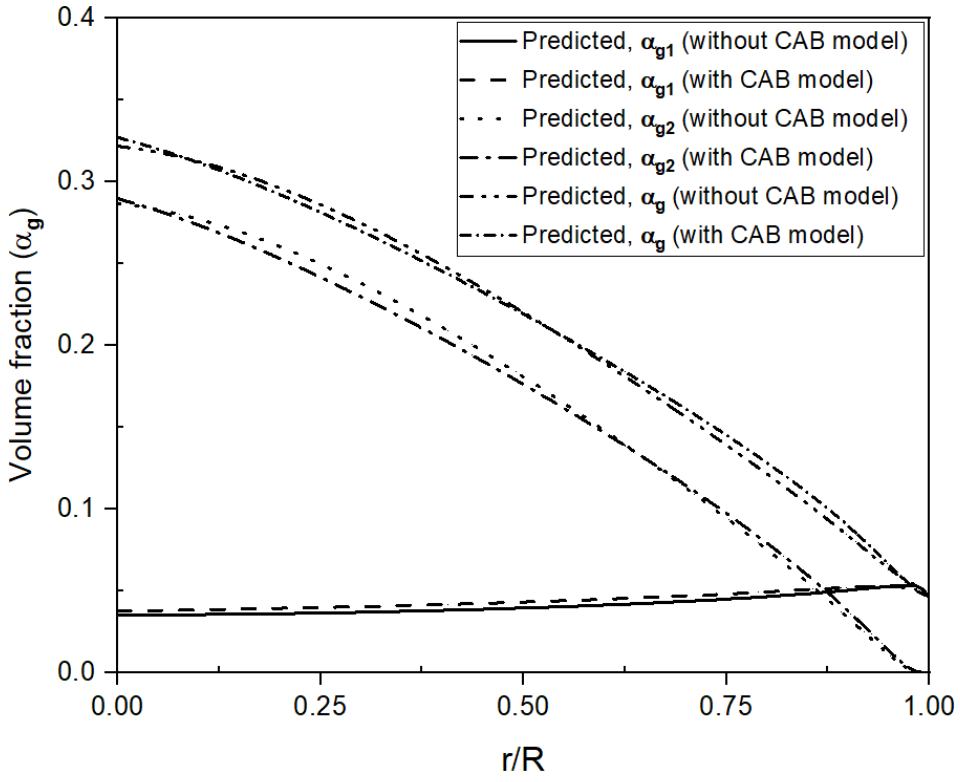

Fig. 4.2. Gas volume fraction profiles with and without coalescence and breakup models.

Fig. 4.2 presents the predicted gas volume fraction profiles with and without the coalescence and breakup model for the case of two bubble groups. For this simulation, the initial bulk volume fraction for each bubble group was specified from Table 4.4. The figure gives the predicted gas volume fraction profile for each bubble group, as well as the total gas volume fraction profile. The bubble group of smaller size with volume fraction α_{g1} and bubble group of larger size with volume fraction α_{g2} represent typical wall-peak and centre-peak gas volume fraction profiles, respectively, as determined by Tomiyama (1998). The change in the gas volume fraction profiles when using the CAB model, compared to the profiles predicted without the CAB model, is due to the gas

exchanged between the bubble groups. Overall, the CAB model resulted in minimal change to the gas volume fraction profiles. This confirms that when the correct bulk gas volume profile is specified, the net change due to coalescence and breakup is negligible.

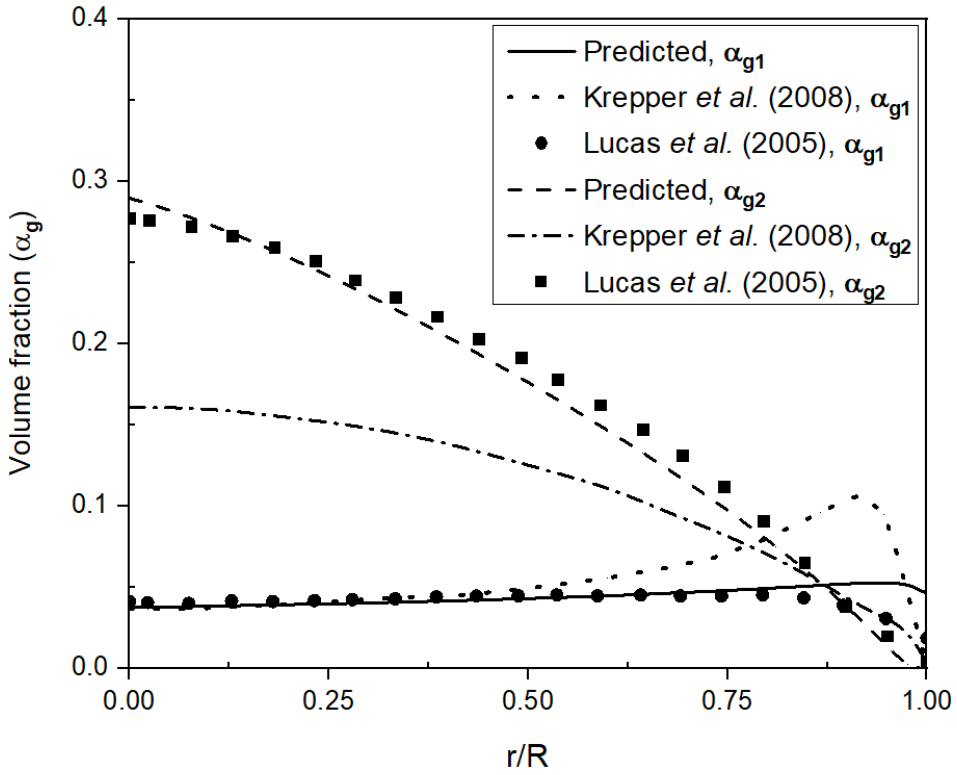

Fig. 4.3. Comparison of predicted gas volume fraction profiles with experimental data for two bubble groups.

For the same two bubble groups, Fig. 4.3 compares the predictions for the gas volume fraction profiles using the CAB model to the experimental measurements of Lucas *et al.* (2005), as well as the simulations of Krepper *et al.* (2008). The predictions with the present model are generally in good agreement with the experimental data, although the gas volume fraction profile for the first bubble group was too high near the wall. In comparison, the profiles predicted by Krepper *et al.* (2008) show significant deviation from the experimental results. This can be partly attributed to the fact that the current model used the CAB model of Liao *et al.* (2015), whereas Krepper *et al.* (2008) used the bubble breakup model of Luo and Svendsen (1996) and the bubble coalescence model of Prince and Blanch (1990).

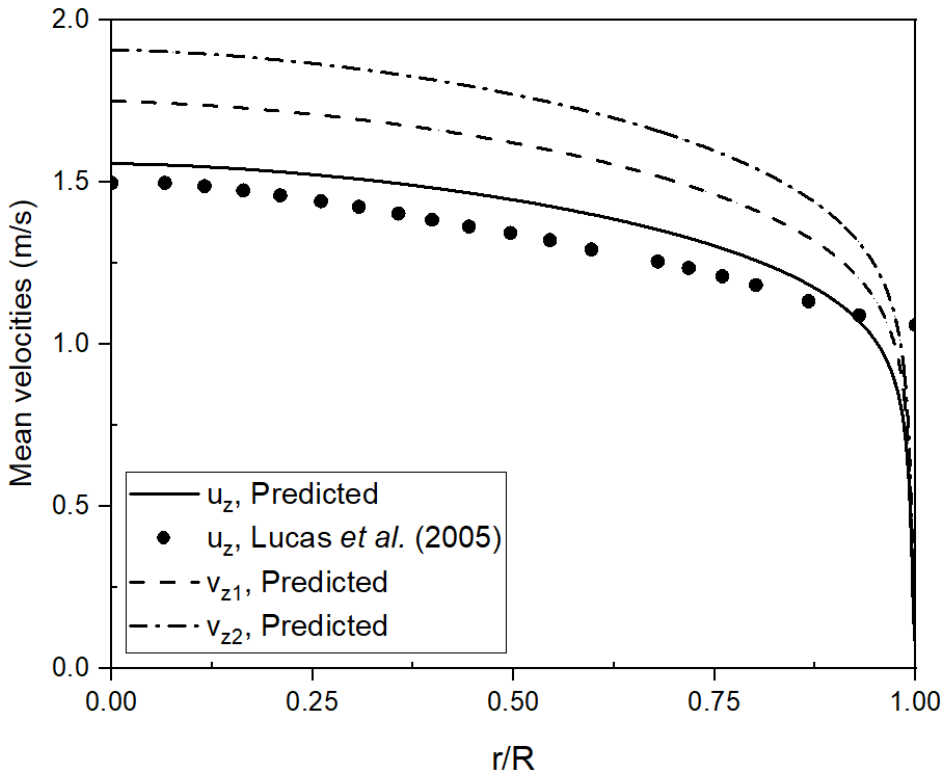

Fig. 4.4. Mean velocity profiles for both phases.

Fig. 4.4 presents the mean velocity profiles of both phases for the two bubble groups given in Table 4.4. Recall that the iMUSIG model adopted in the present study considers a separate momentum equation for each bubble group, which is illustrated in Fig. 4.4. The predicted profile for the liquid phase mean velocity sits somewhat above the measured data, but captures the general shape. At the wall, the experimental data show a finite velocity, whereas the predicted profile drops to zero at the wall due to the no-slip condition. In Fig. 4, v_{z1} and v_{z2} represent the velocity profile corresponding to the small and large bubble groups, respectively. The mean velocity for the large bubble (v_{z2}) group is found to be greater than for the small bubble (v_{z1}) group because of the larger buoyancy force for the larger bubble group.

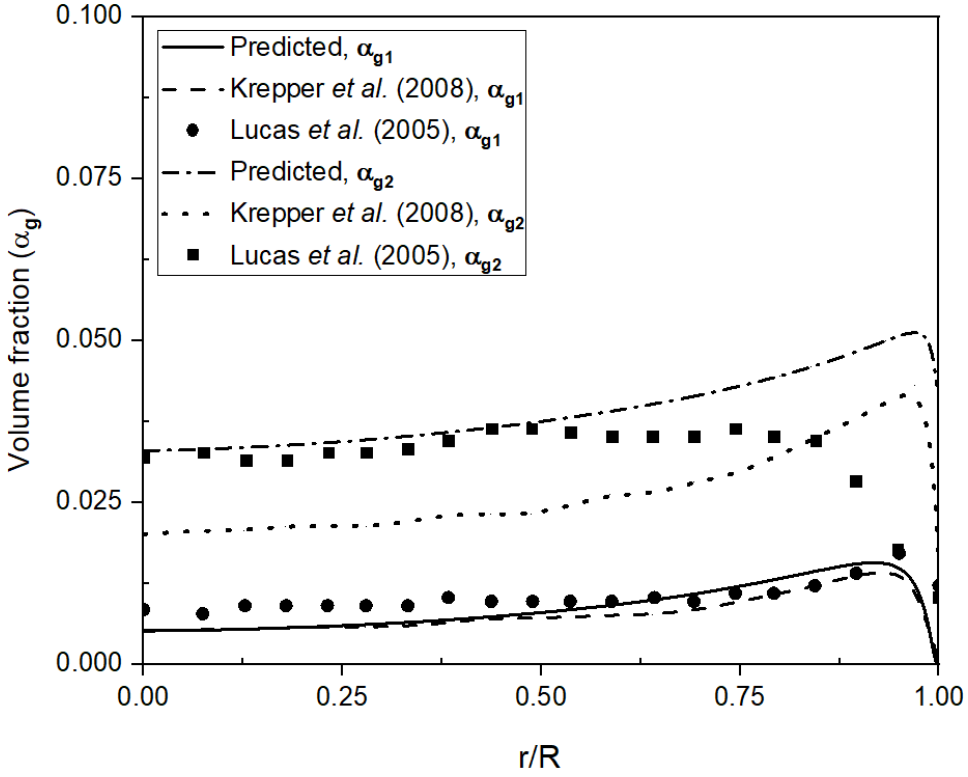
Predicted, α_{g1}
Krepper *et al.* (2008), α_{g1}
Lucas *et al.* (2005), α_{g1}
Predicted, α_{g2}
Krepper *et al.* (2008), α_{g2}
Lucas *et al.* (2005), α_{g2}
Volume fraction (α_g)
0.100
0.075
0.050
0.025
0.000
0.00
0.25
0.50
0.75
1.00
r/R

(a)

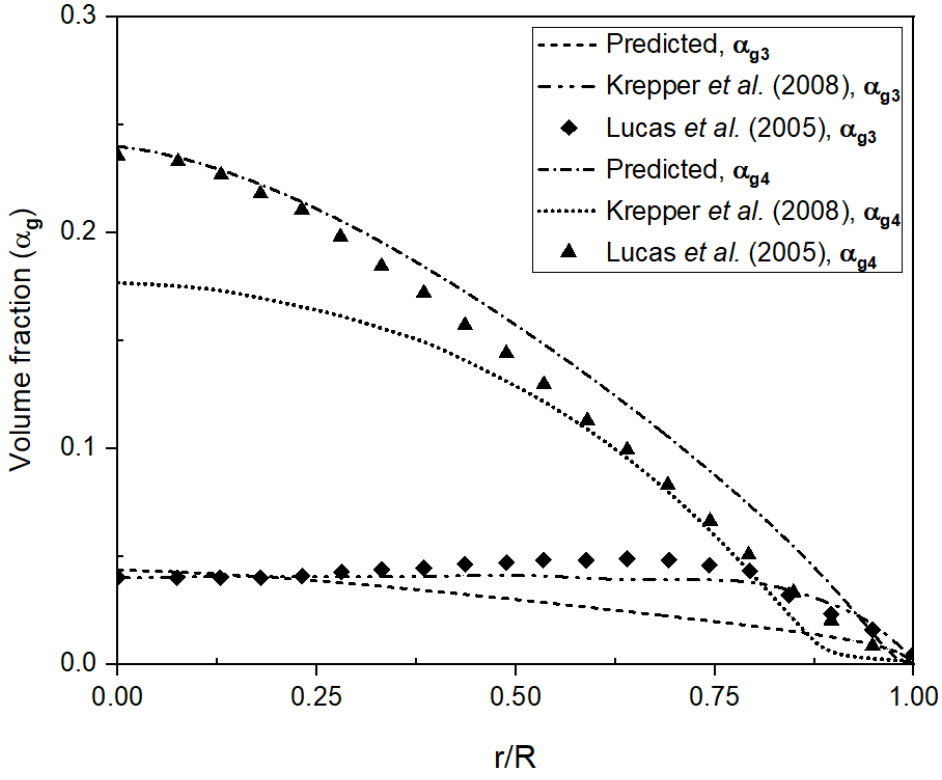
Predicted, α_{g3}
Krepper *et al.* (2008), α_{g3}
Lucas *et al.* (2005), α_{g3}
Predicted, α_{g4}
Krepper *et al.* (2008), α_{g4}
Lucas *et al.* (2005), α_{g4}
Volume fraction (α_g)
0.3
0.2
0.1
0.0
0.00
0.25
0.50
0.75
1.00
r/R

(b)

Fig. 4.5. Comparison of predicted gas volume fraction profiles with experimental data for four bubble groups: a) groups 1 and 2, and b) groups 3 and 4.

Fig. 4.5 compares the predicted gas volume fraction profiles with the experimental data of Lucas *et al.* (2005) as well as the numerical simulations of Krepper *et al.* (2008) for four bubble groups using the CAB model. The equivalent bubble diameter for the four bubble groups and their corresponding average gas volume fractions were used as the input parameters for the current simulation (see Table 4.5). Both the present model and that of Krepper *et al.* (2008) do a good job of reproducing the experimental profile for the first bubble group (α_{g1}). For the second bubble group (α_{g2}), the present model captures the experimental profile in the core of the pipe, but predicts a peak value at the wall that is not present in the experimental results. The profile predicted by Krepper *et al.* (2008) is uniformly too low, and also includes an erroneous wall-peak value. Note that the bubble size of the second group is close to the transition range between the centre-peak and wall-peak case, which may explain the prediction of a wall-peak value. For the third bubble group (α_{g3}) the profile predicted by Krepper *et al.* (2008) is very close to the experimental profile, whereas the present model under-predicts the gas volume fraction in the near-wall region. For the fourth bubble group (α_{g4}) the present model over-predicts the experimental gas-volume fraction profile in the region near the wall, whereas the model of Krepper *et al.* (2008) under-predicts the experimental profile near the centre of the pipe. Overall, for the case of four bubble groups, both numerical models generally capture the gas volume fraction distribution measured for each bubble group, but also show some deviation from the experimental result in specific regions of the pipe. As such, the present CAB model, as well as that of Krepper *et al.* (2008), distribute the gas phase between bubble groups in a manner that is close to the experimental result. The individual gas mean velocity profiles were also calculated for the four bubble groups and they show a similar trend (not shown) to the behavior of the two bubble groups, i.e. the larger bubble groups have a higher bulk mean velocity.

To further assess the ability of the present iMUSIG model formulation to correctly redistribute the gas phase between different bubble groups, the four bubble group case considered by Lucas *et al.* (2005) was simulated using an iterative procedure based on different initial values of the bulk volume fractions of each bubble group. More specifically, in the first case the experimentally measured (correct) values were used as the initial conditions, and in the second case, the initial

values were specified to be quite different (unknown) compared to those in the experiment. The initial and final values are documented in Table 4.6 below. Note that for both sets of initial values, the overall bulk gas volume fraction was conserved.

Table 4.6 Comparison between the predicted and experimental value of bulk gas volume fraction.

Bubble group no.	Correct initial bulk volume fraction	Erroneous initial bulk volume fraction	Final predicted bulk volume fraction	Experimental bulk volume fraction
$j = 1$	0.01	0.125	0.007	0.01
$j = 2$	0.03	0.035	0.037	0.03
$j = 3$	0.035	0.03	0.027	0.035
$j = 4$	0.125	0.01	0.129	0.125

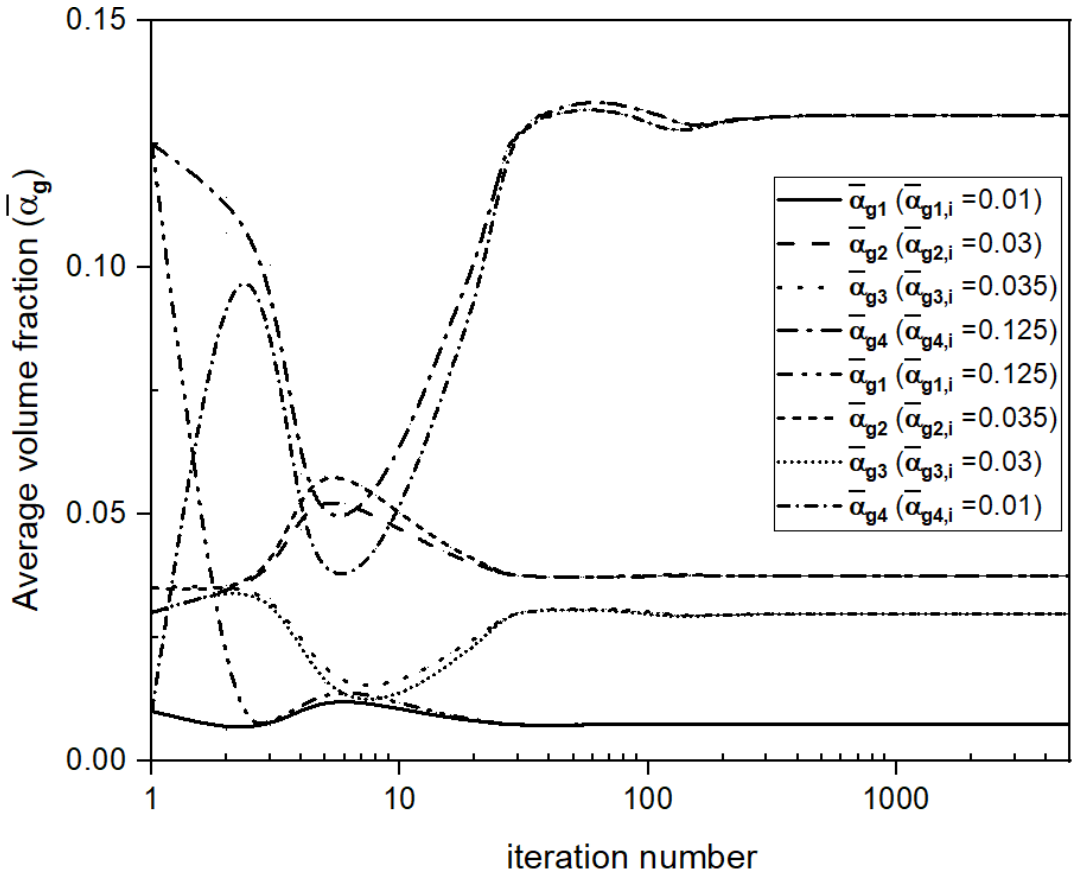

Fig. 4.6. Bulk gas volume fraction values for an iterative calculation using the present CAB model with different initial values for each bubble group.

The variation of the bulk volume fraction values ($\overline{\alpha_g}$) for each bubble group (j) are shown in Fig. 4.6. The results indicate that the present CAB model was able to redistribute the gas phase in a manner that converged to a final distribution consistent with the values measured by Lucas *et al.* (2005). Some specific observations are as follows: for both sets of initial values, the CAB model predicted the same final distribution of bulk volume fraction among the four bubble groups. For both sets of initial values, the iterative procedure resulted in an oscillatory behavior for the bulk volume fraction for each bubble group, which reflected the exchange of gas (mass transfer) between the different bubble groups. After approximately 100 iterations, the values of the bulk volume fraction for each bubble group converged. The final values predicted by the present CAB model differ somewhat from the experimental values measured by Lucas *et al.* (2005). The percent difference in the final bulk volume fraction value was approximately 30, 23, 23 and 3 percent for bubble group 1, 2, 3 and 4, respectively.

4.3.2 Mean flow properties

This section discusses the profiles predicted for the mean velocity of the gas phase and volume fraction distribution using the CAB model with two bubble groups. The purpose is to further investigate the effect of the coalescence and breakup on the mean flow of the gas. The simulated profiles are compared against the experimental data of Lucas *et al.* (2005) and the numerical results of Liao *et al.* (2015) also using a CAB model formulation. The numerical predictions of Liao *et al.* (2015) using the PBLS CAB model are also included for comparison. The flow conditions for test cases 061 and 074 of Liao *et al.* (2015) are described in Table 4.7. The present model and the model of Liao *et al.* (2015) both used the same experimental data (Lucas et al., 2005), following the classification of measured data for bubble groups as reported by Krepper *et al.* (2008), for the model assessment. For test case 061, the gas phase consists of two bubble groups with diameters of 0.0035 m and 0.005 m, while, for test case 074, the gas phase bubble diameters are 0.004 m and 0.005 m.

Table 4.7 Flow conditions for select test cases of Liao *et al.* (2015)

No.	Parameters	Case 061	Case 074
1	Superficial liquid velocity, J_L [m/s]	0.405	1.017
2	Superficial gas velocity, J_G [m/s]	0.0269	0.0413
3	Pipe diameter, D [m]	0.0512	0.0512
4	Equivalent bubble diameter, d_b [m]	0.0043	0.0045
5	Average gas volume fraction, $\overline{\alpha_g}$	0.045	0.037

Figs. 4.7 and 4.8 present the gas volume fraction profiles predicted by the present CAB model compared to the experimental data and other numerical results. The test cases considered correspond to the wall-peak gas volume fraction case, since the mean bubble size for both cases is smaller than the critical bubble size. It can be observed from the Fig. 4.7 that the gas phase volume fraction profile for case 061 predicted by the present CAB model closely matches the experimental data. Both of the other numerical predictions predict an erroneous peak value near the centerline. For case 074 shown in Fig. 4.8, the present model predicts a gas volume fraction profile that fails to reproduce details of the experimental profile near the wall and centerline. The model of Liao *et al.* (2015) with their CAB model does a better job of resolving the near-wall peak value, whereas the model of Liao *et al.* (2015) with PBLS CAB model prediction is still much too large near the centerline. Note that the model of Liao *et al.* (2015) not only used a different CAB model, but also a different model for the turbulence modulation, i.e. their time scale was based on the turbulence kinetic energy and bubble diameter i.e. $\tau = \frac{d_b}{\sqrt{k}}$.

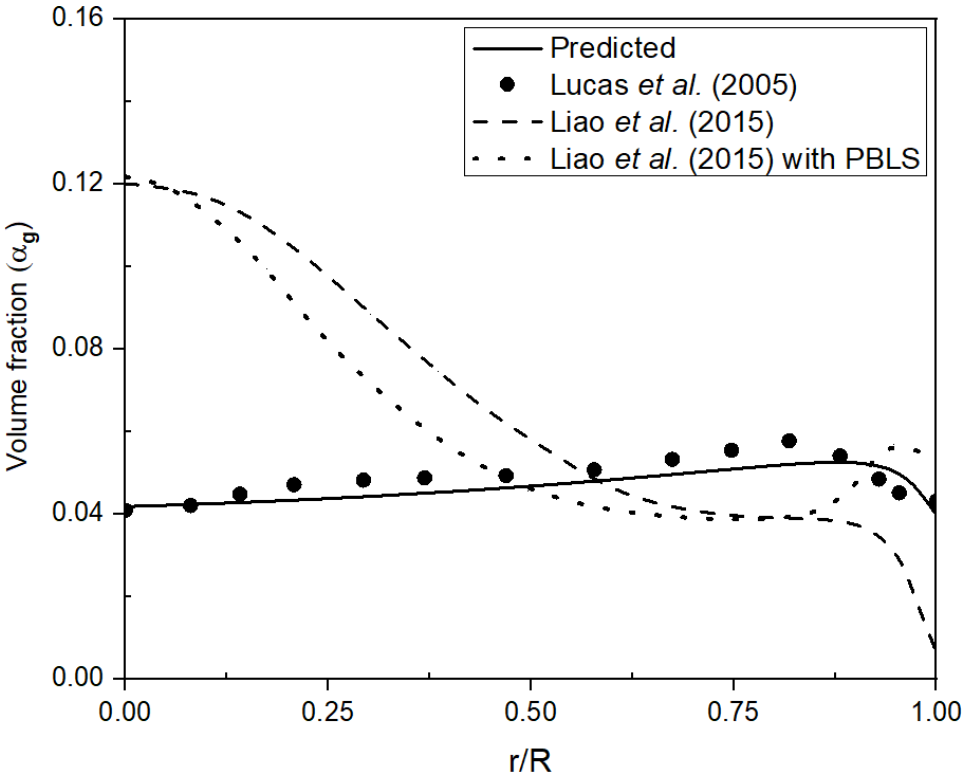

Fig. 4.7. Gas volume fraction profiles for case 061.

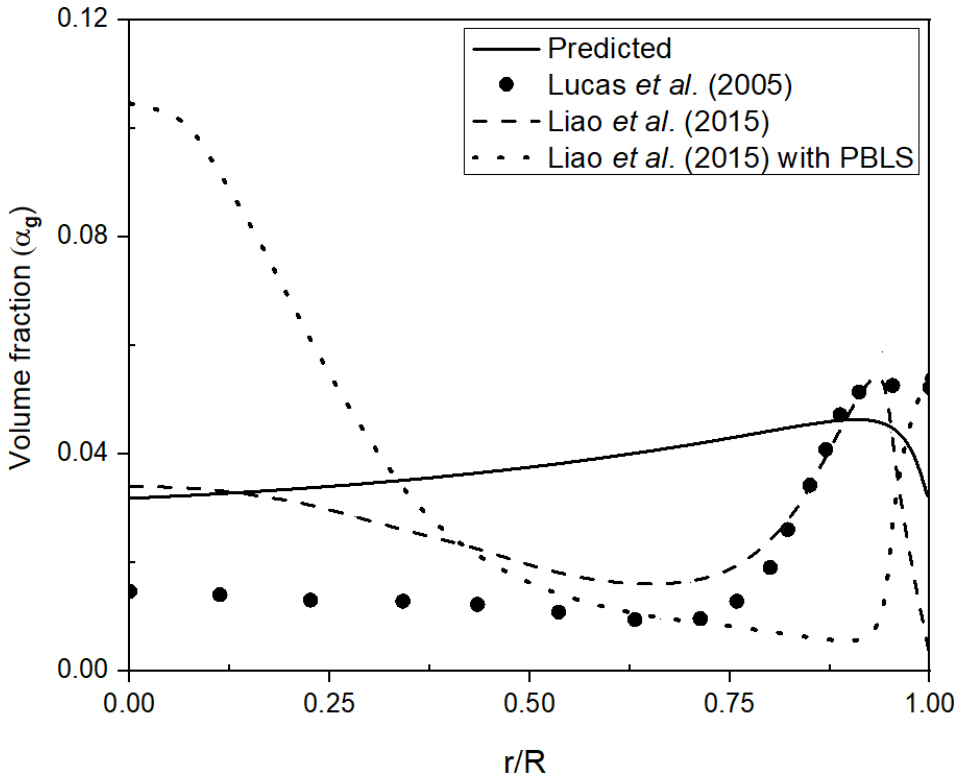

Fig. 4.8. Gas volume fraction profiles for case 074.

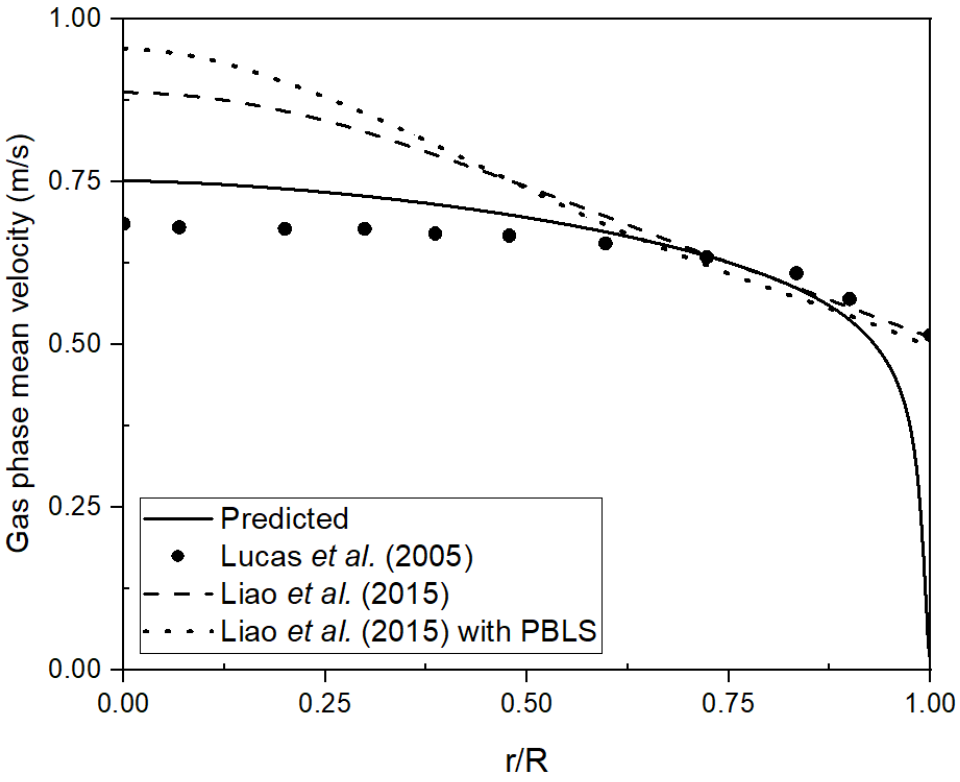

Fig. 4.9. Gas phase mean velocity profiles for case 061.

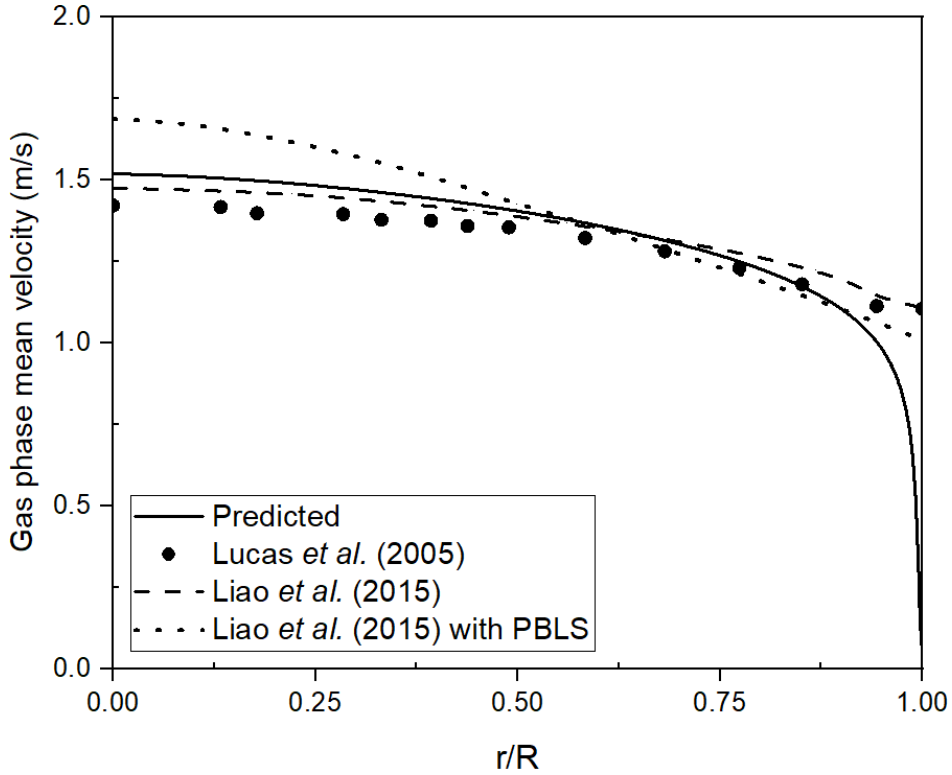

Fig. 4.10. Gas phase mean velocity profiles for case 074.

Figs. 4.9 and 4.10 compare the gas phase mean velocity profiles predicted by the present CAB model to the experimental data and other numerical results. The simulated mean velocity profiles for the gas phase are in good agreement with the experimental data of Lucas *et al.* (2005) except at the wall, where the measurements indicate a finite value of the gas velocity and the present model uses a no-slip condition. The model slightly over-predicts the value of the mean gas velocity near the centre of the pipe. Both of the other numerical models significantly over-predict the mean gas velocity near the centre of the pipe for case 061. For case 074, the prediction of Liao *et al.* (2015) with their CAB model is very close to the experimental data, while their PBLS CAB model again over-predicts the velocity near the centre of the pipe. The mean gas velocities for both cases are found to be greater than the mean liquid velocity as expected due to the effect of buoyancy. However, no experimental data for the liquid phase mean velocity profiles were available for comparison. Overall, the present model shows somewhat better performance than the other numerical simulations based on the void fraction distribution and gas phase mean velocity.

4.3.3 Bubble coalescence and breakup frequency

This section presents some examples of the profiles predicted by the present CAB model for the coalescence and breakup frequency considering the different mechanisms associated with the coalescence and breakup events. The purpose is to show the contribution of each mechanism to the respective coalescence and breakup process for a specific flow condition based on a simulation that considers multiple bubble groups.

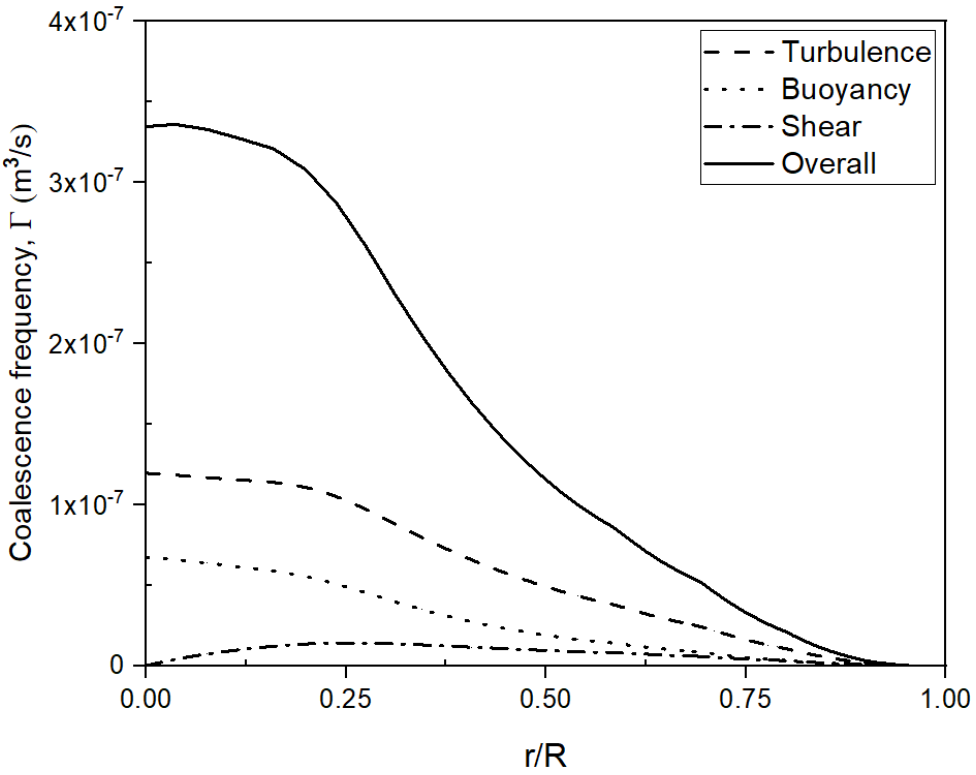

Fig. 4.11. Contribution of different physical mechanisms to the coalescence frequency for the second bubble group.

Fig. 4.11 presents the coalescence frequency profile for the second bubble group with a mean bubble size of $d_b = 4.95$ mm for the case of four bubble group and the flow conditions given in Table 4.5. In addition to the overall profile, it presents the individual profiles for the three different mechanisms considered, i.e. turbulence, buoyancy and shear. In Fig. 4.11, the bubble coalescence frequency has units of m^3/s, which is consistent with the development in Eqs. (4.12) and (4.13), where it is multipled by a factor which represents the inverse of the bubble mass. In contrast, the bubble breakup frequency shown in Fig. 4.13 has units of 1/s. It is evident from the figure that for the flow conditions considered, the coalescence due to turbulence makes the largest contribution to the exchange of volume fraction from one bubble group to another, followed by the coalescence due to buoyancy and shear. Note that the overall coalescence frequency is not equivalent to the profiles of the three different mechanisms, but is given by the cumulative frequency of the different mechanisms multiplied by a factor that depends on the quotient of volume fractions, see Eq. (4.16). For the buoyancy, turbulence and overall coalescence frequency profiles in Fig. 4.11, the peak values occur at the centreline, while for the case of shear the peak occurs near $\frac{r}{R} = 0.25$. For all of

the profiles shown, the value in the near-wall region is negligible. This implies that coalescence occurs primarily in the centre region of the pipe.

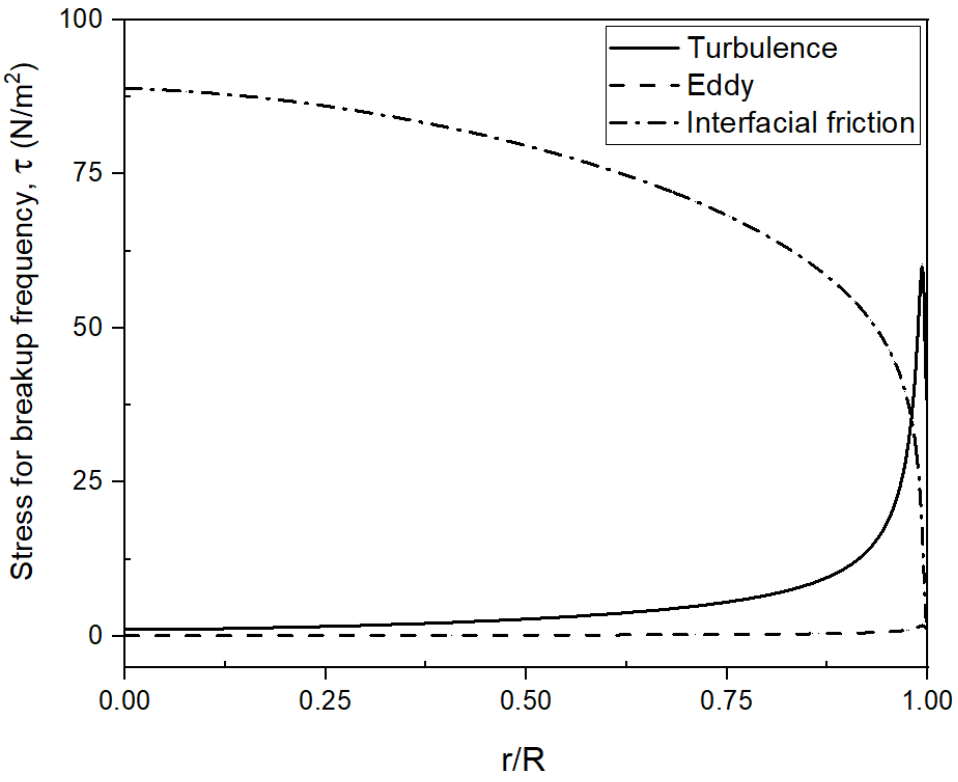

Fig. 4.12. Contribution of different stress mechanisms for the breakup frequency for the second bubble group.

Fig. 4.12 presents the stress profile for each mechanism associated with the bubble breakup process considering four bubble group (Table 4.5) for the second group with mean bubble size $d_b = 4.95$ mm. A similar profile trend was obtained for the other mean bubble sizes, but those results are not shown here due to space limitations. Fig. 4.12 considers three separate mechanisms: bubble breakup due to the effect of turbulence, laminar shear and interfacial friction (or drag). The stress profile representing the effect of interfacial friction is dominant, whereas the profile related to laminar shear is negligible. The profile associated with turbulence is mostly minimal, except near the wall where it shows a sharp peak. The stress due to the interfacial friction has maximum and minimum values at the centreline and the wall of the pipe, respectively, which is to be expected since it depends on the terminal velocity which is likely to be a maximum at the centreline and a

minimum at the wall. For the complete set of bubble groups, the stress profile due to turbulence was found to be greater for larger bubbles than for smaller bubbles, while the stress profile due to interfacial friction was found to be greater for smaller bubbles than for larger bubbles.

Recall that the breakup frequency is determined based on the largest stress associated with the different breakup mechanisms. The bubble breakup frequency for the bubble group considered above is depicted in Fig. 4.13. Note that the frequency profile closely follows the stress distributions shown in Fig. 4.12, specifically the contributions due to the effects of interfacial friction and turbulence.

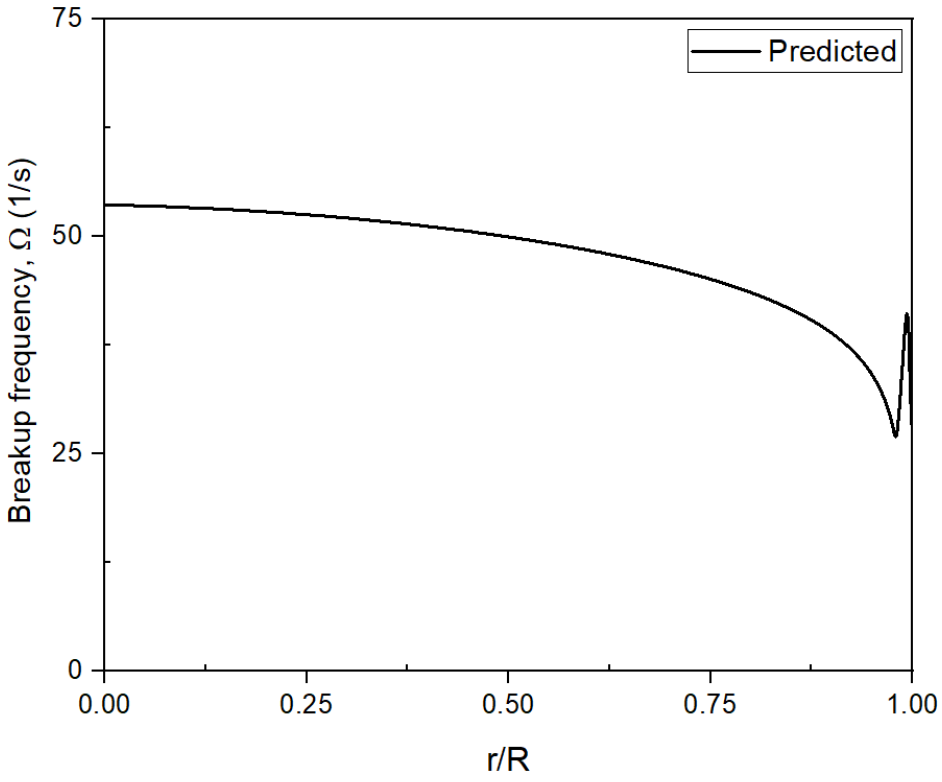

Fig. 4.13. Bubble breakup frequency for second bubble group.

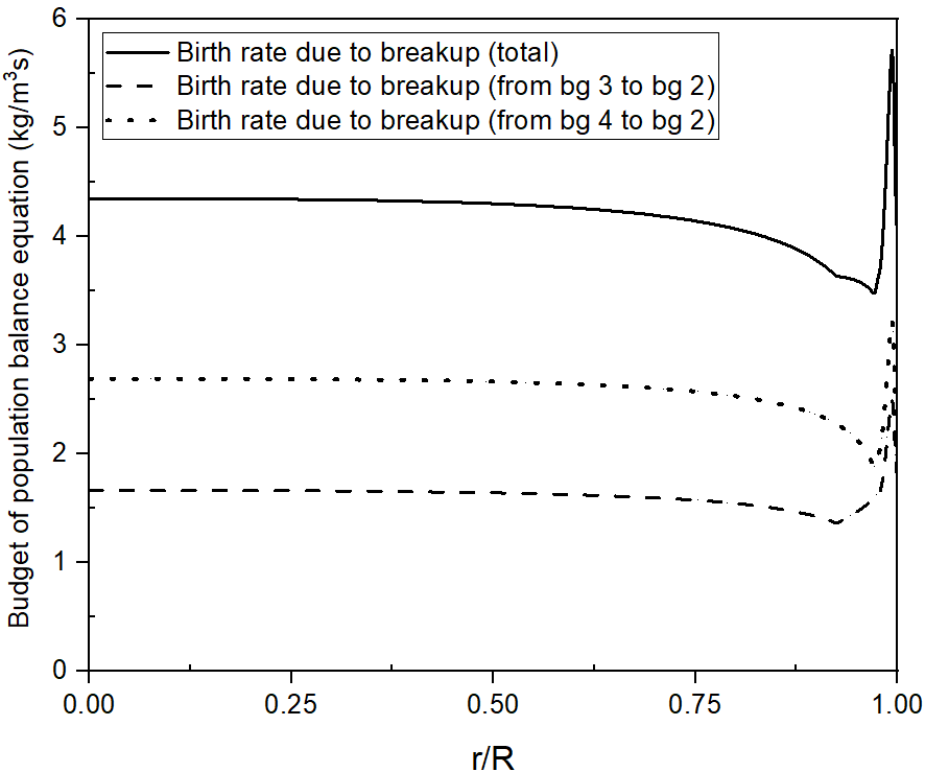

Fig. 4.14. Combined contribution due to breakup of larger bubble groups to the population balance equation for the second bubble group.

As described in the methodology section, the coalescence and breakup frequencies are used to determine the birth rates and death rates of bubbles calculated using Eqs. (4.10) - (4.13), which in turn are used to calculate the exchange of gas volume fraction for a given bubble group (bg). Fig. 4.14 above demonstrates that the net contribution to the population balance equation due to breakup for bubble group 2 is the sum of the contributions from the two larger bubble groups, i.e. bubble group 3 and 4. The population balance equation includes all of the exchanges of gas volume fraction between the different bubble groups, considering the breakup and coalescence processes.

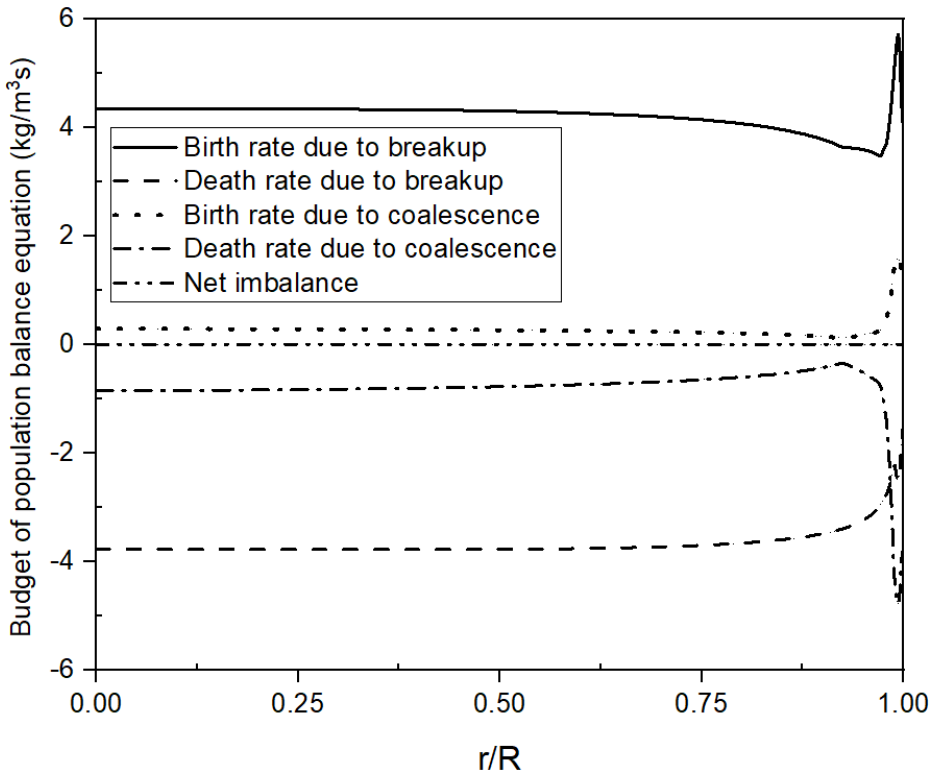

Fig. 4.15. Population balance equation budget (equilibrium) for the second of four bubble groups.

Fig. 4.15 presents the different terms in the population balance equation for the second bubble group for an equilibrium state (at iteration number 5000) for which the net rate of transfer of gas volume fraction to the bubble group is approximately zero. From the figure, it is clear that the birth and death rate associated with the bubble breakup process are greater than those associated with the coalescence process. The breakup of larger bubble groups results in significant transfer of gas volume fraction to the second bubble group; however, breakup also removes significant gas volume fraction from the second bubble group. The coalescence of bubbles from group 1 results in only a small transfer of gas volume fraction to bubble group 2, and likewise, coalescence of bubbles in bubble group 2 only results in a small transfer of gas volume fraction to larger bubbles. The results in Fig. 4.15 reveal that the effect of the wall on both the coalescence and breakup processes is significant. For example, the profile for the birth rate due to breakup is almost constant over most of the pipe, until near the wall it first dips and then increases to a sharp peak value very close to the wall. On the destruction side, the death rate due to coalescence is relatively small and uniform over most of the pipe, however, near the wall the magnitude first decreases and then increases sharply to a peak value close to the wall. Recall that both bubble group 1 and 2 are

characterized by a wall peak behavior. The accumulation of smaller bubbles near the wall may partly explain the near-wall peaks in the birth and death rate profiles due to coalescence shown in Fig. 4.15. Since this case represents an equilibrium state, the net imbalance is approximately zero across the pipe.

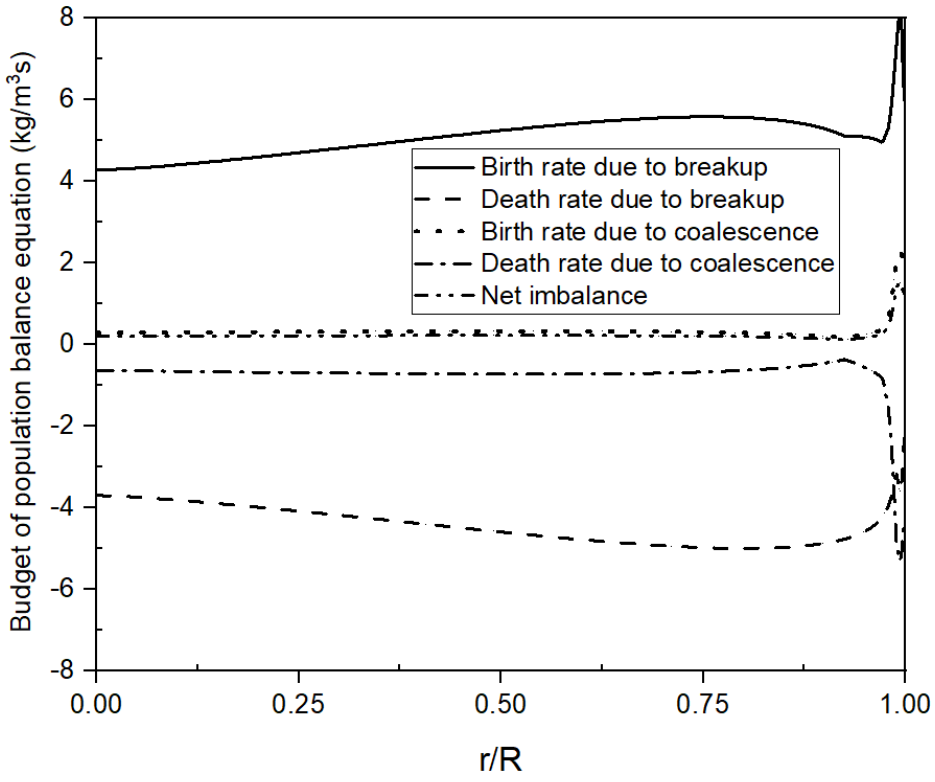

Fig. 4.16. Population balance equation budget (non-equilibrium) for the second of four bubble groups.

Fig. 4.16 gives the population balance equation budget for a non-equilibrium case (at iteration number 10) for the second bubble group. Overall, the behavior in terms of birth and death rate profiles is very similar to that observed in Fig. 4.15 for the equilibrium case. However, for the case shown in Fig. 4.16, the net transfer of gas volume fraction is finite and positive, indicating that overall the bulk gas volume fraction has increased due to the various exchanges of gas volume fraction with the other bubble groups. The net addition of gas volume fraction is largest in the region next to the pipe wall.

4.3.4 Turbulence modulation

This section concisely investigates the effect of the CAB model on the turbulence modulation (TM) in the transport equations for the turbulence kinetic energy (TKE) and its dissipation rate. The turbulence modulation for the turbulence kinetic energy distribution will be compared for both mono- and poly-disperse bubbly flow for the same flow condition as noted in Table 4.5. However, it should be noted that the bubble diameter, i.e. $d_b = 0.006$ m and same bulk gas volume fraction $(\overline{\alpha_g} = 0.20)$ were used for the mono-disperse case in the comparison.

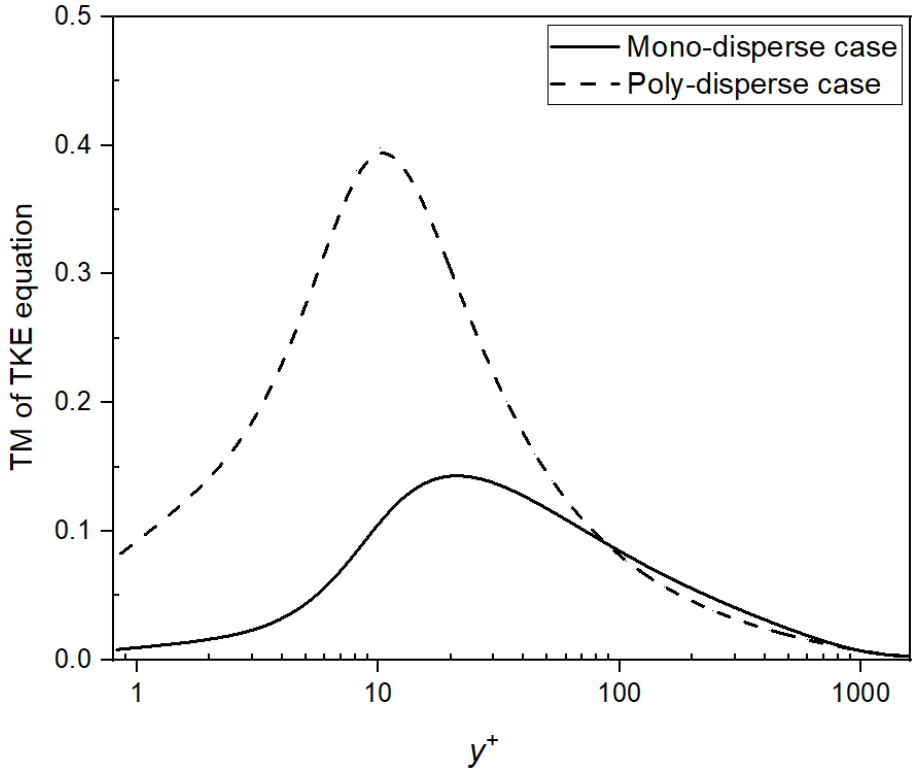

Fig. 4.17. Comparison of the turbulence modulation of TKE equation for mono- and poly-disperse flow.

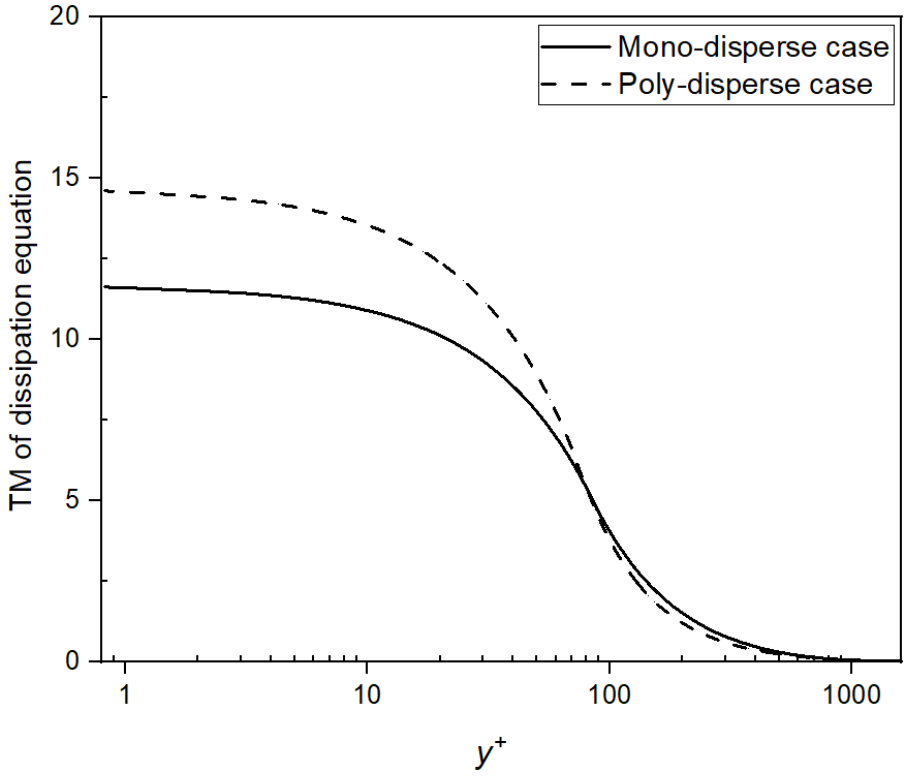

Fig. 4.18. Comparison of the turbulence modulation of dissipation equation for mono- and poly-disperse flow.

Figs. 4.17 and 4.18 depict the profiles for the turbulence modulation terms for the turbulence kinetic energy and dissipation rate equations, respectively, as predicted by the CAB model. The turbulence modulation terms were predicted for the case of four bubble groups (see Table 4.5) and plotted as a function of dimensionless wall normal distance $\left(y^+ = \frac{yu_\tau}{\nu}\right)$, using a log scale to expand the near-wall region. Recall from the methodology section, that each bubble group, characterised by its own slip-velocity, makes a contribution to the total turbulence modulation. For both the mono- and poly-disperse flow cases, similar trends were obtained for the turbulence modulation terms in each equation. However, the maximum values of the turbulence modulation term in each transport equation, located near the wall of the pipe, were observed to be larger for the poly-disperse case compared to the mono-disperse case. This was especially true for the turbulence kinetic energy equation, where the TM was much enhanced throughout the near-wall region.

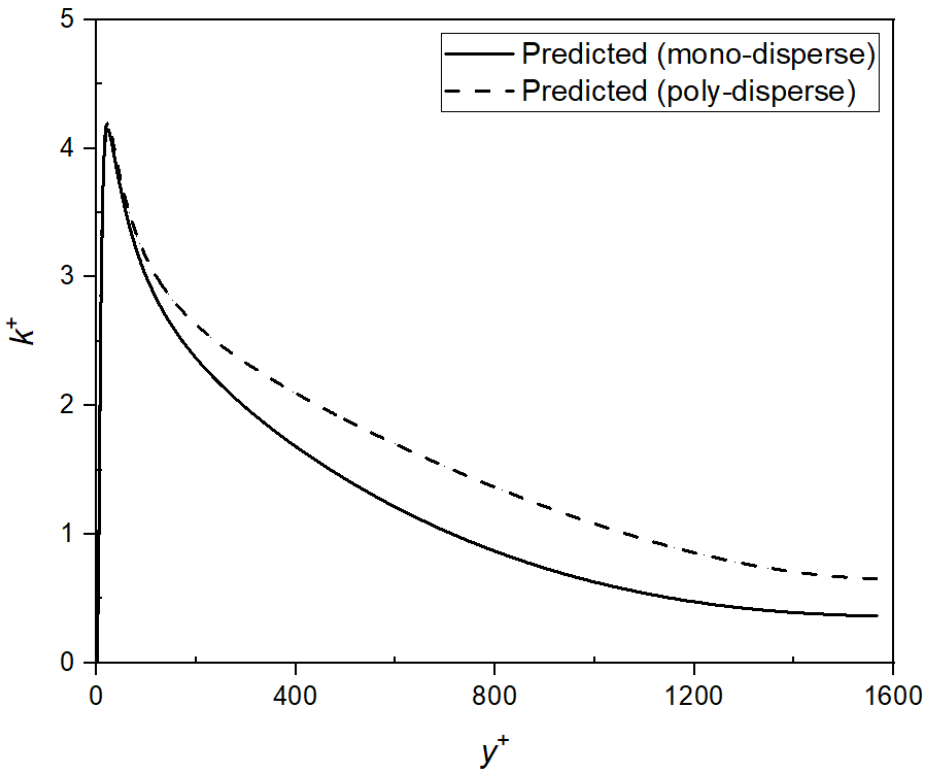

Fig. 4.19. Comparison of the predicted turbulence kinetic energy profiles for the mono- and poly-disperse flow.

Fig. 4.19 examines the predicted profiles of the dimensionless turbulence kinetic energy ($k^+ = \frac{k}{u_\tau{}^2}$) for the mono- and poly-disperse bubbly flows for the same flow conditions. The shape of the turbulence kinetic profile is the same for both flows, i.e. a sharp near-wall peak and a much lower value in the central region of the pipe. The effect of poly-dispersity is to noticeably enhance the level of the turbulence kinetic energy across most of the pipe. This enhancement can be attributed to the increase in the TM for the poly-disperse case.

4.4 Conclusion and further recommendations

A two-fluid model has been successfully implemented in a one-dimensional code for the prediction of gas-liquid poly-disperse bubbly flow in a pipe using the iMUSIG approach with a simplified bubble coalescence and breakup model. The numerical predictions for the gas volume fraction and

mean velocity profiles were used to assess the performance of the model for both two-bubble and four-bubble groups based on comparisons to experimental and other numerical results. The model was shown to correctly redistribute the gas volume fraction among different bubble groups based on the coalescence and breakup processes. In particular, when an unknown bulk gas fraction distribution among bubble groups was used as the initial condition, the model redistributed the gas volume fraction among the different bubble groups such that the final prediction for each bubble group closely approximated the measured gas volume fraction values. The present paper also reports the mean velocity profiles for the individual bubble groups, which is an important feature of the iMUSIG model. This study also investigated the effect of the iMUSIG model on the predictions for the turbulence kinetic energy of the liquid phase, which is used to determine the turbulent transport. The results available in the literature for the mono-disperse case indicate that the effect of a bubble on the liquid phase turbulence is strongly dependent on the bubble size, which also holds true for the poly-disperse case. The turbulence modulation predicted for the poly-disperse bubbly flow was found to be larger than for the mono-disperse case, for both the turbulence kinetic energy and its dissipation rate.

Notwithstanding the promising performance of the iMUSIG model documented in the present study, the model itself requires further testing and development. Given the complexity of the coalescence and breakup processes that are responsible for the redistribution of gas volume fraction among the different bubble groups, the model formulation is highly empirical and includes many parameters that have not yet been widely tested against experimental data. In this regard, a DNS study that resolved the bubble structure could be used to provide a data base that would allow many features of the model itself to be more thoroughly and critically tested. Finally, the present study only considered the relatively simple case of fully-developed upward bubbly flow in a vertical pipe. Practical applications will entail more complex geometries that may require more complex turbulence models for the liquid phase and its interaction with the bubble phase.

4.5 Acknowledgements

The authors are grateful to the Natural Sciences and Engineering Research Council of Canada (NSERC) for providing financial assistance for this research project.

Chapter 5

Conclusions

The following section summarizes the thesis, documents the conclusions and research contributions, and outlines future work based on the numerical results.

5.1 Thesis summary

An in-house CFD model was developed based on the two-fluid formulation for the prediction of fully developed turbulent gas-liquid upward flow in a vertical pipe. The overall model was implemented to achieve the three specific objectives of the thesis.

For the first objective, the radial force balance method of Lucas *et al.* (2001) was used to predict the gas volume fraction for mono-disperse bubbly flow. The radial forces such as lift, wall, and turbulent dispersion were considered in the momentum balance. More specifically, the lift force of Zun (1980), wall force of Tomiyama *et al.* (1995), turbulent dispersion force of Lahey *et al.* (1993), and turbulent dispersion force based on Eötvös number of Lucas *et al.* (2001) were adopted for the analysis. The lift and wall force coefficients of Tomiyama (1998) were incorporated in the model. An adjusted value of the lift force coefficient, as reported by Tomiyama (1998), was employed for the wall-peak volume fraction case. Modification of the turbulent dispersion and lift force coefficient gave improved agreement between the predicted and experimental results. The interphase force for the streamwise momentum equations was modelled by the drag force term using the model formulation of Monahan and Fox (2009).

The turbulent viscosity of the liquid phase was modelled using a two-equation turbulence closure. This thesis implemented the low Reynolds number $k-\varepsilon$ model of Myong and Kasagi (1990) to accommodate the damping of turbulence near the wall of the pipe. The bubble induced turbulent viscosity model of Sato and Sekoguchi (1975) was also included in the model. For the same flow conditions, the predicted eddy viscosity profiles for gas-liquid and single-phase flow were

compared in order to see the effect of the gas phase. In addition, the effect of the turbulence modulation on the eddy viscosity and turbulence kinetic energy was also reported. The predicted outcomes from the two-fluid model were compared to select experimental data of Lucas *et al.* (2005) and simulated results of Lucas *et al.* (2001). Based on the predicted gas volume fraction profiles, the performance of the present model was also compared to other models such as those of Hosokawa *et al.* (2002) and Rzehak *et al.* (2012).

For the second objective, the thesis documents a comprehensive analysis to understand the effect of gas bubbles on the liquid phase turbulence in mono-disperse bubbly flow. The effect of bubbles on the liquid phase turbulence was implemented using the turbulence modulation model originally developed by Dhotre *et al.* (2007). However, the coefficients of the turbulence modulation terms in the turbulent transport equations were modified as compared to the values recommended by Dhotre *et al.* (2007).

The numerical results were compared to the experimental measurements of Liu (1998), Lucas *et al.* (2005), Shawkat *et al.* (2008), and Hosokawa and Tomiyama (2009), as well as the numerical simulation of Rzehak and Krepper (2013). The time-scale formulations of Rzehak and Krepper (2013), and Yao and Morel (2004) for the turbulence modulation were also investigated. For select experimental flow conditions, the effect of the turbulence modulation on predictions for the gas volume fraction, gas and liquid phase mean velocity profiles, eddy viscosity, and turbulence kinetic energy was investigated. A budget analysis of the turbulence transport equations was performed in order to assess the relative importance of the turbulence modulation.

With respect to the third objective, this thesis reports an in-depth numerical study of poly-disperse bubbly flow using the two-fluid model. The poly-disperse distribution of the gas bubbles was treated using the iMUSIG concept of Krepper *et al.* (2008). The model implemented in this study also included a bubble coalescence and breakup formulation, as originally developed by Liao *et al.* (2015), to capture the exchange of gas volume fraction among the different bubble groups.

For the poly-disperse flow, the same radial force balance method of Lucas *et al.* (2001) was used for the volume fraction calculation. However, for multiple bubble groups, a separate force balance equation was solved for each bubble group. The iMUSIG model was tested considering the case of two and four bubble groups. The coalescence and breakup model used a different

implementation than that of by Liao *et al.* (2015). The effect of turbulence, buoyancy and shear stress on the bubble coalescence frequency is included in the model. Similarly, the effect of turbulence, laminar shear and interfacial friction is included in the model for the bubble breakup frequency.

The simulated results were validated against select experimental measurements of Lucas *et al.* (2005), and numerical results of Krepper *et al.* (2008) and Liao *et al.* (2015). The effect of the coalescence and breakup model on the predicted results for gas volume fraction was explored. The thesis also documents the mean velocity profiles for the individual bubble groups, which is an inherent characteristic of the iMUSIG model. An analysis of the different terms in the population balance equation, which accounts for the birth and death rates of bubbles due to breakup and coalescence, was presented in the thesis. Finally, the predictions for the turbulence modulation for the poly-disperse and mono-disperse case were compared.

5.2 Conclusions

This thesis attempts to better understand the physics of turbulent gas-liquid bubbly flow and in that context develop an improved computational model in a RANS framework. This was achieved use of theoretical knowledge, numerical simulation, and comparison to experimental measurements. This section documents the conclusions of the research.

A one-dimensional two-fluid model was implemented for the prediction of fully developed gas-liquid flow in a vertical pipe. The model was able to predict the effects of bubble diameter on the gas volume fraction distribution across a pipe, e.g. larger bubbles tend to form a center-peak, while smaller bubbles form a wall-peak gas volume fraction profile. Turbulence modulation source terms in the turbulence transport equations were used for the eddy viscosity calculation. In addition, the bubble induced turbulent viscosity model of Sato and Sekoguchi (1975) was included in the effective viscosity of the liquid phase. For the center-peak case, the bubble induced turbulence was greater than the shear driven turbulence, whereas for the wall-peak case the bubble induced turbulence was smaller than the shear driven turbulence. It should be noted that the bubble induced turbulence viscosity model of Sato and Sekoguchi (1975) was not included in the second and third study of this thesis, because in some sense it was redundant.

To include the effect of bubbles on the liquid phase turbulence via turbulence modulation terms in the turbulence transport equations remains a challenging task for RANS modeling of bubbly flows. The available experimental data shows both enhancement and attenuation of the turbulence kinetic energy, in different regions of the pipe for the same flow condition, by the presence of bubbles. In some cases, the effect of the turbulence modulation on the turbulence quantities was negligible. In other cases, the effect of the turbulence modulation on the mean flow properties was minimal even though the turbulence quantities were modified by the bubbles. As such, the turbulence modulation can modify the turbulence properties of a flow without having much impact on the mean flow properties. The effect of the superficial gas and liquid phase velocities on the turbulence modulation was also explored. For low gas volume fractions, the turbulence modulation of the turbulence kinetic energy is observed to increase as the liquid superficial velocity increases. In contrast, the effect of the gas superficial velocity on the turbulence modulation was observed to be negligible.

Modelling of the poly-disperse gas-liquid flow using the iMUSIG approach presents a major challenge for the two-fluid model related to the bubble coalescence and breakup processes. The poly-disperse distribution of different sized bubbles can exhibit the exchange of gas volume fraction between bubbles. For the present model, the exchange of gas volume fraction between bubbles due to the coalescence and breakup processes was evaluated using ad hoc and highly empirical model relations. The results available in the literature for the mono-disperse case indicate that the effect of a bubble on the liquid phase turbulence is strongly dependent on the bubble size, which also holds true for the poly-disperse case. Therefore, the effect of bubbles on the turbulence properties in poly-disperse flow can be more significant than in mono-disperse flow. Apart from the bubble coalescence and breakup process, the two-fluid formulation of poly-disperse flow is more complex than mono-disperse flow as it deals with multiple physics based on bubbles of different sizes.

Overall, this thesis considered the relatively simple case of fully developed turbulent gas-liquid bubbly flow in a vertical pipe to understand the fundamental flow physics. However, practical applications will consists of complex flows depending on the type of applications. Therefore, the turbulence modulation needs to be re-formulated based on the non-isotropic turbulence closures, which are not limited to use of a two-equation turbulence model formulation.

5.3 Research contributions

This section documents the contributions of the thesis research. A one-dimensional formulation of the CFD model was implemented for the prediction of turbulent gas-liquid flow in pipe. One advantage of studying this one-dimensional flow is that it allows the effects of the individual models, both turbulent and multiphase, to be readily evaluated against benchmark data, which is not possible for most complex three-dimensional flows. The numerical model was able to predict the essential flow properties successfully, when the results were validated against experimental measured data.

This thesis documents the sequential improvement of a two-fluid model related to the prediction of mean flow properties, turbulence modulation formulation, and coalescence and breakup approach for the poly-disperse case. The numerical results, in terms of gas volume fraction, mean velocity, and turbulence kinetic energy profiles, show that the present model performs overall as well as and sometimes better than other model formulations in the literature.

For the one-dimensional formulation, the thesis provides a thorough investigation of the radial force balance mechanism considering the effect of bubble size on the evaluation of gas volume fraction. The present model used a revised value of the turbulent dispersion and lift force coefficient, which resulted in an improved prediction compared to Lucas *et al.* (2005) for the center-peak and wall-peak gas volume fraction profiles. The present model did not formulate a new turbulence modulation model, but rather introduced a modification in the coefficient values of an existing model (Dhotre *et al.*, 2007). The adjusted value of the turbulence modulation coefficients in the turbulence transport equations was justified by the improved agreement of the predicted results to the measured data. For the source term in the dissipation rate equation, the selection of the time scale had a significant effect on the magnitude and distribution of the turbulence modulation. For the poly-disperse flow, the present model was developed using a different approach than the baseline (BSL) model of Liao *et al.* (2015). The thesis implemented the iMUSIG model considering two and four velocity groups, where the number of velocity and bubble groups are same. Whereas, the iMUSIG approach was implemented using only two velocity groups in the BSL model. The current model did not introduce a new bubble coalescence and

breakup model, but implemented a simplified version of an existing coalescence and breakup model (Liao *et al.*, 2015).

This thesis demonstrates the effect of turbulence modulation on the mean flow variables and turbulence quantities explicitly. A relatively novel feature of this research is the documentation of a budget analysis for the turbulence kinetic energy and its dissipation rate. One advantage of this budget analysis is that it assesses the relative importance of the turbulence modulation by comparing the source term to the shear production. This thesis also demonstrates the effect of bubble size on the time scale of the turbulence modulation. For the poly-disperse flow, a significant feature of the iMUSIG model is to predict the mean velocity profile for the individual bubble group, which is not typically shown in the literature. The thesis appears to be the first to document the mean velocity profile for the separate bubble groups. The mean velocity for the large bubble group was found to be greater than for the small bubble group, because of the larger buoyancy force of the larger bubble group. The model was shown to correctly redistribute the gas volume fraction among different bubble groups based on the coalescence and breakup processes. More specifically, when an unknown bulk gas volume fraction distribution among bubble groups was used as the initial condition, the model redistributed the gas volume fraction among the different bubble groups such that the final prediction for each bubble group closely approximated the measured gas volume fraction values. An analysis of the different terms in the population balance equation was documented in this thesis for the first time. This analysis clearly shows the exchange of gas volume fraction among different bubble groups associated with the birth and death rates of bubbles due to coalescence and breakup processes.

In summary, this thesis presents a predictive model, clearly documents the model implementation, and provides a comprehensive and informative investigation of results.

5.4 Future work

Some suggestions for future work based on the thesis research include the following:

The numerical simulation of gas-liquid turbulent flow was performed using a one-dimensional two-fluid model. However, many practical problems will require a two-dimensional or three-dimensional model formulation to explore a spatially developing flow. The volume fraction distribution would then be evaluated using the continuity equation, instead of using the radial force balance. It will be interesting to observe the prediction of wall and center peak cases based on the continuity equation, as noted previously.

In spite of the promising performance of the present turbulence modulation, it has limitations since it is based on an eddy viscosity model. The turbulence modulation needs to be implemented considering turbulence closures for the prediction of more complex flows, which are not limited by the use of a two-equation turbulence closure. Furthermore, it would be helpful to formulate the turbulence modulation based on a full Reynolds stress model and observe the prediction of flow parameters.

The bubble coalescence and breakup model was used for two and four bubble groups. A thorough investigation with a larger number of bubble groups would allow for a more careful analysis of poly-disperse flow, which might be useful for further refinement of the coalescence and breakup model. In addition, the empirical constants used for the highly empirical correlations in the coalescence and breakup model would be better expressed as a function of local flow properties.

In some cases, the present model does not match the value of the experimental mean velocity at the wall. The model uses a no-slip condition for the liquid and gas velocity at the wall, whereas the measurements (Liu, 1998; Lucas *et al.,* 2005; and Shawkat *et al.,* 2008) indicate a finite value for select test cases. Implementation of either a free-slip or a partial-slip boundary condition, instead of using the no-slip boundary condition at the pipe wall for the gas phase, could improve the prediction of the mean velocity fields for some flow conditions.

The numerical analysis using the present model should be performed considering the downward vertical pipe flow configuration. It would be interesting to observe the changes in the predicted mean flow parameters compared to the upward flow configuration. Furthermore, it would be advantageous for the present model if it had the ability to predict both the upward and downward pipe flow configurations, which will increase the versatility.

The lack of appropriate experimental measured data related to gas-liquid flow analysis is a significant challenge to the development of a robust computational model. As a whole, the measured data available for assessment of a predictive model for turbulent gas-liquid flow is insufficient and inconsistent. With the availability of new instrumentation and improved technology, more refined and comprehensive experimental data and direct numerical simulation (e.g. Ma *et al.*, 2017) should be able to provide further insight related to this type of flow.

References

Antal, S. P., Lahey, R. T., Flaherty, J. E., 1991. Analysis of phase distribution in fully developed laminar bubbly two-phase flow. International Journal of Multiphase Flow 17, 635-652.

Auton, T. R., 1987. The lift force on a spherical body in a rotational flow. Journal of Fluid Mechanics 183, 199-218.

Brennen, Christopher E., 2005. Fundamentals of Multiphase Flow. Cambridge University Press, New York, USA.

Burns, A. D., Frank, T., Hamill, I., Shi, J.-M., 2004. The Favre averaged drag model for turbulence dispersion in Eulerian multiphase flows. 5th International Conference on Multiphase Flow, ICMF2004, 392.

Cheung, S. C. P., Yeoh, G. H., Tu, J. Y., 2007. On the numerical study of isothermal vertical bubbly flow using two population balance approaches. Chemical Engineering Science 62, 4659-4674.

Colombo, Marco, Fairweather, Michael, 2015. Multiphase turbulence in bubbly flows: RANS simulations. International Journal of Multiphase Flow 77, 222-243.

Dhotre, M. T., Smith, B. L., Niceno, B., 2007. CFD simulation of bubbly flows: random dispersion model. Chemical Engineering Science 62, 7140-7150.

Drew, D. A., Passman, S. L., 1998. Theory of Multicomponent Fluids. Springer.

Drew, D. A., Lahey, R. T., 1987. The virtual mass and lift force on a sphere in rotating and straining inviscid flow. International Journal of Multiphase Flow 13, 113-121.

Duan, X. Y., Cheung, S. C. P., Yeoh, G. H., Tu, J. Y., Krepper, E., Lucas, D., 2011. Gas-liquid flows in medium and large vertical pipes. Chemical Engineering Science 66, 872-883.

Ekambara, K., Dhotre, M. T., Joshi, J. B., 2005. CFD simulations of bubble column reactors: 1D, 2D and 3D approach. Chemical Engineering Science 60, 6733-6746.

Frank, Th., Zwart, P. J., Krepper, E., Prasser, H. M., Lucas, D., 2008. Validation of CFD models for mono- and polydisperse air–water two-phase flows in pipes. Nuclear Engineering and Design 238, 647-659.

Hibiki, T., Ishii, M., Xiao, Z., 2001. Axial interfacial area transport of vertical bubbly flows. International Journal of Heat and Mass Transfer 44, 1869-1888.

Hosokawa, S., Tomiyama, A., Misaki, S., Hamada, T., 2002. Lateral migration of single bubbles due to the presence of wall. Proc. ASME Joint U.S.-European Fluids Engineering Division Conference, FEDSM 2002, Montreal, Canada.

Hosokawa, S., Tomiyama, A., 2004. Turbulence modification in gas-liquid and solid-liquid dispersed two-phase pipe flows. International Journal of Heat and Fluid Flow 25, 489-498.

Hosokawa, S., Tomiyama, A., 2009. Multi-fluid simulation of turbulent bubbly pipe flows. Chemical Engineering Science 64, 5308-5318.

Islam, A S M Atiqul, Adoo, N A, Bergstrom, D J, 2016. Prediction of mono-disperse gas-liquid turbulent flow in a vertical pipe. International Journal of Multiphase Flow 85, 236-244.

Islam, A S M Atiqul, Bergstrom, D J, 2019. Modelling bubble induced turbulence for gas-liquid bubbly flow in a vertical pipe. Chemical Engineering Science 197, 159-171.

Issa, S. Al, Lucas, D., 2009. Two phase flow 1 D turbulence model for poly-disperse upward flow in a vertical pipe. Nuclear Engineering and Design 239, 1933-1943.

Kariyasaki, A., 1987. Behaviour of a gas bubble in a liquid flow with a linear velocity profile. Transactions of the Japan Society of Mechanical Engineers Series B 53, 744-749.

Krepper, E., Lucas, D., Prasser, H.-M., 2005. On the modelling of bubbly flow in vertical pipes. Nuclear Engineering and Design 235, 597-611.

Krepper, E., Lucas, D., Frank, T., Prasser, H.-M., Zwart, P. J., 2008. The inhomogeneous MUSIG model for the simulation of poly-dispersed flows. Nuclear Engineering and Design 238, 1690-1702.

Lahey, R. T., Lopez de Bertodano, M., Jones, O. C., 1993. Phase distribution in complex geometry conduits. Nuclear Engineering and Design 141, 177-201.

Liao, Y., Lucas, D., Krepper, E., Schmidtke, M., 2011. Development of a generalized coalescence and breakup closure for the inhomogeneous MUSIG model. Nuclear Engineering and Design 241, 1024-1033.

Liao, Y., 2013. Development and Validation of Models for Bubble Coalescence and Breakup. PhD thesis, Dresden University of Technology, Germany.

Liao, Y., Rzehak, R., Lucas, D., Krepper, E., 2015. Baseline closure model for dispersed bubbly flow: Bubble coalescence and breakup. Chemical Engineering Science 122, 336-349.

Lin, T.-J., Tsuchiya, K., Fan, Liang-Shih., 1999. On the measurements of regime transition in high-pressure bubble columns. Canadian Journal of Chemical Engineering 77, 370-374.

Liu, T. J., 1997. Investigation of the wall shear stress in vertical bubbly flow under different bubble size conditions. International Journal of Multiphase Flow 23, 1085-1109.

Liu, T. J., 1998. The role of bubble size on liquid phase turbulent structure in two-phase bubbly flow. In: Proceedings of the 3rd International Conference on Multiphase Flow, ICMF1998, Lyon, France.

Lopez de Bertodano, M., Lee, S. J., Lahey, R. T., Drew, D. A., 1990. The Prediction of Two-Phase Turbulence and Phase Distribution Using a Reynolds Stress Model. Journal of Fluids Engineering 112, 107-113.

Lucas, D., Krepper, E., Prasser, H.-M., 2001. Prediction of radial gas profiles in vertical pipe flow on the basis of bubble size distribution. International Journal of Thermal Science 40, 217-225.

Lucas, D., Krepper, E., Prasser, H.-M., 2005. Development of co-current air–water flow in a vertical pipe. International Journal of Multiphase Flow 31, 1304-1328.

Lucas, D., Krepper, E., Prasser, H.-M., 2007. Use of models for lift, wall and turbulent dispersion forces acting on bubbles for poly-disperse flows. Chemical Engineering Science 62, 4146-4157.

Luo, H., Svendsen, H. F., 1996. Theoretical model for drop and bubble breakup in turbulent dispersions. AIChE Journal 42, 1225-1233.

Ma, T., Santarelli, C., Ziegenhein, T., Lucas, D., Fr¨ohlich, J., 2017. Direct numerical simulation-based Reynolds-averaged closure for bubble-induced turbulence. Physical Review Fluids 2, 034301.

Masood, R. M. A., Delgado, A., 2014. Numerical investigation of the interphase forces and turbulence closure in 3D square bubble columns. Chemical Engineering Science 108, 154-168.

Monahan, S. M., Fox, R. O., 2009. Validation of two fluid simulations of a pseudo two dimensional bubble column with uniform and nonuniform aeration. Industrial and Engineering Chemistry Research 48, 8134-8147.

Myong, H. K., Kasagi, N., 1990. A new approach to the improvement of turbulence model for wall-bounded shear flows. JSME International Journal 33, 63-72.

Ohnuki, Akira, Akimoto, Hajime, 2000. Experimental study on transition of flow pattern and phase distribution in upward air-water two-phase flow along a large vertical pipe. International Journal of Multiphase Flow 26, 367-386.

Patankar, S. V., 1980. Numerical Heat transfer and Fluid Flow. Hemisphere, New York, USA.

Pfleger, D., Becker, S., 2001. Modelling and simulation of the dynamic flow behaviour in a bubble column. Chemical Engineering Science 56, 1737-1747.

Politano, M. S., Carrica, P. M., Converti, J., 2003. A model for turbulent polydisperse two-phase flow in vertical channels. International Journal of Multiphase Flow 29, 1153-1182.

Prasser, H.-M., Beyer, M., Carl, H., Gregor, S., Lucas, D., Pietruske, H., Schutz, P., Weiss, F.-P., 2007. Evolution of the structure of a gas-liquid two-phase flow in a large vertical pipe. Nuclear Engineering and Design 237, 1848-1861.

Prince, M. J., Blanch, H. W., 1990. Bubble coalescence and breakup in air-sparged bubble columns. AIChE Journal 36, 1485-1499.

Ruzicka, M. C., Drahos, J., Fialova, M., Thomas, N. H., 2001. Effect of bubble column dimensions on flow regime transition. Chemical Engineering Science 56, 6117-6124.

Rzehak, R., Krepper, E., Lifante, C., 2012. Comparative study of wall-force models for the simulation of bubbly flows. Nuclear Engineering and Design 253, 41-49.

Rzehak, R., Krepper, E., 2013. CFD modeling of bubble-induced turbulence. International Journal of Multiphase Flow 55, 138-155.

Rzehak, R., Krepper, E., 2015. Bubbly flows with fixed polydispersity: validation of a baseline closure model. Nuclear Engineering and Design 287, 108-118.

Santarelli, C., Roussel, J., Fr¨ohlich, J., 2016. Budget analysis of the turbulent kinetic energy for bubbly flow in a vertical channel. Chemical Engineering Science 141, 46-62.

Sato, Y., Sekoguchi, K., 1975. Liquid velocity distribution in two-phase bubble flow. International Journal of Multiphase Flow 2, 79-95.

Sato, Y., Sadatomi, M., Sekoguchi, K., 1981a. Momentum and heat transfer in two-phase bubble flow-I: theory. International Journal of Multiphase Flow 7, 167-177.

Sato, Y., Sadatomi, M., Sekoguchi, K., 1981b. Momentum and heat transfer in two-phase bubble flow-II: a comparison between experimental data and theoretical calculations. International Journal of Multiphase Flow 7, 179-190.

Sattar, M. A., Naser, J., Brooks, G., 2013. Numerical simulation of two-phase flow with bubble breakup and coalescence coupled with population balance modeling. Chemical Engineering and Processing 70, 66-76.

Shaikh, A., Al-Dahhan, M. H., 2007. A Review on flow regime transition in bubble columns. International Journal of Chemical Reactor Engineering 5, Review R1.

Shawkat, M. E., Ching, C. Y., Shoukri, M., 2008. Bubble and liquid turbulence characteristics of bubbly flow in a large diameter vertical pipe. International Journal of Multiphase Flow 34, 767-785.

Sheng, Y. Y., Irons, G. A., 1993. Measurement and modeling of turbulence in the gas liquid two-phase zone during gas injection. Metallurgical Transactions B 24, 695-705.

Shi, J.-M., Frank, T., Krepper, E., Lucas, D., Rohde, U., Prasser, H.-M., 2004. Implementation and validation of non-drag interfacial forces in CFX-5.6. 5th International Conference on Multiphase Flow, Yokohama, Japan.

Tomiyama, A., Zun, I., Sou, A., Sakaguchi, T., 1993. Numerical analysis of bubble motion with the VOF method. Nuclear Engineering and Design 141, 69-82.

Tomiyama, A., Sou, A., Zun, I., Kanami, N., Sakaguchi, T., 1995. Effects of Eötvös number and dimensionless liquid volumetric flux on lateral motion of a bubble in a laminar duct flow. Advances in Multiphase Flow 3-15.

Tomiyama, A., 1998. Struggle with computational bubble dynamics. Multiphase Science and Technology 10, 369-405.

Tomiyama, A., Kataoka, I., Zun, I., Sakaguchi, T., 1998. Drag coefficients of single bubbles under normal and micro gravity conditions. JSME International Journal B 41, 472-479.

Tomiyama, A., Tamai, H., Zun, I., Hosokawa, S., 2002. Transverse migration of single bubbles in simple shear flows. Chemical Engineering Science 57, 1849-1858.

Troshko, A. A., Hassan, Y. A., 2001. A two-equation model of turbulent bubbly flows. International Journal of Multiphase Flow 27, 1965-2000.

Vitankar, V. S., Dhotre, M. T., Joshi, J. B., 2002. A low Reynolds number $k-\varepsilon$ model for the prediction of flow pattern and pressure drop in bubble column reactors. Chemical Engineering Science 57, 3235-3250.

Wellek, R. M., Agrawal, A. K., Skelland, A. H. P., 1966. Shapes of liquid drops moving in liquid media. AIChE Journal 12, 854-862.

Yao, W., Morel, C., 2004. Volumetric interfacial area prediction in upward bubbly Two-Phase Flow. International Journal of Heat and Mass Transfer 47, 307-328.

Ziegenhein, T., Rzehak, R., Krepper, E., Lucas, D., 2013. Numerical Simulation of Polydispersed Flow in Bubble-Columns with the Inhomogeneous Multi-Size-Group Model. Chemie Ingenieur Technik 85, 1080-1091.

Ziegenhein, T., Rzehak, R., Lucas, D., 2015. Transient simulation for large scale flow in bubble columns. Chemical Engineering Science 122, 1-13.

Ziegenhein, T., Rzehak, R., Ma, T., Lucas, D., 2017. Towards a unified approach for modeling uniform and non-uniform bubbly flows, Canadian Journal of Chemical Engineering 95, 170-179.

Zun, I., 1980. The transverse migration of bubbles influenced by walls in vertical bubbly flow. International Journal of Multiphase Flow 6, 583-588.

Zun, I., 1986. The non-rectilinear motion of bubbles rising through a stagnant and disturbed liquid. Proc. World Cong. III of Chem. Eng. 2, 214-217.

Appendix

Permissions

Title: Prediction of mono-disperse gas–liquid turbulent flow in a vertical pipe

Author: A.S.M. Atiqul Islam,N.A. Adoo,D.J. Bergstrom

Publication: International Journal of Multiphase Flow

Publisher: Elsevier

Date: October 2016

LOGIN

If you're a copyright.com user, you can login to RightsLink using your copyright.com credentials.

Already a RightsLink user or want to learn more?

Please note that, as the author of this Elsevier article, you retain the right to include it in a thesis or dissertation, provided it is not published commercially. Permission is not required, but please ensure that you reference the journal as the original source. For more information on this and on your other retained rights, please visit: https://www.elsevier.com/about/our-business/policies/copyright#Author-rights

BACK CLOSE WINDOW